THERMAL PERFORMANCE CHARACTERIZATION OF FLAT GROOVED HEAT PIPES

A THESIS SUBMITTED TO

THE GRADUATE SCHOOL OF ENGINEERING AND SCIENCE

OF BILKENT UNIVERSITY

IN PARTIAL FULFILLMENT OF THE REQUIREMENTS FOR

THE DEGREE OF

MASTER OF SCIENCE

IN

MECHANICAL ENGINEERING

By

Hossein ALIJANI ALIJANVAND

July 2017

THERMAL PERFORMANCE CHARACTERIZATION OF FLAT GROOVED HEAT PIPES

By Hossein ALIJANI ALIJANVAND

July 2017

We certify that we have read this thesis and that in our opinion it is fully adequate, in scope and in quality, as a thesis for the degree of Master of Science.

Barbaros Çetin(Advisor)

Zafer Dursunkaya(Co-advisor)
Middle East Technical University, Department of Mechanical Engineering

Murat Köksal
Hacettepe University, Department of Mechanical Engineering

Özgür Bayer
Middle East Technical University, Department of Mechanical Engineering

Approved for the Graduate School of Engineering and Science:

Ezhan Karaşan
Director of the Graduate School

ABSTRACT

THERMAL PERFORMANCE CHARACTERIZATION OF FLAT GROOVED HEAT PIPES

Hossein ALIJANI ALIJANVAND
M.S. in Mechanical Engineering
Advisor: Barbaros Çetin
July 2017

Heat pipes are promising heat removal devices widely used in a variety of fields ranging from thermal management of electronic components to terrestrial and aerospace applications. Their working principle, phase change of a working fluid, makes them superior to other conventional cooling methods. This thesis study focuses on flat grooved heat pipes and the effects of working fluid, filling ratio, groove density, and input heat flux on their thermal performance are investigated. During the study, two aluminum heat pipe generations and one silicon heat pipe configuration, each having a set of different groove densities, are fabricated. In each set, different methods of heating and cooling are applied. In all the experiments on aluminum heat pipes, the working fluid is isopropyl alcohol due to its wetting characteristics that makes it compatible with the aluminum surface. For the case of silicon, the heat pipes are charged with isopropyl alcohol and water. The optimum filling ratio, corresponding to the minimum temperature difference along the heat pipe and maximum effectiveness, is reported for each heat pipe. Moreover, as one of the operational limitations of heat pipes, the occurrence of dryout is visually observed and its extent is reported for each heat pipe operating at different filling ratios under different heat inputs. Furthermore, to find the heat input to the heat pipes of first generation and to simulate the phase change in one of the heat pipes of second generation, two 3-D computational models are developed and temperature distribution along the heat pipes are verified by the experimental results.

Keywords: Flat grooved heat pipe, thermal performance, filling ratio, dryout.

ÖZET

DÜZ OLUKLU ISI BORULARININ ISIL PERFORMANS KARAKTERİZASYONU

Hossein ALIJANI ALIJANVAND
Makine Mühendisliği, Yüksek Lisans
Tez Danışmanı: Barbaros Çetin
Temmuz 2017

Isı boruları elektronik, uzay ve havacılık uygulamalarında elektronik ekipmanların soğutulmasında sıklıkla kullanılan ısı uzaklaştırma cihazlarıdır. Faz değişimi ile ısı transferi sağlamaları ile diğer soğutma yntemlerine gre üstünlük sağlamaktadırlar. Bu tez çalışması düz oluklu ısı boruları üzerine odaklanmakta ve kullanılan akışkanın, doldurma oranın, oluk yoğunluğunun ve verilen ısı akısı ısıl performans üzerindeki etkilerini incelemektedir. Bu çalışma kapsamında farklı oluk yoğunluklarına sahip iki tane alüminyum ve bir silikon ısı borusu konfigürasyonu üzerinden çalışmalar yürütülmüştür. Yürütülen farklı set deneysel çalışmalarda farklı ısıtma ve soğutma yntemleri uygulanmıştır. Alüminyum ile yapılan deneylerde alüminyum ile uyumu nedeniyle izopropil alkol, silikon deneylerinde ise hem izopropil alkol hem de su kullanılmıştır. Isı borusu iki ucu arasında en düşük sıcaklığı ve ısı borusu için en yüksek etkinlik katsayısı veren optimum doluluk oranı her ısı borusu rapor edilmiştir. Ayrıca, ısı borularının çalışma limitine karar veren kuruma grsel olarak gzlemlenmiş, ve kuruma başlangıç noktası farklı dolum oranları ve ısı girdileri için deneysel olarak irdelenmiştir. Yapılan n deneylerde ısı borusuna verilen ısı girdisini belirlemek ve optimum doluluk oranında çalışan bir ısı borusu içerisindeki sıcaklık dağılımını belirleyebilmek için 3-boyutlu sayısal bir model geliştirilmiş ve ısı boruları üzerindeki sıcaklık dağılımı ile doğrulanmıştır.

Anahtar sözcükler: Düz oluklu ısı borusu, sl performans, doldurma oran, kuruma.

Acknowledgement

I'd like to appreciate my supervisor Dr. Barbaros Çetin for his kind guidance, scientific support and advice, and patience during my thesis research from the very first day of my M.Sc. studies.

I also express my gratitude to my co-adviser Dr. Zafer Dursunkaya for his scientific support in every step of this work. Additionally, I thank Dr. Yiğit Akkuş for his beneficial collaboration in my research. I'm also thankful to Dr. Mehmet Yılmaz, Mr. Semih Yaşar, Murat Güre, Abdullah Kafadenk, Mustafa Kılıç, Şakir Duman, and Semih Bozkurt for their kind helps during the fabrication of the heat pipes.

Financial support from the Scientific and Technological Research Council of Turkey (TÜBİTAK) under project no. 213M351 is hereby appreciated.

I'm grateful to my friends too, who supported me during my master's studies, including Serdar Taze (for transferring his laboratory skills), Reza Rasooli, Arsalan Nikdoost, Mohammad Asghari, Masoud Ahmadi, and Mehrdad Vasheghani Farahani (for his long-distance emotional support.) I also thank Cem Kurt, Atakan Atay, and Büşra Sarıarslan for their help in preparing some figures in this thesis.

My deepest appreciation goes to my mother, Parvin, my father, Majdoddin, and my brother, Mohammad, for their overseas support. Last but not least, I'd like to express my warmest thanks to Gamze, without her encouragement, this thesis would not have been written.

Contents

List of Figures

List of Tables

Chapter 1

Introduction

Heat pipes are promissing heat removal devices which utilize phase change of a working fluid to dissipate heat from a heat source. Importantly, the phase change mechanism enables them to operate under small temperature gradients along their length. They also benefit from high heat removal capacity caused by high heat of vaporization of working fluids, needing no external pumping power, and requiring relatively low amount of working fluid [1–3]. Every heat pipe has two major sections of evaporator (on the heat source side) and condenser (on the heat sink side). Based on the application area and available space, there might be an adiabatic section in between. Operation of a typical heat pipe initiates with vaporization of the liquid working fluid in the evaporator, by absorbing its latent heat of vaporization from the heat source. The resultant vapor then moves to the condenser section with the help of its pressure difference, where it releases its latent heat of condensation to the heat sink. Next, the condensate flows back to the evaporator by a capillary force caused by a wick structure. This process continues as long as there is a temperature difference between the evaporator and condenser. Figure 1.1 depicts schematic of the operation of a typical heat pipe.

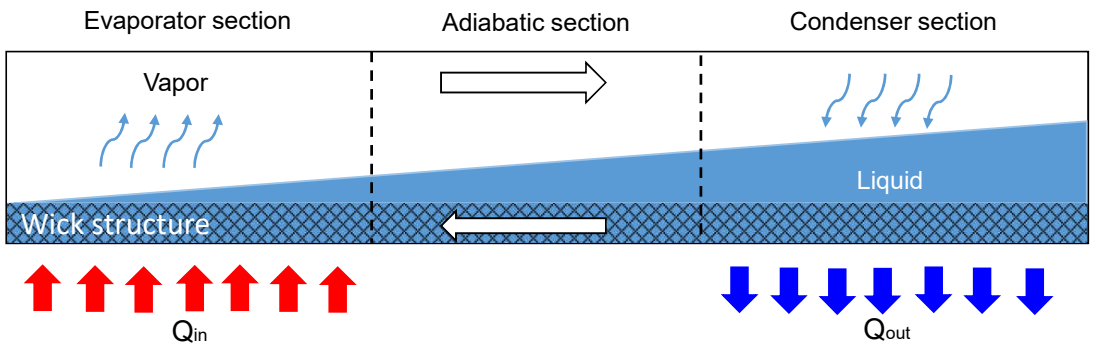

Figure 1.1: Schematic of the working principle and sections of a typical heat pipe, with direction of the vapor and liquid flows

1.1 Wick Structures

The wick structure of a heat pipe provides sufficient capillary force for the liquid flow from the condenser to the evaporator. The wicks can be categorized into sintered, mesh, groove, or occasionally a combination of them.

(i) Sintered wick: This type of wick is made by sintering a metal powder in temperatures between half of and close to melting point of the material. A sintered wick can be of mono-porous or bi-porous type. The high hydraulic resistance of mono-porous wicks at high heat fluxes may cause the evaporator to dryout. In such a case, a bi-porous wick increases the performance, while the bigger pores exhibit a lower hydraulic resistance and smaller pores supply the adequate capillary force. Figures 1.2–(a) and (b) shows the cross-sectional and cut-up views of a typical cylindrical heat pipe with sintered wick structure. A summary of recent developments in heat pipes with sintered wick structures are given in [5].

(ii) Groove wick: Axial grooves are also capable of providing capillary pressure for liquid flow in a heat pipe. The cross-section of the grooves may be in different shapes, including triangular, square, rectangular, trapezoidal, or even Ω-shaped. However, fabricating miniature sized grooves may increase the fabrication cost of a heat pipe. Figures 1.2–(c) and (d) demonstrate the cross-sectional and cut-up views of a cylindrical heat pipe with

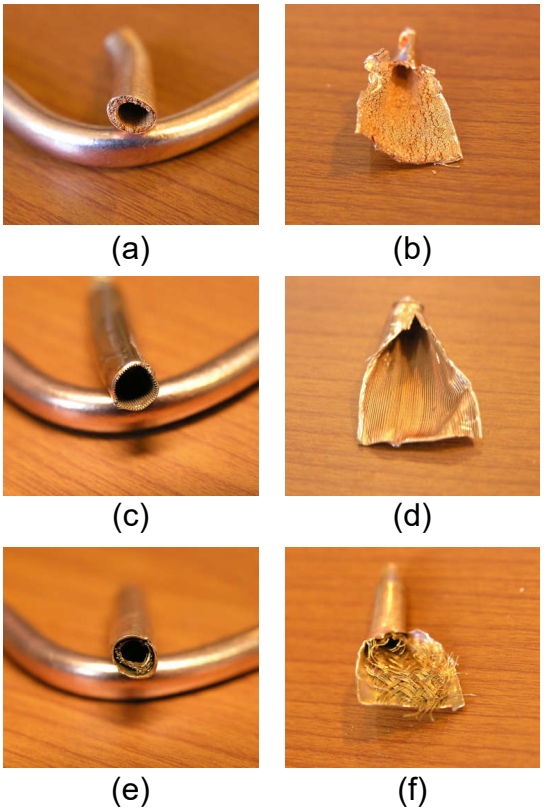

Figure 1.2: Three types of wick structures [4], sineterd wick: **(a)** cross-sectional view, **(b)** cut-up heat pipe, groove wick: **(c)** cross-sectional view, **(d)** cut-up heat pipe, mesh wick: **(e)** cross-sectional view, **(f)** cut-up heat pipe.

axial grooves. Rectangular grooves are of common interest due to easier fabrication and simpler geometry to be numerically modeled.

(iii) **Mesh wick:** Another type of wick structure is composed of a number of screen mesh layers. In this case, the sharp corners between the mesh wires act as the capillary structure for the liquid flow [6]. The cross-sectional and cut-up views of a cylindrical heat pipe with a mesh wick structure is shown in Figures 1.2–(e) and (f).

It is worth mentioning that depending on the application and design, the aforementioned wick structures can be combined to be used as the capillary structure of a heat pipe. As an instance, Lefevre *et al.* [7] investigated thermal performance of a flat plate heat pipe with axial grooves covered with screen meshes. As

another, Li *et al.* [8] manufactured a heat pipe with compound wick of sintered copper powder on axial grooves.

1.2 Types of Heat Pipes

Heat pipes can be in various configurations and types, including two-phase closed thermosyphon, capillary-driven heat pipe, annular heat pipe, vapor chamber, rotating heat pipe, gas-loaded heat pipe, loop heat pipe, capillary pumped loop heat pipe, pulsating heat pipe, micro and miniature heat pipe [2]. Three of the most common heat pipes are described in detail as follows:

1.2.1 Micro Heat Pipes

First defined by Cotter [9] in 1984, a micro heat pipe consists of a single channel of a non circular cross-section, with sharp corners acting as liquid arteries providing sufficient capillary force for the liquid flow. Figure 1.3–(a) shows different cross-sections of micro heat pipes studied in the literature. Cotter proposed a triangular cross-section in a theoretical study to determine the maximum heat transfer capacity of a microchannel. Other cross-section shapes include rectangular or square with straight or incurved walls, trapezoidal, and circular with incurved walls, and triangular with concave walls. While the liquid flows at the sharp corners, the vapor flow occurs in the inner hollow core. The typical hydraulic diameter of a micro heat pipe is in the range of $10 - 500\,\mu$m [10].

1.2.2 Loop Heat Pipes

Having evaporation and condensation processes similar to conventional heat pipes, loop heat pipes consist of a capillary pump, a compensation chamber, a condenser, and liquid and vapor lines. They are capable of heat dissipation

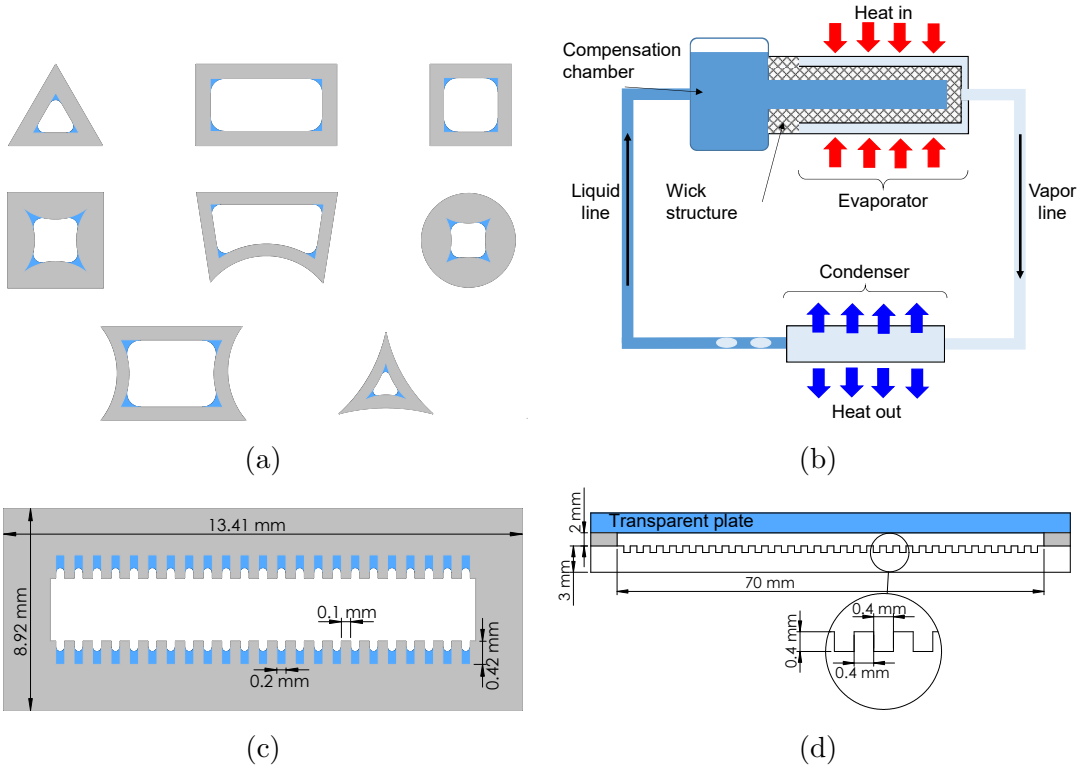

Figure 1.3: Different types of heat pipes: **(a)** common micro heat pipe cross-sections (adapted from [12]), **(b)** schematic of a loop heat pipe (adapted from [13]), **(c)** cross-section of a flat heat pipe with axial rectangular grooves (adapted from [14]), **(d)** cross-section of a flat plate heat pipe with axial rectangular grooves(adapted from [15])

over long distances between the heat source and heat sink, against gravity forces. They have application areas in thermoregulation systems of spacecraft and electronics and computers cooling [11]. Figure 1.3–(b) shows the working cycle and sections of a typical loop heat pipe.

1.2.3 Grooved Heat Pipes

Capillary-driven heat pipes with groove wick structure are often called grooved heat pipes. The grooves might be of triangular, rectangular, or trapezoidal cross-section, but compound wick structures, such as screen mesh or sintered powder covering the grooves, may also be used. Cylindrical heat pipes with axial grooves

on the inside wall are the most common type of grooved heat pipes. Unlikely, flat heat pipes mostly have a bulk with outer rectangular cross-section. Electric Discharge Machining (EDM), CNC milling process, CNC machining, and drawing and extrusion processes are some of the techniques used to fabricate flat heat pipes [16]. It should be noted that the grooves might be present on both the top and bottom surfaces as in [14, 17–20] (Figure 1.3–(c)), or just on the bottom surface of the heat pipe as in [15, 21–24] (Figure 1.3–(d)). They are usually called a flat plate heat pipe (FPHP); more specifically, if the wick structure is made of axial grooves, it may be called a flat grooved heat pipe (FGHP). The details of some experimental and analytical studies on FGHPs are described as follows.

In 1999, Hopkins *et al.* [17] performed an experimental and analytical analysis on heat transfer performance of three flat miniature heat pipes on copper with axial trapezoidal and rectangular grooves. The two heat pipes with trapezoidal grooves were fabricated by a rolling method and filled with water with amounts of 0.20 ml for one of them and 20% of the internal volume for the other. The heat pipe with rectangular grooves was fabricated with a different method: first, 62 grooves of cross-sectional dimensions of 0.2 mm × 0.2 mm and top fin width of 0.1 mm were machined on two identical copper plates by a high-speed dicing saw. The symmetric pieces then were attached together by a low temperature silver solder. The length of the heat pipe was 120 mm. Next, it was charged with 0.84 ml of water with weighting method. In their experiments, the maximum heat loads at operating temperatures of 60, 70, 80, 90, and 95 °C were found under horizontal and vertical orientations. According to the results, the heat pipe with rectangular grooves exhibited the lowest value of thermal resistance (see section 1.7.2) of 0.2 K/W. Moreover, maximum heat flux was found to be 92.8 W/cm^2 and 141.8 W/cm^2 for horizontally and vertically oriented heat pipe, respectively.

In 2008, Lim *et al.* [18] evaluated the thermal performance of a flat heat pipe, which could operate under an adverse-gravity condition due to the high capillary pump provided by novel fan-shaped microgrooves. The grooves were 0.30 mm deep with top width of 0.15 mm, machined on two plates of copper using a femtosecond laser micromachining technique. The vapor space was provided with a

hollow middle plate between the two plates with grooves. Then, the heat pipe was charged with 0, 53.9, and 183 μL of degassed water, corresponding to empty, moderately charged, and overcharged heat pipe, respectively. The values of heat input to the heat pipe were from 1 to 8 W with 1 W increments. Moreover, the heat pipe operated at different tilt angles between $-90\,^\circ$ (adverse-gravity orientation) and $90\,^\circ$ (pro-gravity orientation). At the maximum input power of 8 W, the temperature difference between the average of two thermocouples at the evaporator and four thermocouples at the condenser of the moderately charged heat pipe section turned out to be 45.9 °C when the peak temperature approaching a top limit of 120 °C, resulted in a minimum thermal resistance of 5.45 °C/W. In addition, thermal resistance values of overcharged and empty heat pipe, where the heat transfer mechanism is through the conduction alone, were higher than those of moderately charged one for all of the examined heat inputs, showing the efficient phase change heat transfer. Furthermore, the heat transfer rate remains the same (8 W) for tilt angles from $-90\,^\circ$ to $45\,^\circ$, increasing for the case of $90\,^\circ$ tilt angle, indicating the successful operation of the heat pipe under adverse-gravity operating condition. Moreover, the onset of dryout was observed at input power of 13 W with a sudden jump in thermal resistance of the heat pipe after increasing the input power beyond 12 W.

In 2009, nucleate boiling at different filling ratios was experimentally studied for a copper flat plate heat pipe with axial rectangular grooves charged with methanol by Lips *et al.* [15]. Figure 1.3–(d) depicts the schematic cross-section of their FPHP, including the copper plate on which 88 grooves of cross-section $0.4\,\text{mm} \times 0.4\,\text{mm}$ are machined, and a nitrile ring covered with a transparent plate which enables the observation of the liquid/vapor menisci inside the grooves. The experiments performed under different filling ratio (see section 3.1) values of 1.3, 1.6, 2.8 compared to the total volume of the grooves. Under filling ratio of 2.8 and input heat load of $9.6\,\text{W/cm}^2$, boiling was visually observed through the transparent cover and the performance of the heat pipe characterized accordingly. The results revealed that occurrence of boiling could decrease the temperature readings in the evaporator section by approximately 5 K compared to operation without boiling, resulting in a decrease in the thermal resistance of the heat

pipe. This indicated that boiling could improve thermal performance of the heat pipe. Furthermore, the effect of different filling ratios were taken into account by corresponding thermal resistance values of the heat pipe under different input heat flux values. Although at filling ratio of 1.3 the condenser showed the lowest thermal resistance under lower heat fluxes, filling ratio of 1.6 exhibited the best performance under high input heat fluxes. However, the optimum filling ratio was chosen to be 1.6 because of the small thermal resistances in both the condenser and evaporator sections. In 2010, same authors investigated the effect of filling ratio and the vapor space thickness on thermal performance of the same flat plate heat pipe with n-pentane as the working fluid [21]. With vapor space thickness of 2 mm, the optimal amount of filling ratio was chosen to be the one that minimized the overall thermal resistance of the heat pipe under input heat flux of $7.5\,\mathrm{W/cm^2}$, which turned out to be in the range of $10-25\%$ of the internal volume of the heat pipe, corresponding to $1-2.5$ times of the volume of the grooves. For vapor space thickness of 5 mm, optimal filling ratio values were in the range of $1-2$ times the volume of the grooves. Moreover, a very small or very high vapor space thickness resulted in trapping of the working fluid in the corners and sides of the heat pipe or dominating the gravitational forces and flooding the grooves, respectively, both adversely affect the performance of the heat pipe. In other words, a thicker vapor space resulted in the homogeneous distribution of the working fluid all over the condenser section, while a thinner vapor space resulted in trapping the working fluid in the corners of the heat pipe as well as in the distance between the grooves and transparent cover.

The effect of filling ratio on cooling performance of a flat grooved heat pipe was investigated by Chen *et al.* in 2014 [19]. The grooves were of 0.2 mm width and 0.4 mm depth, with 0.2 mm distance between them, fabricated from aluminum with extrusion process. The performance of the heat pipe was characterized when it was charged with acetone with filling ratio values between 5 % and 50 % with 5 % increments under heat inputs from 5 W to 60 W with 5 W intervals. Filling ratio of 25 % demonstrated lowest values of evaporator temperature, minimum thermal resistance of 0.254 K/W, and maximum effective thermal conductivity of $3150\,\mathrm{W/m\cdot K}$. Moreover, the study of the same grooves geometry is

extended to investigate the effect of filling ratio on the heat pipes with different lengths and bending angles [25]. It was found that a shorter heat pipe shows a lower minimum temperature difference between the evaporator and condenser and, consequently, a lower thermal resistance. In addition, the effective thermal conductivity and maximum heat transport capability of the heat pipes could increase with increasing the bending angle from 0° to 90°.

Stubblebine *et al.* [23] studied the effect of inorganic aqueous solutions on the thermal performance of a grooved aluminum flat heat pipe in 2015. The heat pipe consisted of 15 grooves, 1.5 mm wide, 2.0 mm deep, and 130 mm long, machined on an aluminum plate placed under a stainless steel frame, covered with an acrylic plate, and sealed with two o-rings. The heat pipe charged with two different inorganic aqueous solutions and the corresponding thermal resistance values were compared. Accordingly, they showed thermal resistance values similar to those of a copper heat pipe with the same grooves geometry made of copper and charged with water in [24]. However, one of the solutions demonstrated a maximum heat flux 27% higher than that of the copper/water heat pipe under the same operation conditions. Moreover, dryout was visually estimated and its onset calculated by corresponding inflection point in the graph of thermal resistance versus input heat load. Both solutions could delay the onset of dryout compared to the copper/water heat pipe.

Supowit *et al.* studied the effect of a designer fluid and inclination angle on heat removal performance of a flat grooved heat pipe in 2016. The grooves and heat pipe configuration was the same as in [23]. Ease of machining, low cost, and visualization of dryout were of reasons for choosing this relatively large groove dimensions. The heat pipes charged with water and two concentrations of a designer fluid, with the same amount of 7 mL equal to a 1.2 times the total volume of the grooves. For case of the heat pipe charged with water, the onset of dryout occurred at heat inputs near 85 W and noticed by a sudden increase in thermal resistance with power input, verified visually through the transparent cover. Moreover, the effect of two concentrations of an inorganic aqueous solution (IAS) was investigated on the performance of the heat pipe. One of the concentrations could decrease thermal resistance of the heat pipe charged with water by 20%.

Furthermore, it could postpone onset of dryout to an input power higher than 200 W. However, thermal resistance of the heat pipe charged with difference concentrations of the designer fluid did not show a significant improvement. Details of the investigated inclination angles and comparison between the performance of water and the designer fluid can be found in [24].

In 2017, Hao *et al.* [20] experimentally investigated the performance of acetone-based nanofluids on a flat plate heat pipe with axial rectangular grooves of 0.3 mm width and 0.65 mm depth, with 0.55 mm distance between the grooves. To find the optimum filling ratio, 20, 30, and 40 % of the internal volume of the heat pipe charged with acetone and corresponding thermal resistances were calculated under different input heat loads of $10-130$ W with 10 W increments. Since filling ratio of 30 % showed the lowest thermal resistance values in all of the examined heat inputs, it was chosen to be the optimum filling ratio for further experiments. Then, the heat pipe charged with different concentrations of two multiwall carbon nanotubes (MWCNTs) acetone nanofluids and its performance assessed with corresponding thermal resistance and effective thermal conductivity values (see section 1.7.3). For both of the nanofluids, 0.005 wt. % concentration resulted in the lowest thermal resistance and highest effective thermal conductivity and this was chosen to be the optimum mass concentration of the nanofluids. The nanofluids could reduce the thermal resistance of the heat pipe 16 % and 40 % compared to the heat pipe charged with acetone. Moreover, the effective thermal conductivity of the heat pipe compared with thermal conductivity of the heat pipe bulk material which was aluminum. Compared to acetone, both nanofluids showed higher effective thermal conductivity values for all the examined input heat loads. As an instance, the effective thermal conductivity of the heat pipe, peaked at approximately 13 times the thermal conductivity of aluminum under heat input of 160 W. Table 1.1 summarizes some studies on flat grooved heat pipes in the literature.

Table 1.1: Experimental studies on flat grooved heat pipes in the literature

Reference	**Wall material**	**Grooves dimensions width (mm) × depth (mm)**	**Grooves array**	**Working fluid(s)**	**Heat load(s)**	**Different filling ratios**	**Performance characterization method**
Hopkins *et al.* [17]	Copper	0.2×0.42	Double-sided	Water	$4 - 168\,\mathrm{W}$	–	Heat pipe thermal resistance, maximum heat transfer rate
Lim *et al.* [18]	Copper	0.15×0.30 (fan-shaped grooves)	Double-sided	Water	$1 - 14\,\mathrm{W}$	0, 33.5, 114[1]%*	Thermal resistance
Lips *et al.* [15]	Copper	0.4×0.4	One-sided	Methanol	$1.1 - 14.5\,\mathrm{W/cm^2}$	1.3, 1.6, and 2.8 **	Thermal resistance
Lips *et al.* [21]	Copper	0.4×0.4	One-sided	*n*-pentane	$5, 7.5, 10\,\mathrm{W/cm^2}$	$0 - 80\,\%$*	Thermal resistance
Dean *et al.* [22]	Silicon	0.1×0.1	One-sided	Liquid Hg	$0 - 20\,\mathrm{W}$	–	Temperature drop along the top lid, effective thermal conductivity
Chen *et al.* [19]	Aluminum	0.2×0.4	Double-sided	Acetone	$5 - 60\,\mathrm{W}$	5–50% *	Thermal resistance, effective thermal conductivity, ΔT between the evaporator and condenser, maximum heat transport capability
Stubblebine *et al.* [23]	Aluminum	1.5×2	One-sided	Water, inorganic aqueous solutions	$0 - 108\,\mathrm{W/cm^2}$	–	Thermal resistance, ΔT between the evaporator and condenser
Supowit *et al.* [24]	Copper	1.5×2	One-sided	DI-water, inorganic aqueous solutions	$10 - 120\,\mathrm{W}$	–	Thermal resistance
Hao *et al.* [20]	Aluminum	0.3×0.65	Double-sided	Acetone, acetone-based nanofluids	$10 - 170\,\mathrm{W}$	20, 30, 40% *	Thermal resistance, effective thermal conductivity

[1] Considering the fill tube as the extra space
* Compared to internal volume of the heat pipe
** Compared to total volume of the grooves

1.3 Heat Transfer Limitations

Heat pipes are vulnerable to some constraints on their performance, depending on their shape and size, working fluid, wick structure, and operating temperature [2]. There are physical phenomena that limit the maximum transferred heat through a heat pipe. Such limitations can be categorized as: (*i*) those which result in the failure of the heat pipes, known by inadequate liquid flow to the evaporator at a given heat input, including capillary, boiling, and entrainment limits; (*ii*) those which do not fail the heat pipe operation. In such a case, operation at a higher temperature for an increase in the heat input would resolve the failure. Sonic, viscous, and condenser limits are instances of this category [26]. A brief description of the above-mentioned limits is introduced as follows:

(i) Capillary limit: The most common limit in operation of a heat pipe takes place when the sum of the liquid and vapor pressures exceeds the maximum capillary pressure of the wick structure. Consequently, there exists insufficient liquid flow from the condenser to the evaporator and dryout occurs. In addition, the evaporator section undergoes a sudden temperature jump on its outer surface. The physical properties of the wick structure and the working fluid determine the maximum capillary pressure in a heat pipe.

(ii) Boiling limit: Boiling limit occurs when the applied input heat causes nucleate boiling in the evaporator. The resultant vapor bubbles may partially block the liquid flow and result in dryout. It is worth mentioning that this limit is governed by the heat flux in the direction of the heat source towards the working fluid, *e.g.* radial direction for case of conventional cylindrical heat pipes. This is more often in the heat pipes with non-metallic, rather than metallic, working fluids.

(iii) Entrainment limit: Due to the opposing directions of vapor and liquid flows, there exists a shear force at the liquid-vapor interface. At relatively high velocities, the liquid droplets may be torn from the wick surface, entrained into the vapor, and flow towards the condenser. In the case of

high entrainment rates, the evaporator undergoes dryout. Sounds of striking droplets to the condenser end is an indication of the entrainment limit which is often associated with heat pipes of small diameters and low to moderate temperatures, or high temperature heat pipes operating under high heat input values [2]. An analysis based on Weber number can help a better understanding of the onset of the entrainment limit [27].

(iv) Sonic limit: This typically occurs in liquid-metal heat pipes during startup or low-temperature operations. At low densities the vapor flows with high velocities corresponding to its mass flow rate. Hence, sonic flow occurs in the vapor flow passage. However, this does not result in operational failure of a heat pipe. Once a heat pipe operates in this condition, a considerable temperature drop in the axial direction is observed, i.e. the heat pipe may not work in a near isothermal condition [2, 28].

(v) Viscous limit: For a heat pipe operating at low temperatures, the viscous forces in the vapor flow to the condenser may become dominant. In other words, the saturation pressure of the vapor cannot exceed the required pressure drop for vapor flow. As a consequence, the vapor pressure is inadequate to sustain the flow. Viscous limit may also be called vapor pressure limit.

(vi) Condenser limit: Depending on the cooling method, the condenser has a cooling limit. In some heat pipes, the condenser is not able to remove the maximum heat transfer rate of the heat pipe and it may not operate at its full capacity [2]. This is called the condenser limit.

1.4 Working Fluid Selection

The operational temperature range of a heat pipe is a key factor to select the proper working fluid. Some other parameters that need to be considered include compatibility with wall and wick material and being able to wet them, high latent heat of vaporization and high surface tension [2, 29]. Table 1.2 shows the useful

Table 1.2: Operational temperatrue range of some common working fluids and their compatibility with some bulk materials [2]

Working fluid	Melting point at 1 atm [K]	Boiling point at 1 atm [K]	Useful range [K]	Compatible material(s)	Incompatible material(s)
Helium	1.0	4.21	2–4	–	–
Nitrogen	63.1	77.35	70–103	–	–
Methane	90.6	111.4	91–150	–	–
Ammonia	195.5	239.9	213–373	Aluminum, Stainless Steel, Iron, Nickel	–
Acetone	180.0	329.4	273–393	Aluminum, Stainless Steel, Copper, Brass, Silica	–
Methanol	175.1	337.8	283–403	Stainless Steel, Iron, Copper, Brass, Silica, Nickel	Aluminum
Ethanol	158.7	351.5	273–403	–	–
Water	273.1	373.1	303–550	Stainless Steel, Copper, Silica, Nickel, Titanium	Aluminum, Inconel
Mercury	234.2	630.1	523–923	Stainless Steel	Molybdenum, Nickel, Tantalum, Inconel, Titanium, Niobium
Lead	600.6	2013	1670–2200	Tungsten, Tantalum	Stainless Steel, Nickel, Inconel, Titanium, Niobium
Silver	1234	2485	2073–2573	Tungsten, Tantalum	Rhenium

operating temperature range of some common working fluids in addition to their compatibility with materials.

1.5 Evacuation and Charging

Evacuating a heat pipe followed by filling it with the desired amount of working fluid and subsequent sealing are of critical steps before its operation. Since the presence of small amounts of any unwanted fluid in a heat pipe can adversely affect its performance, the working fluid must be cleaned and degassed prior to charging; doing so guarantees eliminating the introduction of any dissolved or non-condensable gases (NCGs) to the heat pipe. Based on the type and size of a heat pipe and working fluid, the charging methods may vary. Faghri [30] described a charging station with multiple containers with which the working fluid distills into the heat pipe. However, such a method might be time consuming. A common and faster charging method is using a three-way connection: one way for vacuuming and one way for charging, while the third one goes to the heat pipe. To charge an embedded heat pipe system, Wits *et. al.* [31] proposed a four-step

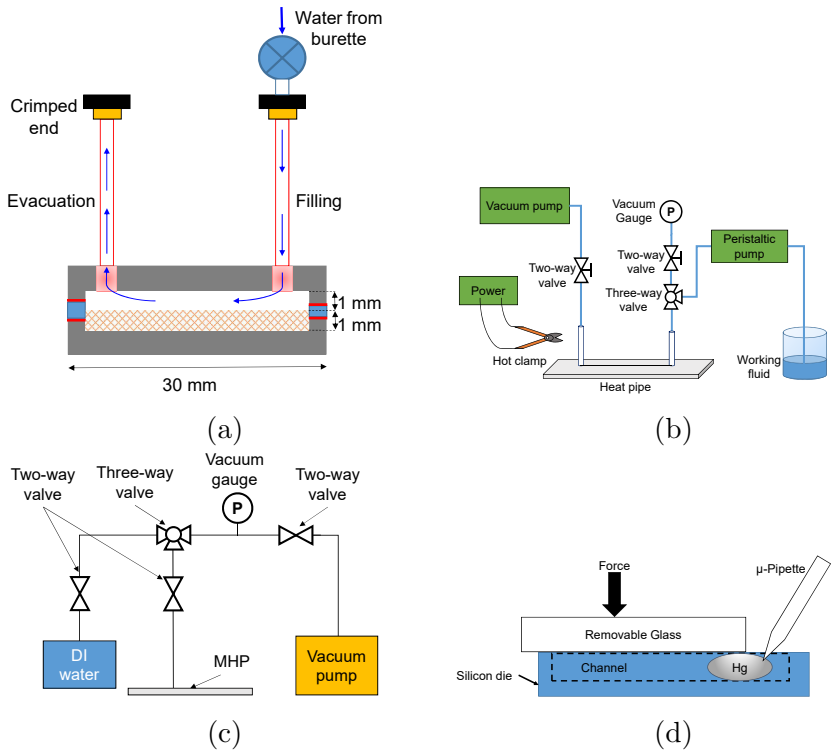

Figure 1.4: Schematic of different charging methods: **(a)** charging of a planar miniature heat pipe (adapted from [32]), **(b)** charging of a micro heat pipe (adapted from [33]), **(c)** charging of a pyrex-silicon heat pipe (adapted from [34]), **(d)** charging of a heat pipe with liquid metal (adapted from [22])

method: mounting, evacuating, filling, and sealing, done through one hole on the heat pipe. Unlike conventional sealing method of pinching the fill tube, he forced a plug into the charge component to seal the heat pipe. The accuracy of his method was 1.5 μL. Ababneh *et al.* [32] evacuated and filled a planar miniature heat pipe thermal ground plane with two holes on its upper surface. Figure 1.4-(a) depicts the schematic of their setup. In their method, the device was first evacuated with connecting the left tube in Figure 1.4-(a) to a vacuum station. Then, it was sealed and the desired amount of previously-purified water enters the device with the help of low pressure in the heat pipe, through the right tube in the figure which was also sealed afterwards. Li *et al.* [33] used a peristaltic pump charging followed by a differential weighting for accurate charging of a micro heat pipe. Figure 1.4-(b) depicts the schematic of their charging station. Wang *et al.* [34] proposed a double air pumping charge method on a pyrex-silicon flat

grooved heat pipe through one hole on the pyrex cover. In the first step, the heat pipe was vacuumed to 0.1 Pa. Then it was connected to a syringe full of degassed DI water, in such a way that water filled the heat pipe with a pressure difference. The heat pipe was then connected to the vacuum pump to pump out some of DI water until its desired amount was reached. The schematic of their charging system is shown in Figure 1.4-(c). Dean *et al.* [22] charged a heat pipe with liquid mercury with help of micropipettes and a micropump. The challenge in charging their heat pipe was the fact that mercury is not a wetting liquid. Hence, the side walls of the grooves were coated with Ti/Pt/Au for easier charging. Their method is sketched in Figure 1.4-(d).

1.6 Heating and Cooling Methods

Based on the application area, type and size of the heat pipe, available space, desired operating temperature, and working fluid the heating and cooling methods at the evaporator and condenser sections may vary from a heat pipe to another. Electrical resistance heaters are mostly used for metal heat pipes, while for silicon heat pipes film heaters are usually used. Moreover, common cooling methods include liquid cooling by water flowing in a cooling jacket, forced convection air cooling, or natural convection to the ambient. Table 1.3 summarizes various heating and cooling methods performed in experimental studies on different types of heat pipes in the literature.

Table 1.3: Different heating and cooling methods for different heat pipes studies in the literature

Reference	Type of the heat pipe	Wall material	Wick structure	Heating method	Cooling method
[35]	Miniature heat pipe	Copper	Axial trapezoidal grooves	A thin film heater	Plate heat sink cooling by a fan
[36]	Flat plate heat pipe	Copper	Axial rectangular grooves	A thick resistor film	A water heat exchanger
[37]	Cylindrical heat pipe	Copper	Axial rectangular grooves	An electrical heater	Liquid cooling (cooling jacket)
[18]	Flat heat pipe	Copper	Axial fan-shaped grooves	Nichrome-resist wire	A refrigerating bath circulator
[38]	Flat micro heat pipe	Copper	Axial rectangular grooves	A thick resistor film	A water heat exchanger
[39]	Flat plate heat pipe	Silicon	Radial rectangular grooves with decreasing width toward the center	A circular thick resistor film	A circular water heat exchanger
[21, 40]	Flat plate heat pipe	Copper	Axial rectangular grooves	A copper block heated by a heating resistor	Water flowing heat sink
[41]	Pulsating heat pipe	Silicon	Axial trapezoidal grooves	A film heater	Liquid cooling
[42]	Pulsating heat spreader	Silicon	Axial grooves	Film heater	Liquid cooling (water jacket)
[43]	Cylindrical heat pipe	Copper	Axial rectangular grooves	Heating rods heated by hot water	Ambient air
[44]	Cylindrical heat pipe	Copper	Axial trapezium grooves covered with sintered copper powder	Copper sheathing heated by an an electrical bar	Liquid cooling
[24]	Flat heat pipe	Copper	Axial grooves	Two cartridge heaters embedded in a copper block	Liquid cooling
[45]	Cylindrical heat pipe	Aluminum	Axial grooves	An electrical resistance heating element	Liquid cooling (cooling jacket)
[46]	Cylindrical heat pipe	Copper	Helical-grooves	Sheath protected Nickel-Chrome heater	Liquid cooling (cooling jacket)
[47]	Multi-branch cylindrical heat pipe	Copper	Sintered copper powder	Heating module	Forced air convection

1.7 Performance Characterization Methods

In the literature, the effect of various parameters on thermal performance of the heat pipes are investigated, including wall material, wick structure, inclination angle, heat load, working fluid, nanofluids, and filling ratio. Several parameters have been used to characterize the thermal performance of the heat pipes. These parameters are discussed in details as follows:

1.7.1 Merit Number

An indicator of the heat transfer performance of a heat pipe [48], Merit number, M, is defined as:

$$M = \frac{\rho_l \sigma_l h_{fg}}{\mu_l} \tag{1.1}$$

where ρ_l is the density of the liquid, σ_l is surface energy per unit area of the liquid, h_{fg} is latent heat of vaporization of the liquid, and μ_l is the dynamic viscosity of the liquid. This grouping of properties is based on the fact that a desired working fluid is expected to have a high surface tension to enhance the capillary pump inside the grooves, high density and latent heat of vaporization to reduce the mass flow rates, and a low viscosity to reduce the frictional losses [26]. Therefor, a working fluid of interest has a higher Merit number among a group of candidates. However, this number is usually used to select the proper working fluid at the working temperature range of a heat pipe [49]. Figure 1.5-(a) shows the variation of Merit number of some common working fluids in intermediate temperatures. Merit number of some other working fluids including several organic fluids, mercury, sulfur/iodine, and halides in the temperature range of $450 - 700\,\mathrm{K}$ can be found in [50].

1.7.2 Thermal Resistance

Thermal resistance is widely used to quantify the heat removal performance of a heat pipe. Based on Fourier law of heat conduction, it is defined as:

$$R_{th} = \frac{\Delta T}{Q} \tag{1.2}$$

where R_{th} is thermal resistance of the heat pipe, Q is the heat input, and ΔT is the temperature difference between the evaporator and condenser sections. However, some assumptions must be considered when calculating thermal resistance of a heat pipe, including: (*i*) negligible temperature difference between the wick structure and the vapor, (*ii*) negligible temperature difference between the vapor at evaporator and condenser sections, (*iii*) no heat loss through the adiabatic section, so the heat input to the evaporator section equals to the heat output from the condenser section [51]. The details of some studies which utilized this parameter to characterize the performance of a heat pipe is discussed as follows:

Supowit *et al.* [24] investigated the effect of a designer fluid on the thermal performance of a flat heat pipe with axial grooves. They reported thermal resistance values between 0.6 and 1.0 K/W for heat loads of 20–180 W at six degrees of inclination. However, the change of R_{th} at different power inputs for two different concentrations of the designer fluid did not show any significan difference. Figure 1.5-(b) shows the values of thermal resistance of the heat pipe charged with two different inorganic aqueous solutions (IASs). In 2016, Solomon *et al.* [45] studied the effect of filling ratio on the thermal performance of a cylindrical heat pipe with axial grooves. They found out that thermal resistance of the heat pipe with anodised surface is lower than that of the one with non-anodised surface. Cheng *et al.* [52] reported thermal resistance values as low as 0.2 °C/W for a circular grooved heat pipe with gradient wettability surface. Aly *et al.* [46] investigated the effect of inclination angle on total thermal resistance of a cylindrical heat pipe with helical grooves with water and nanofluids as the working fluid. They reported values between 0.4 and 0.9 K/W for heat loads of $40 - 65$ W for filling ratio of 80%. Cai *et al.* [47] calculated thermal resistance of a multi-branch cylindrical heat pipe under six filling ratios and a wide range of heating loads. They reported thermal resistance of 0.04 °C/W at the heating load of 160 W.

1.7.3 Effective Thermal Conductivity

Another indicator of the performance of a heat pipe is its effective thermal conductivity, k_{eff}, which is defined as:

$$k_{eff} = \frac{Q \cdot L_{eff}}{(T_{evaporator} - T_{condenser}) \cdot A_{eff}} \tag{1.3}$$

where Q is the heat input, L_{eff} is the effective length of the heat pipe, A_{eff} is the effective cross-sectional area of the heat pipe, $T_{evaporator}$ and $T_{condenser}$ are the wall temperatures at the evaporator and condenser sections, respectively. The value of k_{eff} of a heat pipe can be compared with thermal conductivity of its wall material. Usually, heat pipes exhibit k_{eff} values higher than thermal conductivity of their wall material, as in [20]. Some experimental studies which calculated and reported k_{eff} of heat pipes are described as follows:

In 1993, Peterson *et al.* [53] fabricated a micro heat pipe consisting an array of micro grooves on silicon. According to their findings, the effective thermal conductivity of the heat pipes with an array of rectangular and triangular grooves were 31% and 81%, respectively, higher than thermal conductivity of a silicon piece with no grooves. In 2012, Deat *et al.* [22] reported k_{eff} values up to 324 and 789.2 $\mathrm{W/m \cdot K}$ for a silicon heat pipe with axial grooves, filled with water and liquid metal (Hg), respectively. Mehrali *et al.* [54], in 2016, studied the effect of nitrogen-doped graphene nanofluid on the thermal performance of a cylindrical heat pipe with axial grooves. With the help of such a nanofluid, k_{eff} of the heat pipe could exceed 6000 $\mathrm{W/m \cdot K}$ for 0.06 wt% concentration of the nanofluid. Hao *et al.* [20] studied the effect of acetone-based nanofluids on thermal performance of an aluminum flat plate heat pipe with axial grooves. Figure 1.5-(c) shows the ratio of k_{eff} of their heat pipe to thermal conductivity of aluminum for different concentrations of acetone nanofluids under different input heat loads. Accordingly, charging the heat pipe with acetone nanofluids resulted in k_{eff} values of more than ten times higher than thermal conductivity of aluminum in higher examined heat loads.

The definition of k_{eff} is not limited to the heat pipes, thermal performance of other types of heat removal devices may also be characterized by this parameter.

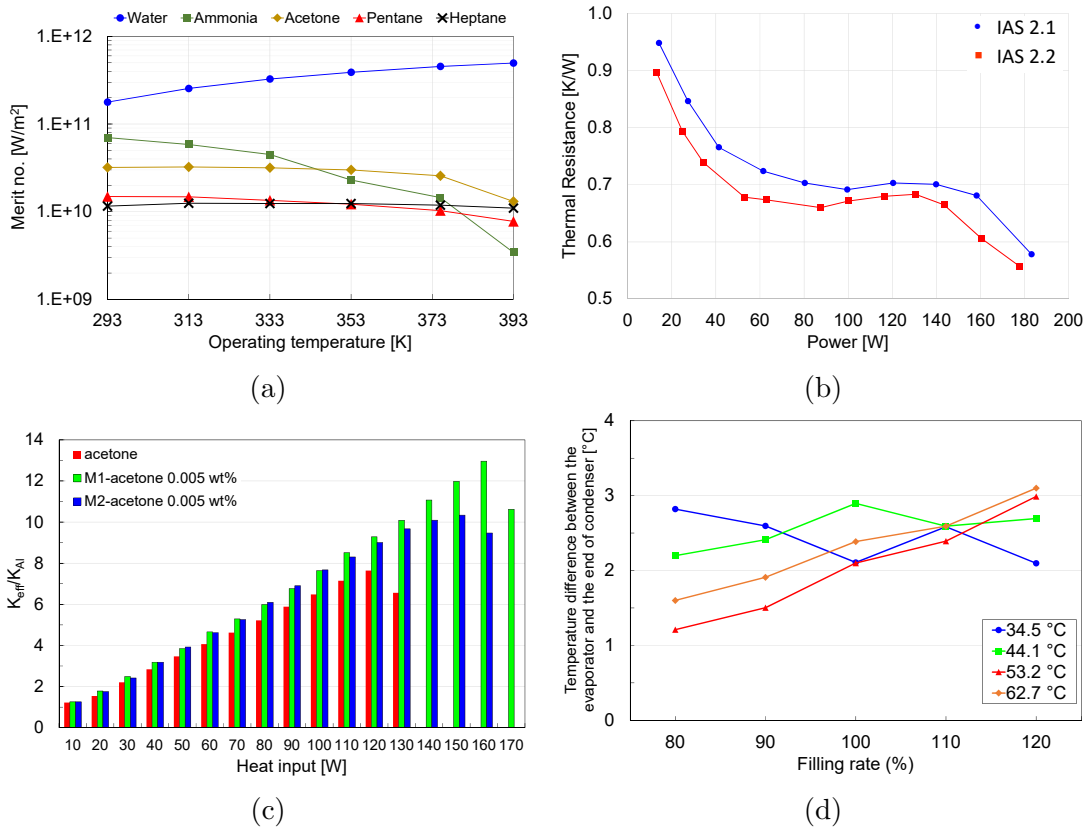

Figure 1.5: Different parameters to characterize the thermal performance of heat pipes: **(a)** Merit number (adapted from [49]), **(b)** total thermal resistance (adapted from [24]), **(c)** effective thermal conductivity (adapted from [20]), **(d)** temperature difference between the evaporator and condenser (adapted from [43])

As an instance, Youn *et al.* [42] studied the effect of filling ratio and heat load on thermal performance of a micro pulsating heat spreader (MPHS). They reported values between 200 and 600 $\mathrm{W/m \cdot K}$ for charged MPHS. As another example, k_{eff} values of a flat polymer heat pipe heat spreader under acceleration can be found in [55]. It should me noted that since k_{eff} is defined based on the heat conduction law, the heat transfer through the hat pipe must not violate the 1-D heat conduction assumption, i.e. the cross-sectional area of the heat pipe should not have the same order of magnitude with the length of the heat pipe, a condition which results in multi-dimensionality in the heat transfer.

1.7.4 Temperature Difference between the Evaporator and Condenser

As mentioned earlier in this chapter, an important advantage of the heat pipes is operating under small temperature gradients between the evaporator and condenser sections. Hence, some researchers report this temperature difference as a parameter of the thermal performance of a heat pipe. In 2007, Park *et al.* [56] investigated the effect of nanofluids on the performance of an oscillating heat pipe (OHP). According to the results of their study, the minimum temperature difference belonged to the OHP filled with 50 % nanofluid because of the strongest oscillatory behavior of the heat pipe. Ji *et al.* [57] studied the effect of size of Al_2O_3 particles on the performance of an oscillating heat pipe. Comparing the temperature difference of the heat pipes charged with nanofluids of different particle sizes, they reported an optimum size of the particles, i.e. 80 nm, which resulted in the best heat transfer capability of the tested heat pipe. Zaghdoudi *et al.* [12] studied thermal performance of a series of flat miniature heat pipes (FMHP) with axial grooves. Compared to a copper plate of the same dimensions, FMHP could operate under a temperature difference with lower slope. Tang *et al.* [43] investigated isothermal performance of a cylindrical heat pipe with axial grooves. Figure 1.5-(d) illustrates the temperature difference between the evaporator and the end of condenser vs. filling ratio at four different heating temperatures. The effect of the filling ratio is noticeable in the case of heating temperatures of 53.2 °C and 62.7 °C, where ΔT increases with filing ratio.

1.8 Motivations and Objectives of the Thesis

Among different types of the heat pipes, flat grooved heat pipes are less experimentally studied in the literature in general, and hence, their heat removal performance is in need of more investigation in terms of stability and heat transfer limitations [58]. However, they have found applications in cooling the electronic components in laptops. In particular, heat pipes with different groove widths

ranging from μm to mm are not reported in a single study in the literature. Besides, combined effects of the filling ratio and grooves dimensions are not studied in the literature. Furthermore, considering promising advantages of aluminum as the bulk material for the heat pipes including low cost, light weight, high thermal conductivity, and relative ease of machining, it has not been studied in the literature as much as copper.

This thesis experimentally investigates the effects of grooves width and filling ratio on thermal performance of flat grooved heat pipes. In this regard, three sets of heat pipes are fabricated: (*i*) first generation prototype aluminum heat pipes (heat pipes coded G1): three aluminum heat pipes with grooves widths of 0.2, 0.4, and 1.5 mm fabricated by CNC machining, (*ii*) second generation aluminum heat pipes (heat pipes coded G2): four aluminum heat pipes with grooves widths of 0.2, 0.4, 0.8, and 1.6 mm fabricated by CNC machining, (*iii*) silicon heat pipes (heat pipes coded S): two silicon heat pipes with grooves widths of 0.2 and 0.4 mm. For first generation heat pipes, thermoelectric units decided to be as the heat source and heat sink. However, the quantification of the heat input and output to and from the heat pipes is challenging because their performance is a function of various operating conditions. Therefore, a 3-D computational model is developed to quantify the heat input to the heat pipes. For second generation heat pipes, an electric resistance heater is chosen to be the heat source and a copper block cooled by cold tap water flow is the heat sink. Moreover, phase change heat transfer is simulated by a 3-D computational model and further verified with the experimental results. For case of silicon heat pipes, two chromium electrodes are used to be the heat source of the heat pipes and cooling water flow through channels in a PDMS piece are removing the heat from the heat pipes. Thermal performance of each heat pipe is investigated and characterized under a wide range of filling ratios from a fully-flooded to a dry heat pipe, and for different input heat loads. Furthermore, as one of the working limitations in performance of a heat pipe, the extent of dryout is carefully observed and reported for different filling ratios and input heat loads. The results of this work can be used for optimization of the groove size and maximum heat transport limits of flat heat pipes with rectangular grooves.

Chapter 2

Experimentation and Simulation

In the present work, three sets of flat grooved heat pipes are fabricated and the heat removal performance of each heat pipe is experimentally investigated. The details about the working fluids, the geometry of the heat pipes and their fabrication steps, along with the experimental setup and procedure, and operating conditions are introduced in this chapter. In this document, "metal base" refers to a metallic piece on which the grooves are fabricated.

In all of the heat pipes, rectangular grooves are used as the wick structure which drive the liquid flow with capillary action. For first and second generation heat pipes, aluminum is selected as the base material due to its desirable properties, namely low cost, high thermal conductivity, light weight, and ease of machining compared to copper. One key parameter for the thermal characterization of a heat pipe is the groove density, which is defined as the number of grooves per unit width. To study the effect of this parameter on the performance of the heat pipes, each set has heat pipes with different groove densities, enabling comparing their performance.

Table 2.1: Physical and thermal properties of water and IPA [59]

Property	**Water**	**IPA**	**Unit**
Density (25 °C)	997.05	780.9	kg/m^3
Thermal conductivity (25 °C)	0.606	0.135	$W/m \cdot K$
Surface tension (25 °C)	71.99	20.93	mN/m
Viscosity (25 °C)	0.890	2.038	$mPa \cdot s$
Boiling point	99.97	82.3	$^\circ C$
Heat of vaporization (at boiling point and 760mmHg)	2258.33	663.06	kJ/kg
Heat of vaporization (at 25 °C and 760mmHg)	2443.33	755.24	kJ/kg

2.1 Working Fluids

Although water has superior thermophysical properties, namely high latent heat of vaporization and surface tension, which makes it the first candidate in intermediate temperatures compared to common fluids, it is not compatible with aluminum surface. Hence, IPA is chosen as the working fluid for aluminum heat pipes in this study. For silicon heat pipes, however, both water and IPA are charged to the heat pipe and their performance compared. Table 2.1 shows some physical and thermal properties of water and IPA.

2.2 First Generation Prototype Aluminum Heat Pipes

Three flat grooved heat pipes with different groove specifications are fabricated. The length of the grooves for all the heat pipes is 75 mm. Table 2.2 shows the groove specifications of the fabricated heat pipes.

Table 2.2: Groove specifications of the first generation prototype aluminum heat pipes

	# of grooves	Groove width W [mm]	Groove height H [mm]	Fin* width F [mm]	Groove density # of grooves/mm width
G1-200	50	0.2	0.2	0.2	2.50
G1-400	25	0.4	0.4	0.4	1.25
G1-1500	7	1.5	2.0	1.5	0.33

* The area between two adjacent grooves is called fin.

2.2.1 Fabrication of the Metal Base

The metal base is a 5 mm-thick piece of aluminum on which the grooves are machined. The fabrication of the metal base starts with the fabrication of the two rectangular o-ring grooves followed by the fabrication of a rectangular recess (78 mm × 23 mm) which is 2.0 mm below the top surface using conventional CNC-machining. This rectangular recess is the base for the fabrication of the grooves and acts as a space for vapor flow. At the bottom side of the metal base, small rectangular holes with a depth of 0.4 mm are machined to attach the thermocouples to the desired locations. The location of these holes are shown in Figure 2.1. The flat grooves are fabricated by a 3-axis micro-machining center (PROINO Z3X Micro Maker) with $\pm 5\mu$m accuracy. The fabrication of flat grooves consists of three major steps. Initially, the top surface of the rectangular recess is machined (with a 1.2 mm cutting tool, feed rate of 2.5 mm/min and rotational speed of 25,000 rpm) to enable the precise control of the depth of the grooves. Next, a fine machining is performed with the following machining parameters:

- **G1-200:** 0.2 mm tool, 1.0 mm/min feed rate, 30,000 rpm rotational speed
- **G1-400:** 0.4 mm tool, 1.0 mm/min feed rate, 30,000 rpm rotational speed
- **G1-1500:** 1.2 mm tool, 2.5 mm/min feed rate, 25,000 rpm rotational speed

In the final step, a soft surface polishing is applied on the entire piece to remove the machining burr at the edge of the grooves. Following the fabrication,

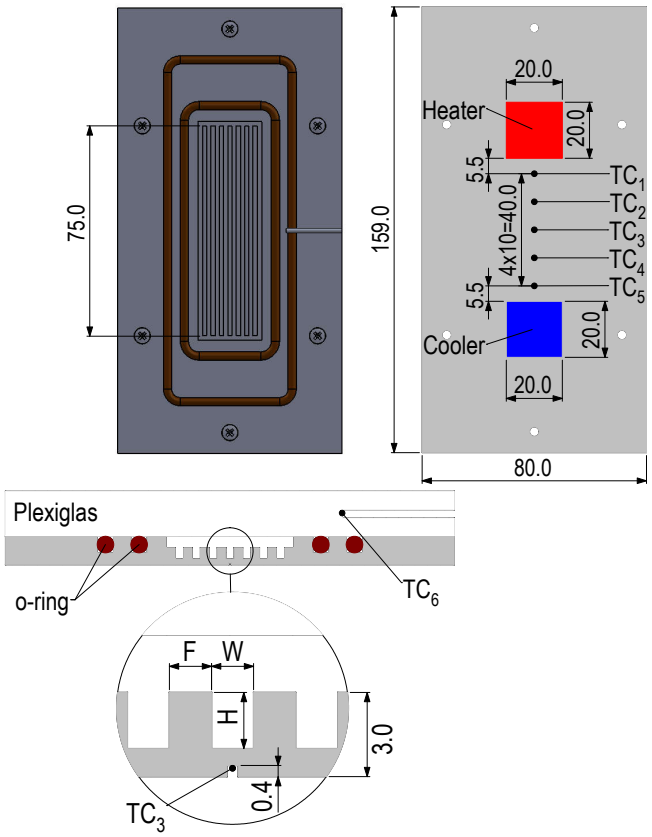

Figure 2.1: Top, bottom, and mid cross-sectional views of G1-1500, and the location of the thermocouples

the sample is ultrasonically cleaned to ensure the removal of any residual debris remaining in the grooves. Finally, the sample is washed by soap and isopropyl alcohol, rinsed with DI water, and blow-dried. Five T-type thermocouples (with an uncertainty of $\pm 0.2\,^{\circ}\mathrm{C}$) are embedded into the metal base at the centerline for temperature measurements. An additional thermocouple is placed at the midpoint of the top plexiglas cover. The locations of the thermocouples together with the thermoelectric heating/cooling units are illustrated in Figure 2.1.

The fabricated pieces together with the groove profiles are shown in Figure 2.2. The groove profiles are also investigated with a 3D Laser Scanning Confocal Microscope (VK-X100, KEYENCE Corporation). The surface roughness of the bottom surface of the grooves and the fin top surfaces are measured using the microscope at different locations. The average surface roughness of the bottom

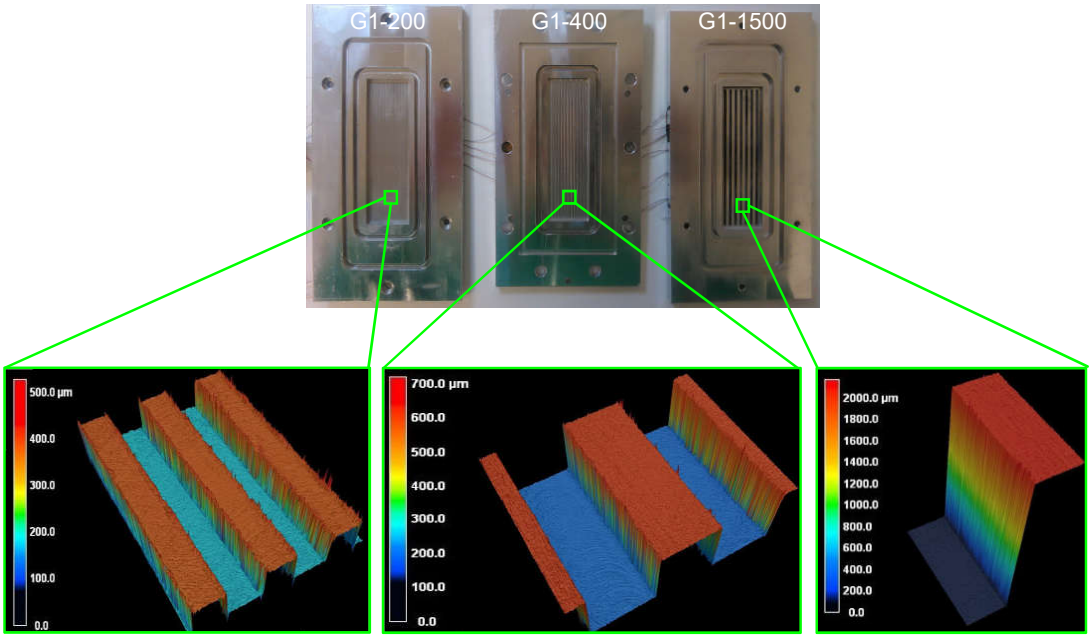

Figure 2.2: Fabricated metal pieces and the groove profiles of the first generation prototype aluminum heat pipes

surface is found to be 3.2 μm, 2.3 μm, and 2.8 μm for G1-200, G1-400, and G1-1500, respectively. The surface roughness of the fin top surfaces are obtained as 2.9 μm, 3.1 μm, and 3.5 μm for the same samples, respectively. It is evident from the measurements that there is no significant variation on the machining quality of the pieces which eliminates surface roughness effect on the comparison between the different groove widths.

2.2.2 Heat Pipe Assembly

Figure 2.3 shows the disassembled components of the heat pipes assembly which consists of an acrylic (plexiglas) top cover, two o-rings, a metal base, thermo-electric heating and cooling units, a fan integrated heat spreader and the acrylic holder. The top cover is made of a transparent material to enable the visualization of evaporation and condensation as well as recording the amount of the working fluid, and location and extent of probable dryout. The two o-rings suitable for vacuum applications are used for sealing. Six screws are placed to assemble the

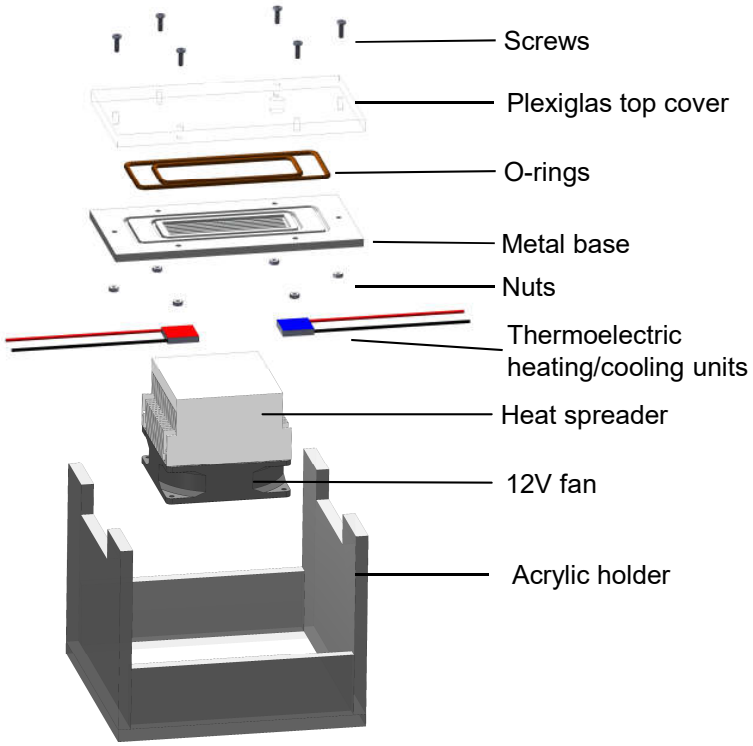

Figure 2.3: The disassembled components of the assembly of the first generation prototype aluminum heat pipes

plexiglas top cover and the metal base as well as fixing the position of the metal base on the micro-machining center. Thermoelectric cooling and heating units are in contact with the metal base on the bottom surface. In order to cool the bottom hot surface of the cooling unit, a heat spreader integrated with a 12V fan is used. The metal base sits on the acrylic holder, which carries the heat pipe and heat spreader.

2.2.2.1 Heating and Cooling Units

Thermoelectric devices capable of converting electricity into thermal energy or vice versa, are a convenient solution for local heating/cooling applications. The thermoelectric modules used in this study are of type TEC1-03106T125 with dimensions of $2\,\text{cm} \times 2\,\text{cm} \times 4\,\text{mm}$. The module whose hot/cold side is in contact with the heat pipe acts as the heat source/sink. Thermal paste is applied on

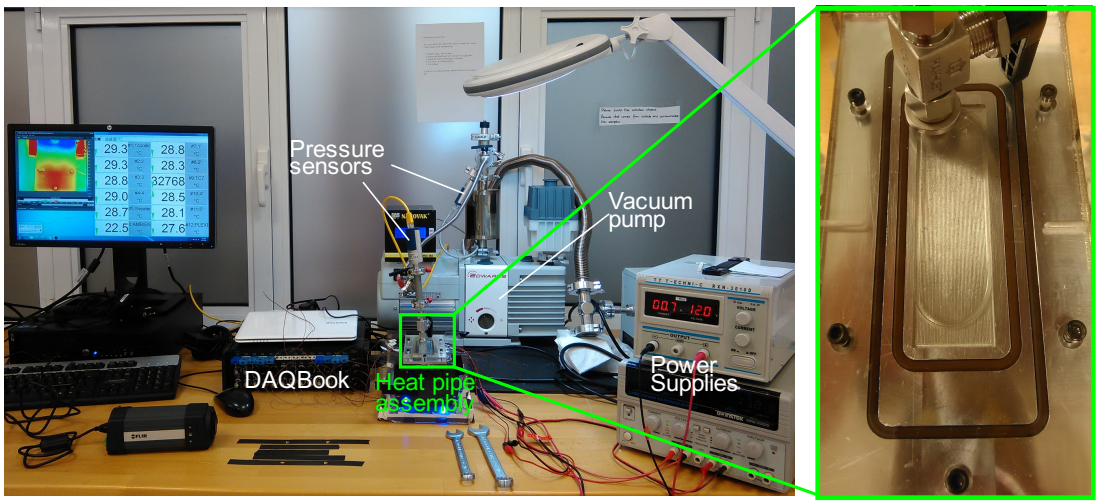

Figure 2.4: Experimental setup and close-up view of test section of the first generation prototype aluminum heat pipes

contact surfaces of the modules to reduce thermal contact resistance. The heat source and heat sink positions are such that they are placed exactly under the grooves array, as shown in Figure 2.1. It should be noted that the input current to both heat source and heat sink is kept constant during all experiments for all samples. Therefore, the heat input and output of all of heat pipes during all experiments are intended to be equal.

2.2.3 Experimental Setup

The experimental setup is built by integrating the vacuum unit, pressure sensors, thermocouples, data acquisition system, and other auxiliary units such as power supplies and a computer to the heat pipe assembly. One two-channel power supply is used to run the thermoelectric units, another power supply is used to drive the fan. The vacuum level of the system is monitored through the pressure sensors. The photograph of the experimental setup is given in Figure 2.4. In order to ensure the removal of all of the air from the system, all the components (valves, connectors etc.) used are gas tight. The working fluid is also degassed for at least 15 minutes prior to charging the heat pipes for the removal of any possibly dissolved air. Figure 2.5 depicts the vacuuming station for the heat

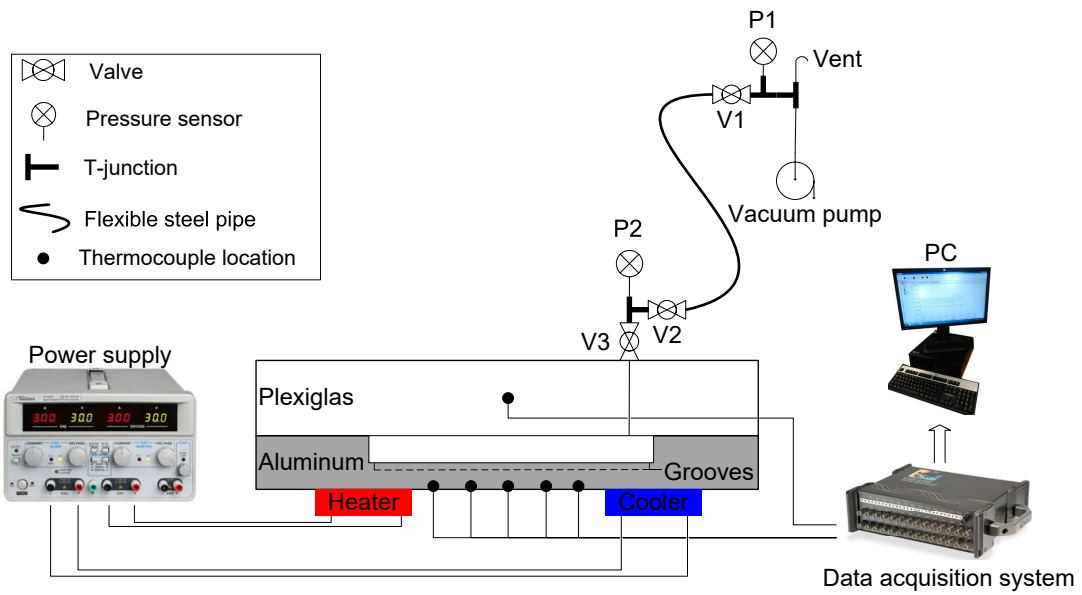

Figure 2.5: Vacuuming station for the first generation prototype aluminum heat pipes (Not to scale.)

pipes. The connection of the heat pipes to the vacuum pump is made by using some ball valves, a T-junction, and flexible pipes. To be assured of removal of any air inside the connections, pressure is monitored in two different locations, one close to the vacuum pump and the other right after the heat pipe.

2.2.4 Experimental Method

The input powers given to the thermoelectric units are recorded during the experiments. In order to minimize the heat transferred to the ambient, the power inputs to the thermoelectric units are adjusted in such a way that the temperature measured at the midpoint of the plexiglas top cover is equal to the ambient temperature.

Each experiment is completed in a single run during which the amount of working fluid is changed from fully-flooded to dry heat pipe. Figure 2.6 shows one sample run of heat pipe G1-200. The duration of each test is 2–3 hours. Initially, all grooves and volumes are fully-flooded with IPA, and the heating

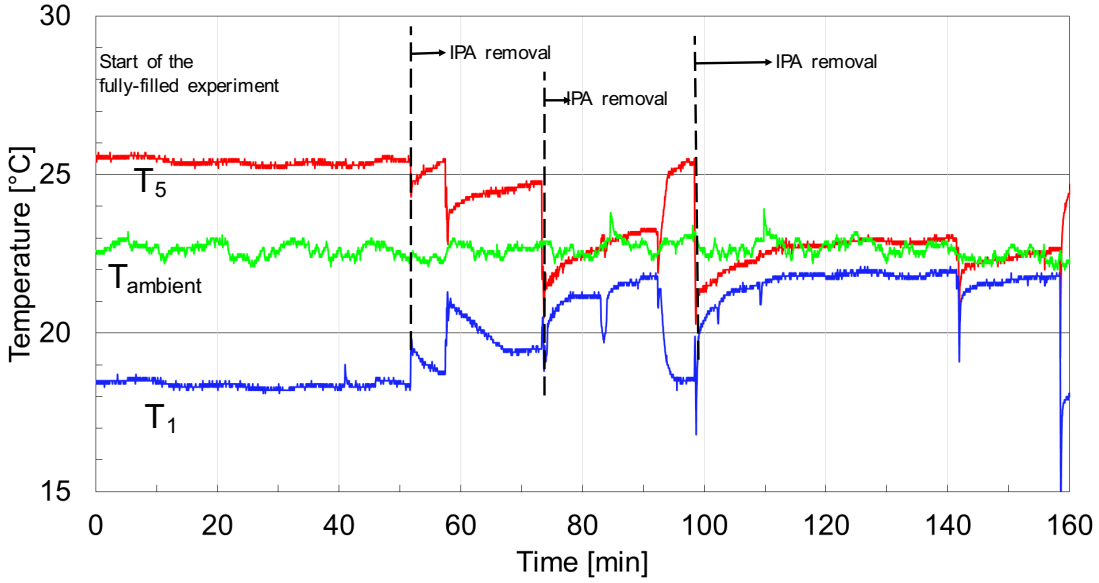

Figure 2.6: Transient temperature variation of heat pipe G1-200

and cooling units are operating. Every sudden change in Figure 2.6 corresponds to removal of IPA with the vacuum pump, to which the system responds with changing temperatures. Once steady operation is reached, more IPA is removed, moving to another operating point. After each IPA removal, the IPA is collected on the condenser side of the heat pipe by tilting, and the extent of the liquid IPA in the grooves is measured under the effect of gravity. Although a vertical orientation is preferred for a more accurate measurement of the liquid extent, it was not possible to tilt the heat pipes by 90 ° because of the heavy weight of the heat pipe assembly. Hence, the measurements performed while the heat pipes are tilted approximately 65 °, as shown in Figure 2.7. This procedure is repeated until all IPA is removed and the unit transfers heat only by conduction in aluminum. After completion of the run, the optimum operating point is found, the point which corresponds to the minimum temperature difference between the heater and the cooler. Strictly speaking, this optimum is not a proper optimum operating point, since IPA removal is performed in discrete steps, which are course, thus rendering the possibility that the true optimum point may be missed between two consecutive steps. Nevertheless, the results are judged to be sufficiently close and further improvements are planned for future studies.

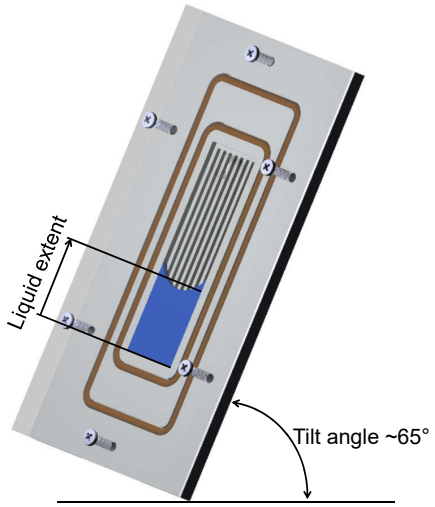

Figure 2.7: Orientation of first generation prototype aluminum heat pipes during the measurements of the liquid extent

2.2.5 Simulation Method

During the experiments, the thermoelectric cooling unit is operated at around its maximum power approximately 6 W, and the power of the heating unit is adjusted to keep the temperature at the midpoint of the top plexiglas cover around ambient. Although the input powers are recorded, the heat addition and removal through the evaporator and condenser sections require the value of the coefficient of performance (COP) of thermoelectric units, which typically is a function of many parameters such as applied current, temperature of the hot and cold surfaces, and temperature difference between the hot and cold sides. Moreover, COP data also shows a variation depending on the manufacturer. A reliable COP data for the thermoelectric units used in this study, however, is not available. Therefore, a simple computational model based on heat conduction alone ($k_{Al} = 140\,\mathrm{W/m \cdot K}$, $k_{IPA} = 0.14\,\mathrm{W/m \cdot K}$, and $k_{plexiglas} = 0.18\,\mathrm{W/m \cdot K}$) is developed using a finite element based commercial software, COMSOL Multiphysics, to quantify the heat input in the experiments. To reduce the computational time, one half of each heat pipe is simulated due to symmetry. Insulated boundary conditions are applied on the side and bottom surfaces, and natural convection is assumed at the top surface with convective heat transfer coefficient of $h = 5\,\mathrm{W/m^2 \cdot K}$. Constant temperature values are assigned on the surfaces

Table 2.3: Groove specifications of the second generation aluminum heat pipes

	# of grooves	Groove width W [mm]	Groove depth H [mm]	Fin width F [mm]	Groove density # of grooves per mm
G2-200	50	0.2	0.2	0.2	2.50
G2-400	26	0.4	0.4	0.4	1.25
G2-800	13	0.8	0.8	0.8	0.63
G2-1600	7	1.6	1.6	1.6	0.31

where the thermoelectric units are located. The model is used to study the two extreme cases of working fluid amount; fully-flooded and dry, and exercised to match the experimentally recorded plexiglas and aluminum temperatures at a total of 6 points.

2.3 Second Generation Aluminum Heat Pipes

Four flat grooved heat pipes with different groove specifications are fabricated. The length of the grooves for all the heat pipes is 100 mm. Table 2.3 shows the groove specifications of the fabricated heat pipes.

2.3.1 Fabrication of the Metal Base

The metal base is a 5 mm-thick piece of aluminum on which the grooves are machined. The first step in its fabrication process is the machining of a groove for an o-ring. Next, a recess of depth 2.5 mm is machined on it to place the vacuum valve 23.2 mm off the grooves end, in order not to block the view of their entire length. At the bottom side of the metal base, then, two rectangles with dimensions of 28.0 mm $\times$ 14.0 mm and 20.0 mm $\times$ 20.0 mm are machined 1 mm deep for placement of the heater and the cooler, respectively. On the center line in between, five rectangular holes of depth 0.4 mm with spacing of 10.0 mm

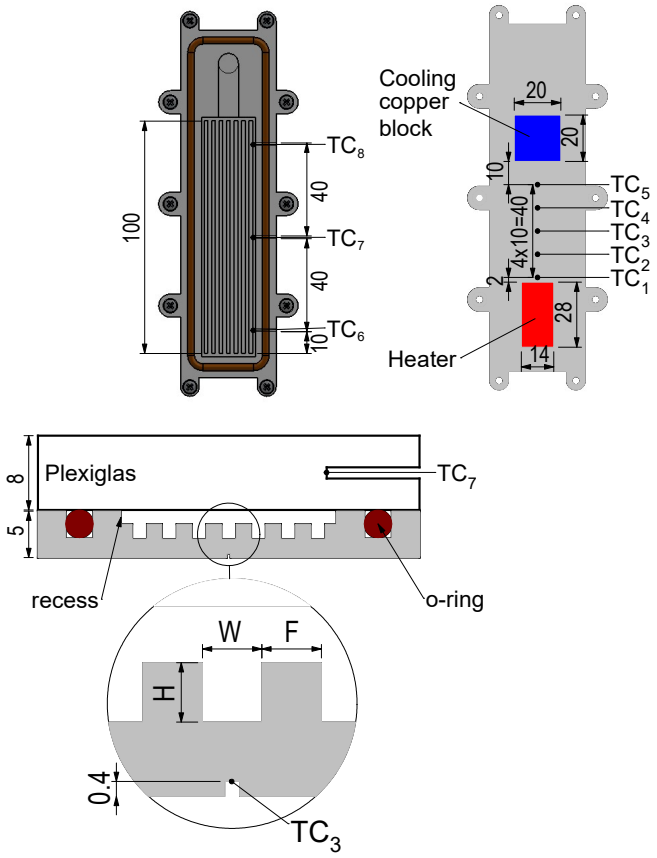

Figure 2.8: Top, bottom and mid cross-sectional views of G2-1600 (all units are in mm)

are machined to attach thermocouples. Lastly, the fabrication of the grooves are performed by a 3-axis micro-machining center (PROINO Z3X Micro Maker) with an accuracy of $\pm 5\,\mu$m. The machining process has two major steps: (i) machining a rectangular recess with area of 103.0 mm $\times$ 23.2 mm performed by a 1.2 mm cutting tool, feed rate of 2.5 mm/min and rotational speed of 25,000 rpm, and (ii) machining of the grooves on the surface of the rectangular recess with the following machining parameters:

- **G2-200:** 0.2 mm tool, 1.0 mm/min feed rate, 30,000 rpm rotational speed
- **G2-400:** 0.4 mm tool, 1.0 mm/min feed rate, 30,000 rpm rotational speed
- **G2-800:** 0.8 mm tool, 2.5 mm/min feed rate, 25,000 rpm rotational speed
- **G2-1600:** 1.2 mm tool, 2.5 mm/min feed rate, 25,000 rpm rotational speed

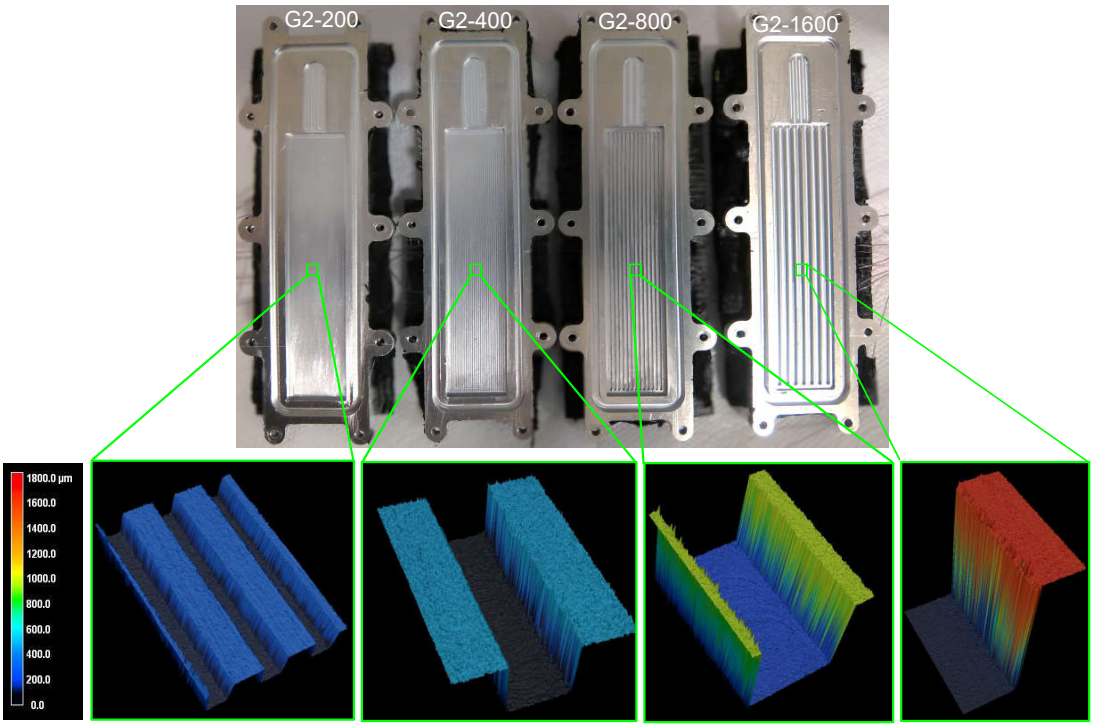

Figure 2.9: Fabricated metal pieces and the groove profiles of the second generation aluminum heat pipes

The rectangular recess creates a space available for the vapor flow during the experiments. The depth of the recess is 2.5 mm for all cases except G2-1600 which is 1.4 mm. These dimensions results in a distance of 0.9 mm, 0.7 mm, 0.3 mm, and 0.6 mm between the thermocouples and bottom of the grooves, respectively for the heat pipes G2-200 through G2-1600. Following the machining, the metal pieces are soft polished and ultrasonically cleaned to remove machining burr at all edges. Prior to the assembly, all metal pieces are washed by soap and isopropyl alcohol, rinsed with DI water, and blow-dried. The detailed dimensions of the metal bases and locations of the o-ring, heater, cooler and thermocouples are shown in Figure 2.8. The top, bottom and mid cross-sectional views of heat pipe G2-1600 can be seen in the figure as an example. Except the groove dimensions specified in Table 2.3, all other dimensions are the same for other heat pipes.

The fabricated pieces together with the grooves profile are shown in Figure 2.9. The grooves profiles are also investigated with a 3D Laser Scanning Confocal Microscope (VK-X100, KEYENCE Corp.). Moreover, the surface roughness of

Table 2.4: Average surface roughness of bottom of the grooves and the fins surface of the second generation aluminum heat pipes

	Bottom surface of the grooves [μm]	**Surface of the fins** [μm]
G2-200	3.66	4.99
G2-400	4.57	6.67
G2-800	5.44	7.34
G2-1600	3.63	5.00

the bottom surface of the grooves and the top surface of the fins are measured using the microscope at five different locations and the average values are reported in Table 2.4. According to the measurements, no significant variation is observed on the machining quality of the pieces. Hence, the effect of surface roughness on the comparison between the heat pipes is eliminated.

2.3.2 Heat Pipe Assembly

The heat pipe assembly consists of layers of a metal base, an o-ring and a transparent plexiglas cover screwed together as seen in Figure 2.10. The o-ring is of Viton type of durometer A75, specified for high vacuum purposes. The top cover is fabricated out of plexiglas to visualize the evaporation and condensation inside the heat pipe, and to enable the measurement of the amount of the working fluid inside the heat pipe, as well as the location and extent of a probable dryout.

2.3.2.1 Heating, Cooling and Temperature Reading

The heater used in the experiments is an electric resistance heater (ARCOL HS25 2R F) with peak power of 25 W. Considering its surface area in touch with the bottom of the heat pipe, it is capable of introducing heat fluxes up to approximately 6 W/cm^2 to the heat pipes. The current passes the heater is measured with a power supply and the voltage is measured with a voltmeter at

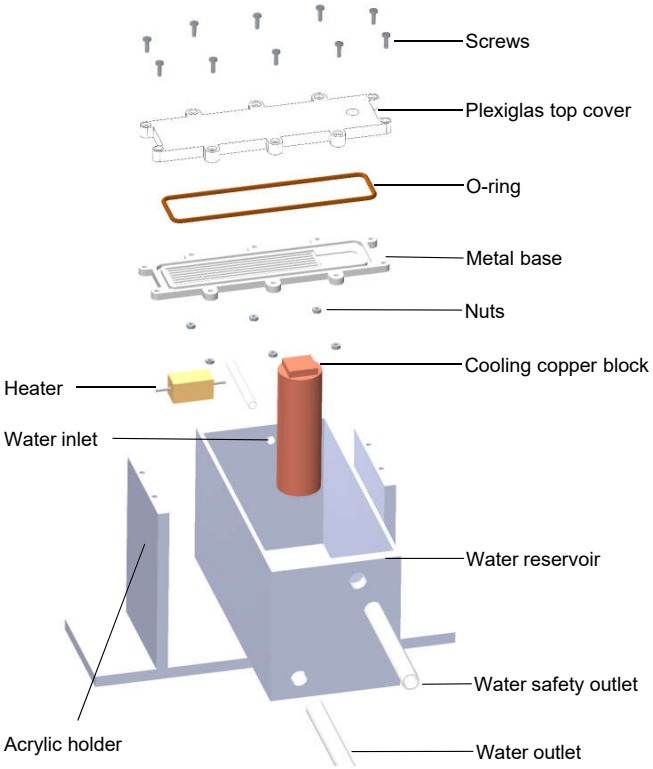

Figure 2.10: The disassembled components of the assembly of the second generation aluminum heat pipes

two sides of the heater. To cool down the heat pipes, a cylindrical copper block of height 100 mm with top surface of square cross-section of 20 mm × 20 mm is in touch with the bottom of the aluminum base. The copper block is submerged 90 mm in a water reservoir with continuous flow of cold tap water. The water flow rate for all of the experiments is around 1.6 to 1.8 L/min. It is worth mentioning that to avoid thermal contact resistance in the contact areas of the heat pipes with the heater and the cooler, silicon thermal paste is applied all over the contact surfaces. For temperature reading purposes, five T-type thermocouples (with an uncertainty of $\pm 0.1\,^{\circ}\mathrm{C}$) are embedded into the metal base at desired locations between the heater and cooler. Three thermocouples, additionally, are placed at the half thickness of the plexiglas cover. The locations of all the thermocouples together with the heater and cooler are illustrated in Figure 2.8.

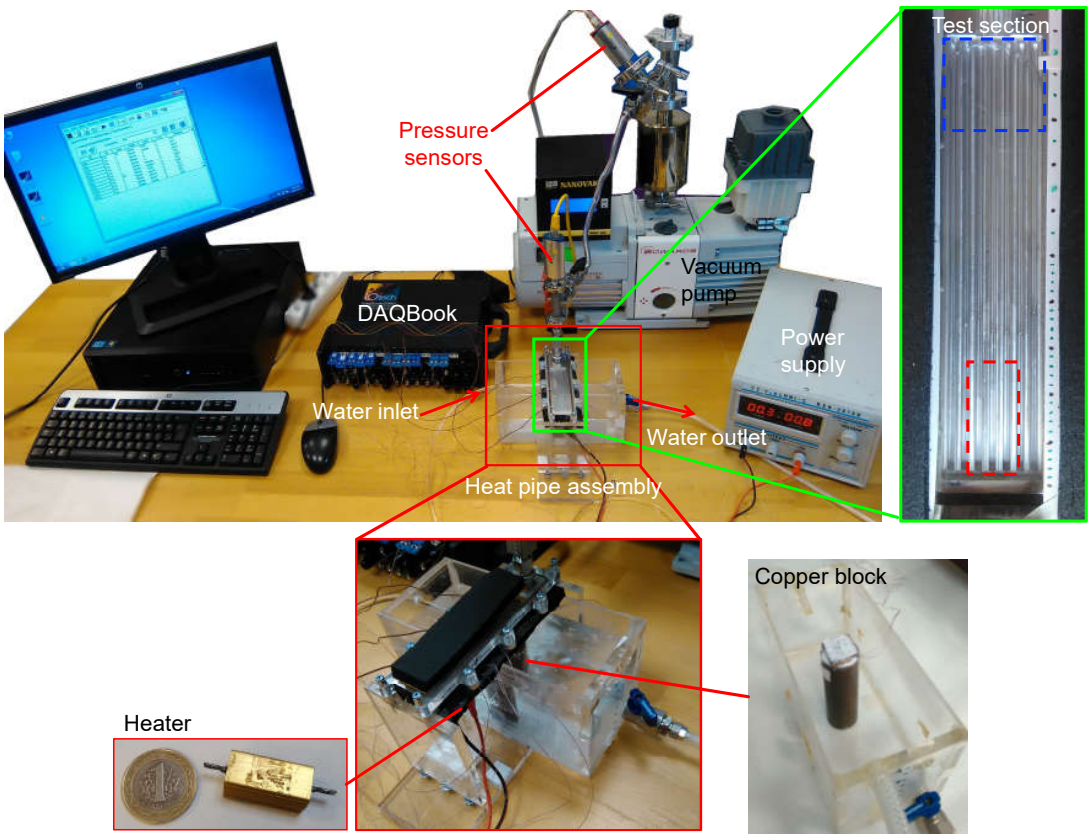

Figure 2.11: Experimental setup table of the second generation aluminum heat pipes

2.3.3 Experimental Setup

In order to eliminate the environmental effects on the performance of the heat pipes, all exterior surfaces of the metal base and the plexiglas cover are insulated. However, the insulation of the top surface of the plexiglas is removed temporarily to visually observe the evaporation and condensation inside the heat pipes, measure the amount of IPA and locate the extent of a probable dryout. In order to keep the heat pipes at a fixed horizontal orientation during the experiments, it is screwed to an acrylic holder. Figure 2.11 shows the assembled components on the setup bench. The heat pipes are intended to operate using the vapor and liquid phases of a pure substance at equilibrium. The presence of even minute quantities of any other fluid adversely affects their thermal performance; therefore, the removal of air from the entire cavity of the heat pipes before admitting

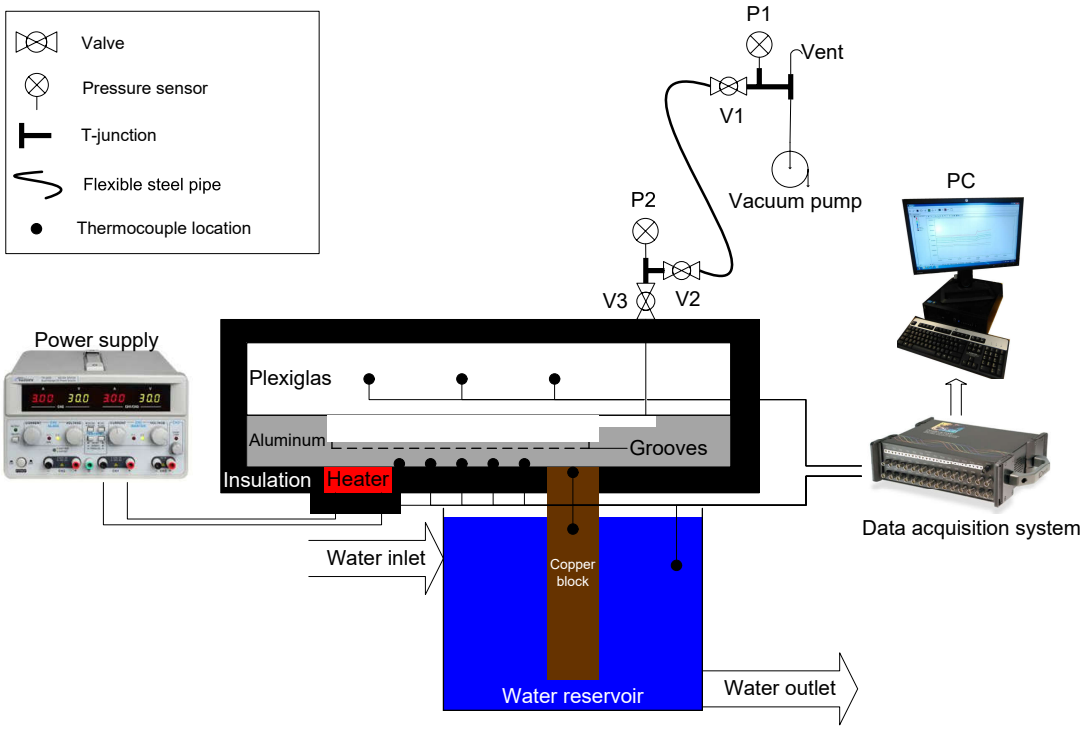

Figure 2.12: Vacuuming station for the second generation aluminum heat pipes (Not to scale.)

the working fluid is crucial. In addition, any air dissolved in the liquid IPA must also be eliminated. To achieve this, IPA is degassed for 15 minutes under 0.2 bar vacuum prior to charging in the heat pipes. Figure 2.12 shows the components used in the vacuuming process of the heat pipes. All the valves and connections used in this work are gas tight to ensure no air penetration to the heat pipe.

2.3.4 Experimental Method

The experimental procedure is as follows:

1. All space in the heat pipes is filled with IPA (the so called "fully-flooded" operating condition that corresponds to the highest values of filling ratio which will be discussed later in chapter 3 for each heat pipe).

2. Four different heating conditions corresponding to heat fluxes 2.1, 3.2, 4.2,

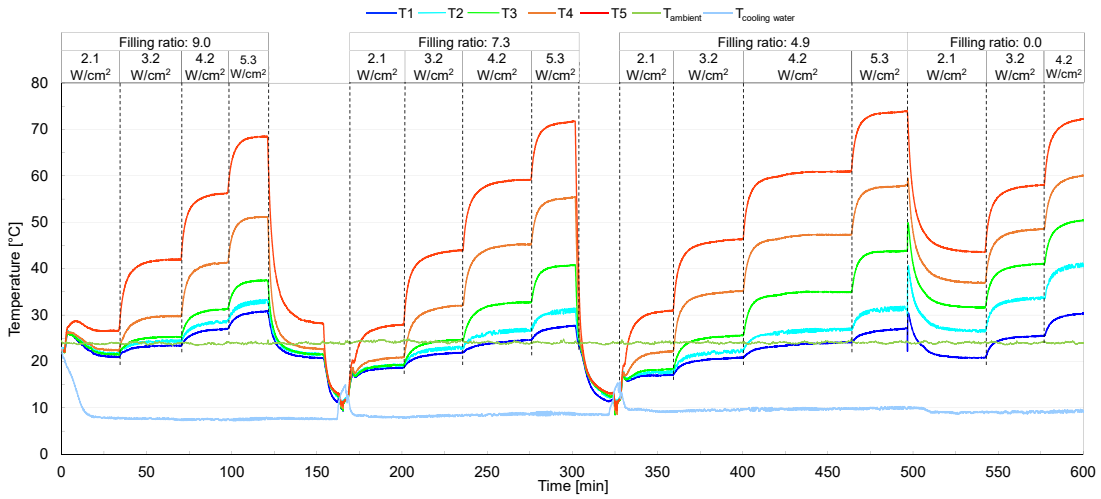

Figure 2.13: Transient temperature variation of heat pipe G2-200

and 5.3 W/cm^2 are applied to the heat pipes and transient temperatures are recorded until steady-state is reached.

3. The heater is turned off and the cooling water reservoir is drained. When the system reaches thermal equilibrium with the environment the heat pipes are tilted to a vertical orientation, some IPA is extracted from the heat pipe (with help of the valves shown in Figure 2.12) for the new operating point, and the new IPA extent is measured. Before each IPA removal, the pressure inside the cavity is less than 7.5×10^{-2} Torr assuring that no air is present in the the connections or pipes. All pipes and connections beyond V3 in Figure 2.12, are subject to vacuum conditions.

4. The procedure is repeated starting from step 2 until the heat pipes are entirely drained of IPA (the so called "dry" operating condition that corresponds to the filling ratio of zero which will be discussed later in chapter 3 for each heat pipe).

Figure 2.13 shows the transient and steady-state temperature readings of thermocouples for different filling ratios and heat inputs for a sample run of heat pipe G2-200. The duration of the test depends on the number of filling ratios realized and it differs for the heat pipes. On the average, each experiment takes two days to complete in two 10–12 hour sessions. There is a limitation in the range of

experiments due to failure. In some filling ratios—especially fully-flooded and dry operating conditions and higher heat inputs—temperatures peak and exceed 60°C. In such a case, the plexiglas is damaged and cracking or surface burning occurs. In order to avoid this incident, only a safe operating zone is exercised, where peak plexiglas temperatures are not allowed to go beyond the failure limit. This reflects itself in the results, where the corresponding data points are absent.

2.3.5 Simulation Method

To assess the thermal performance of G2-800 heat pipe, a 3-D computational model is developed in "`Heat Transfer in Solids`" module of COMSOL Multiphysics, where it solves the stationary heat conduction equation, $\nabla \cdot (k_i \nabla T_i) = 0$ inside the domains, in which k_i represents the thermal conductivity of metal base, IPA, and plexiglas cover. The model is then verified by the experimental results.

2.3.5.1 Computational Model

The modeling starts with a simplified CAD model of the heat pipe, including metal base and plexiglas cover. In addition, to reduce the computational time and because of the symmetry of the heat pipe and boundary conditions, the simulations are performed for half width of the heat pipe only. Figure 2.14 depicts the computational domain used in the simulations. The length and width of both metal base and plexiglas cover in the CAD model are 11.8 cm and 2 cm; and their thickness are 5 mm and 8 mm, respectively.

For heat input and heat output of the heat pipe, boundary condition of "`Overall heat transfer rate`" is assigned to two rectangles placed on the bottom surface of the metal base. The heater and cooler areas are 27 mm × 7 mm and 20 mm × 10 mm, respectively; and their locations on the bottom side of the metal base are shown in Figure 2.8. The simulations are run for four equal input and output heat fluxes of 2.1, 3.2, 4.2 and 5.3 W/cm^2. Since the boundary condition of heater and cooler is "`Overall heat transfer rate`", there will be

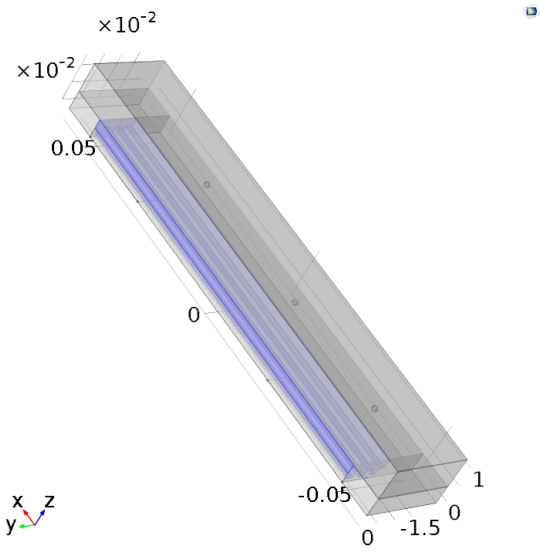

Figure 2.14: Computational domain of heat pipe G2-800 (all units are in m).

infinitely many solutions to the problem. To find the solution of interest, temperatures at three locations in the plexiglas cover measured during the experiments (TC_6, TC_7, and TC_8 in Figure 2.8) are assigned to their corresponding locations in the CAD model to be the reference temperatures of the system. Moreover, since all outer boundaries of the heat pipe are insulated in the experiments, their boundary condition correspond to "`Thermal Insulation`" in the model. The heat transfer between the vapor of the working fluid and the bottom surface of the plexiglas cover, and between the vapor of the working fluid and the side walls of the recess on the metal base is estimated by obtaining the convective heat transfer coefficients through the appropriate Nu correlation which was studied in detail in [3].

Phase change heat transfer, the dominant physical mechanism of the heat pipes, is implemented in the model by defining equivalent convective heat transfer coefficients for evaporator and condenser sections that match the phase change, the values which are obtained from a comprehensive numerical study on a unit cellin which the 3-D heat transfer in the solid and working fluid are coupled with a 1-D analysis of the momentum equation [16] . They were further curve-fitted in [3] and extrapolated for the current geometry. Figure 2.15 shows the variation of effective phase change heat transfer coefficients of the evaporator and condenser

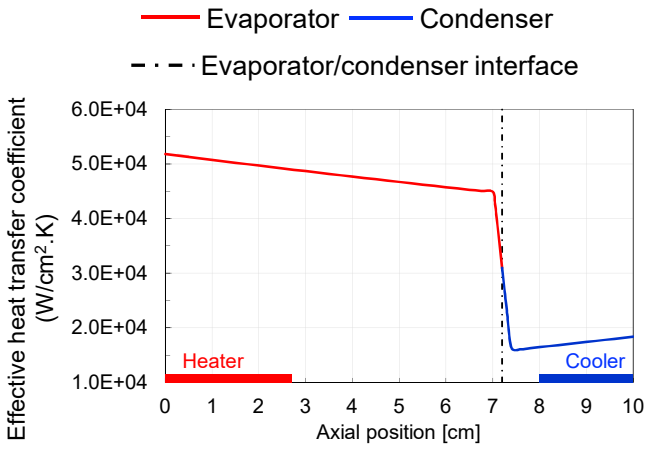

Figure 2.15: Phase change heat transfer coefficients of the evaporator and condenser sections of heat pipe G2-800

sections, as well as their interface, and heater and cooler locations. The effective heat transfer coefficients in the evaporator is assigned to the top 33 μm height of the groove walls as a convective heat transfer boundary condition, considering the fact that most of the evaporation of the working fluid occurs in the thin film region at the contact line. Those of the condenser, are assigned at the surfaces of the fins, knowing that the condensation of working fluid generally takes place at the top of the grooves. Moreover, the external temperature of the convective heat transfer boundary conditions is set to T_{vapor} all along the grooves. It is worth mentioning that the evaporator/condenser transition location is not set *a priori*, rather it is the axial position at which the vapor temperature, T_{vapor}, is equal to the wall temperature and its location is found in successive iterations. In the current case, the transition location is 7.2 cm away from the starting point of the evaporator section.

Furthermore, two operating conditions corresponding to cavities fully-flooded with IPA and dry are simulated. In the former, the CAD model consists of three domains of aluminum, working fluid, and plexiglas cover. The latter includes aluminum base and the plexiglas cover. In this case, all surfaces of the grooves are thermally insulated.

Table 2.5: Groove specifications of silicon heat pipes

	# of grooves	Groove width W [mm]	Groove depth H [mm]	Fin width F [mm]	Groove density # of grooves per mm
S-200	57	0.214	0.195	0.186	2.52
S-400	29	0.422	0.229	0.378	1.27

2.4 Silicon Heat Pipes

In this set, two heat pipes with different groove specifications are fabricated on silicon. Table 2.5 shows the groove specifications of silicon heat pipes. The grooves length is 82 mm for the both heat pipes. It is noteworthy that although the width of the grooves and fins were 0.2 and 0.4 mm in the photolithography mask, grooves width is a bit larger than those values, which is attributed to the shrinkage of the photoresist during hard bake. Figure 2.16 exhibits the fabricated silicon heat pipes and the 3-D grooves profile.

2.4.1 Fabrication of the Silicon Piece

Silicon wafers used in this study are single side poilshed of diameter 100 mm and thickness 1 mm. Fabrication of the silicon heat pipes include five major steps, as depicted in Figure 2.17. First step (Figure 2.17–(a)) is to etch the unpolished side of the silicon wafer by deep reactive ion etching (DRIE). In this regard, the desired geometry of the grooves must first be developed by a standard photolithography process. The details of the photolithography parameters can be found in [3]. The parameters of the DRIE recipe to etch the silicon are in Table 2.6. The second step is deposition of a 400 nm chromium layer on polished side of the wafer by metal sputtering (Figure 2.17–(b)). This step is subsequent to a photolithography process to pattern the geometry of the chromium electrodes on the wafer. It should be noted that to place the electrodes exactly under one end of the grooves array, a back-side alignment is performed in the photolithography process. Next, the silicon wafer is diced to the designed dimensions (Figure 2.17–(c)). Then, the

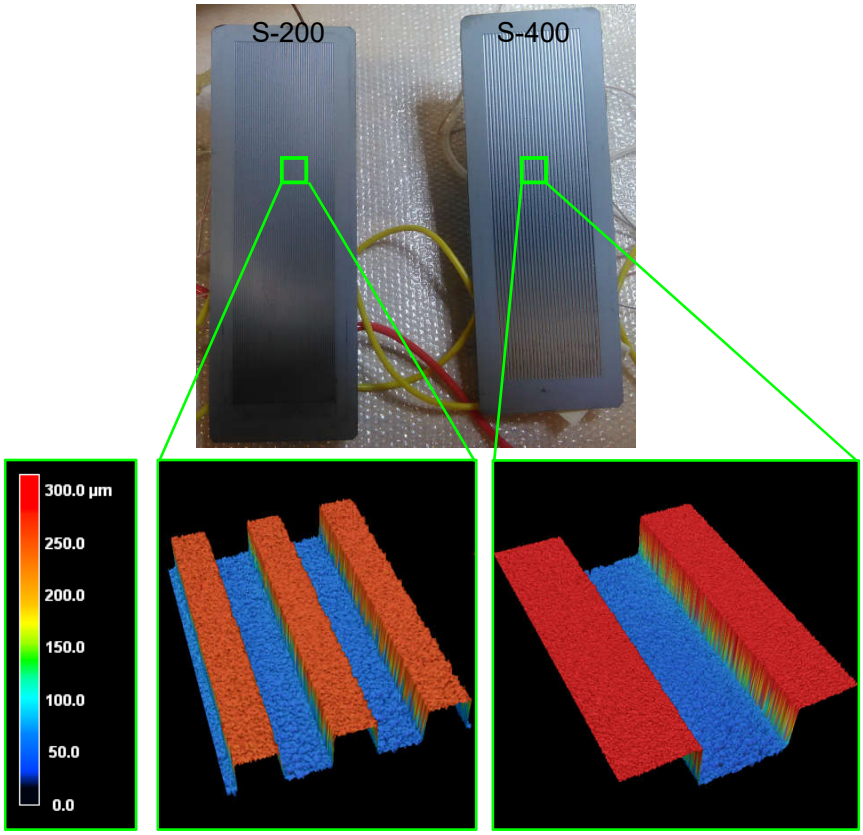

Figure 2.16: Fabricated silicon heat pipes and groove profiles

water cooling channels, embedded in a piece of PDMS, is bonded to the silicon piece by a standard plasma bonding technique (Figure 2.17–(d)). The last step is attaching wires to the electrodes with a conductive epoxy, the thermocouples to the silicon piece by an epoxy, the water inlet and outlet tubes to the PDMS and insert thermocouples in the tubes with epoxy. Figure 2.17–(e) shows the bottom view of a prepared silicon heat pipe. The exact location of the electrodes, cooling water channels, and thermocouples are shown in Figure 2.18.

2.4.2 Heat Pipe Assembly

Heat pipe assembly consists of a plexiglas frame screwed to a plexiglas top cover with an o-ring in between. The plexiglas frame has a window for the silicon piece to be put on and sealed with a smaller o-ring. The assembly, then, is screwed

Table 2.6: Parameters of the DRIE recipe to fabricate silicon heat pipes

	Deposition	**Etching**
Cycle time	7 s	10 s
Pressure	20 mTorr	35 mTorr
C_4F_8 flow	70 sccm	–
SF_6 flow	–	80 sccm
O_2 flow	–	5 sccm
13.56 MHz Coil Power	400 W	600 W
13.56 MHz Platen Power	–	25 W

Table 2.7: Average surface roughness of bottom of the grooves and the fins surface of silicon heat pipes

	Bottom surface of the grooves [μm]	**Surface of the fins** [μm]
S-200	5.78	3.79
S-400	5.93	3.77

to an acrylic holder to keep the heat pipes in a horizontal orientation during the experiments. Figure 2.19 shows the disassembled components of the silicon heat pipes. The electrodes are sputtered on the bottom side of the silicon, but they are shown detached in this figure for clarity.

2.4.2.1 Heating, Cooling, and Temperature Reading

Two chromium electrodes are sputtered on the bottom side of the silicon as the heat source of the silicon heat pipes. Their resistance is in the order of kΩ and by applying a voltage to their two ends, they can act as a resistance heater. The power is from the potential difference and current. The length of the adiabatic section (between the heat source and heat sink) is approximately 2 cm when

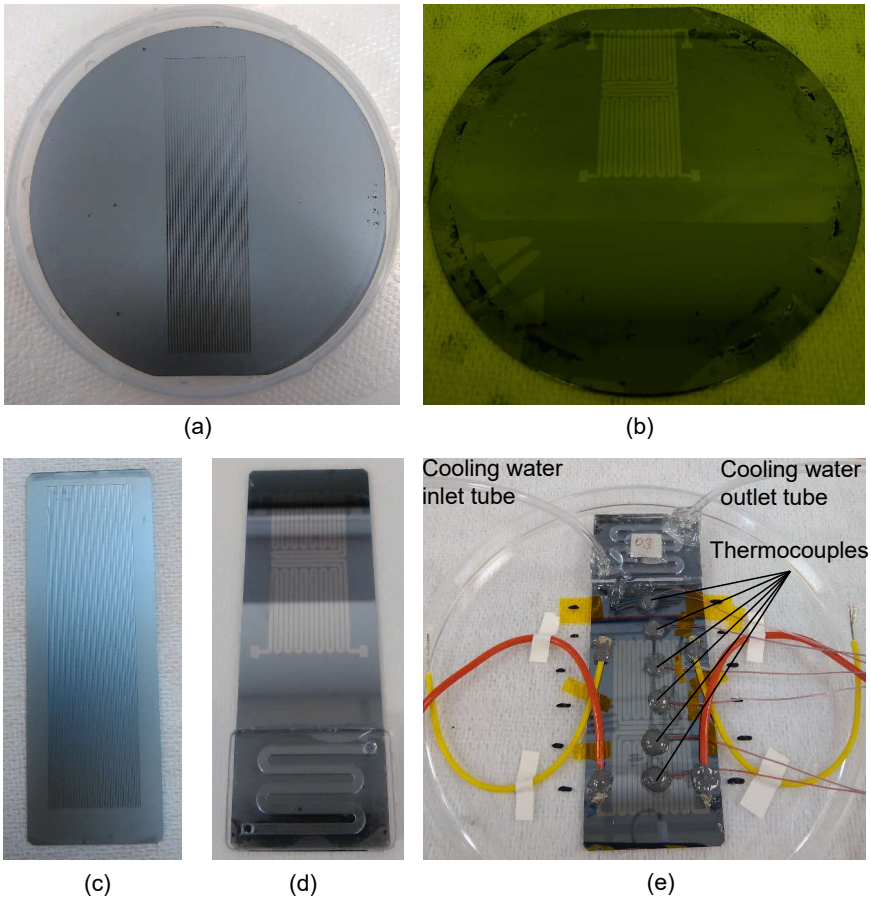

Figure 2.17: Fabrication steps of silicon heat pipes

both electrodes are operating, and about 4 cm when only one (outer) heater is in operation. In this study, only one heater is used during the experiments. To cool the heat pipes, cooling water flows in a series of channels in a PDMS piece, bonded to the silicon (Figure 2.17–(d)). Cooling water flows from an ice water reservoir (placed about 40 cm higher than the heat pipe, shown in Figure 2.20) and the outlet tube is put on the floor of the lab to increase the natural head. Since the distance between the water reservoir and the outlet is constant and the ice water bath is kept at a fixed temperature, the water flow rate is almost constant during all the experiments. The accumulated water is weighed with a scale over a short period of time and corresponding flow rate is calculated. The water temperature is measured by two thermocouples inserted inside the tubes before the PDMS piece. The silicon temperature is read by means of six thermocouples placed in 1 cm increments on the bottom surface of the silicon.

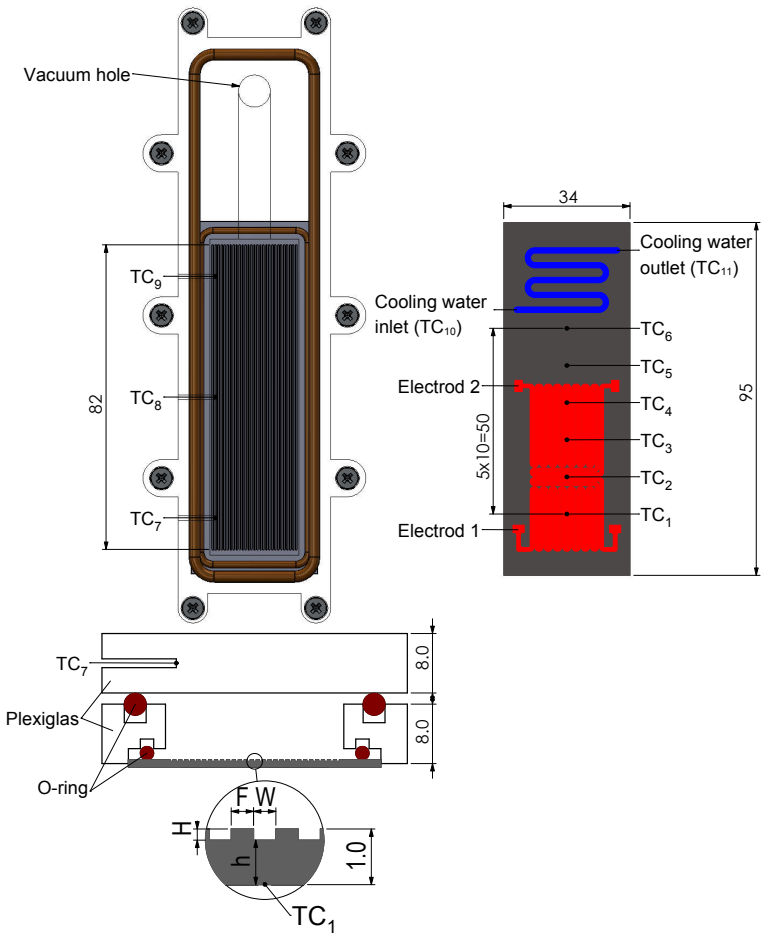

Figure 2.18: Top, bottom, and cross-sectional views of heat pipe S-400

Moreover, three thermocouples are placed inside the plexiglas top cover to record its temperature. All of the thermocouples are T-type.

2.4.3 Experimental Setup

Figure 2.20 illustrates the assembled components on the setup table in addition to other essential equipment, including a PC, data acquisition system, vacuum pump and its necessary connections and valves, two power supplies, ice water reservoir, and a cylindrical piston filled with the degassed working fluid. Figure 2.21 depicts the schematic of the evacuation and charging station of silicon heat pipes. After screwing the plexiglas top cover to the plexiglas frame and to the acrylic holder,

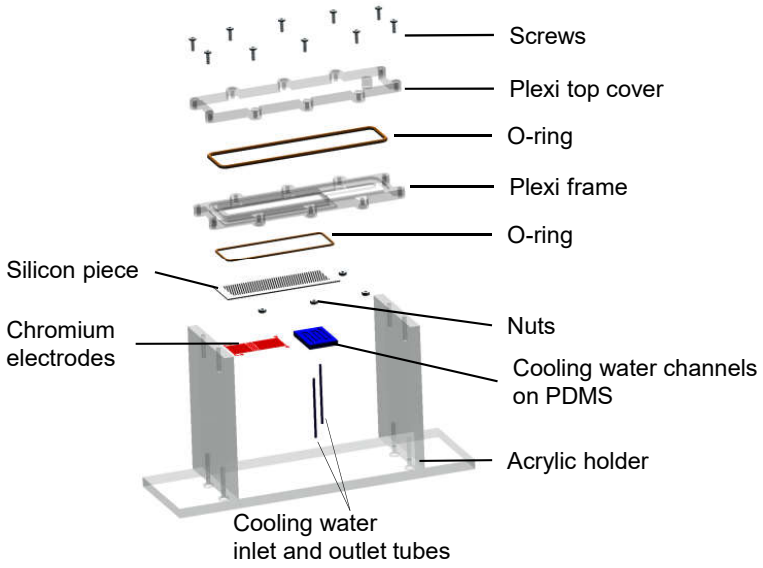

Figure 2.19: The disassembled components of the assembly of silicon heat pipes

the silicon piece must be put in place. To do so, all the valves shown in Figure 2.21 are opened and while the vacuum pump is turned on, the silicon piece is put in place. Once placed, it can be kept in position with the help of the vacuum inside.

2.4.4 Experimental Method

It should be noted that the experiments are performed on heat pipe S-200 only because of lack of enough time prior to publishing this document. The experimental method consists of the following steps:

1. The empty heat pipe is kept under vacuum for about 15 minutes to assure the removal of any non-condensable gas inside (V1, V2, V3: open; V4: closed).

2. The connection of the heat pipe to the vacuum pump is cut by closing V3 and the working fluid cylinder is connected to the vacuum pump, by opening V4, for a few seconds for final degassing step. Then, V4 is closed again so the vacuum pump removes the released working fluid in the connections.

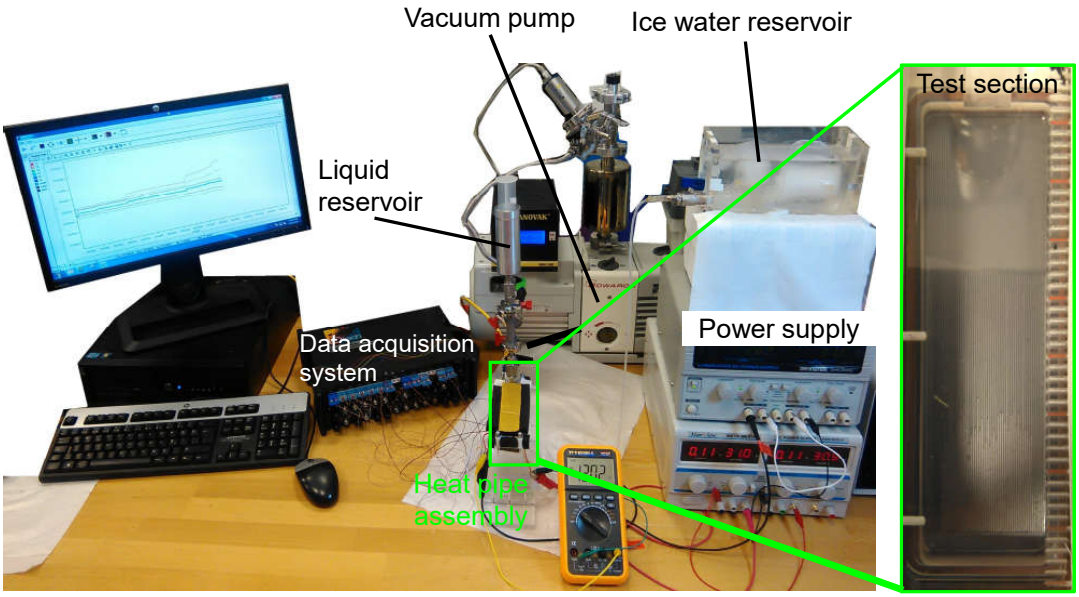

Figure 2.20: Experimental setup table of silicon heat pipes

3. Once the desired amount of vacuum is reached, V2 is closed and the heat pipe is connected to the working fluid reservoir by opening V3 and V4. This lets the working fluid fill the entire heat pipe (The so-called "fully-flooded" operating condition). Next, V3 is closed to isolate the heat pipe from other connections.

4. The valve of the water reservoir is opened to start the cooling water flow. Then, heat fluxes of 1.1, 2.0, 3.0, and 4.2 W/cm^2 are applied to the heat pipe and steady-state temperature readings are recorded.

5. The heater is turned off while the cooling water is let to flow for a few more minutes in order to condense all of the vapor inside the heat pipe. Next, it is tilted to a vertical orientation, V3 is opened slowly to pump out some of the working fluid and closed. The new extent of the working fluid is measured to calculate the filling ratio.

6. The experiment continues by going to step 3 until the heat pipe is empty of the working fluid, corresponding to dry operating condition.

Figure 2.22 shows the transient and steady-state operations of heat pipe S-200

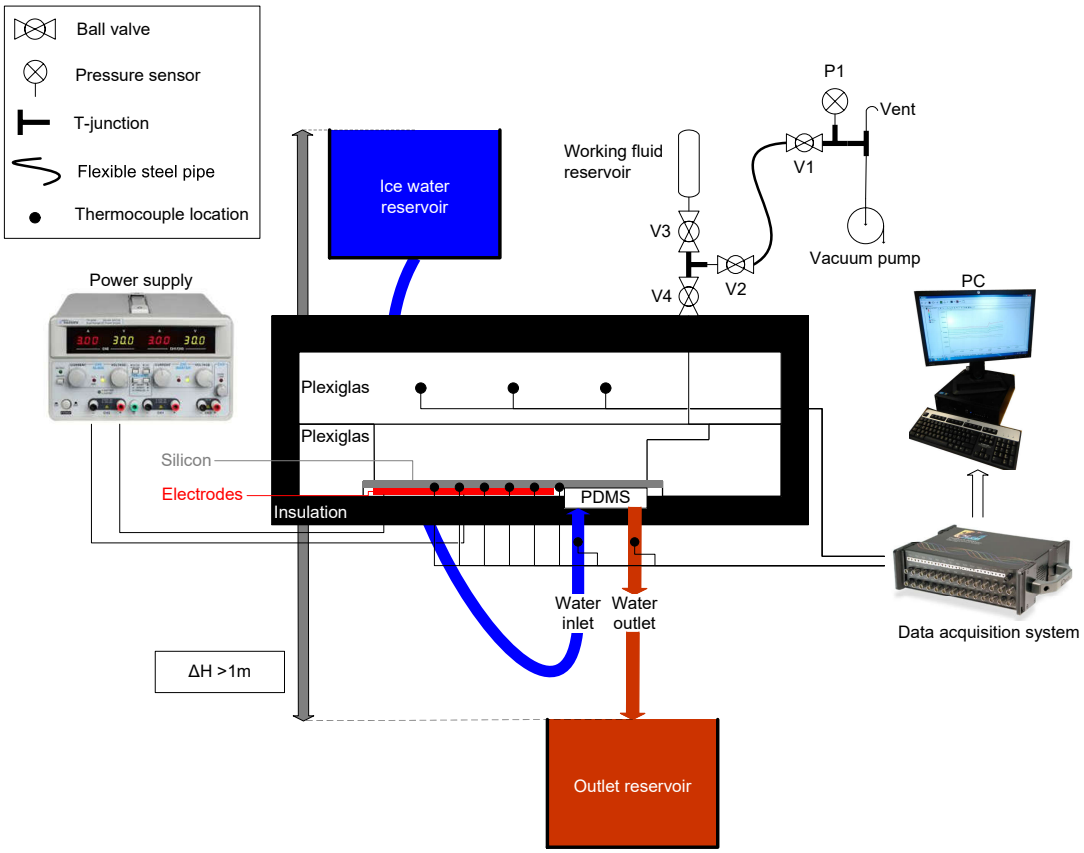

Figure 2.21: Charging and vacuuming station for silicon heat pipes

charged with DI water. It should be noted that due to the low chemical resistance of plexiglas against IPA, at filling ratios near fully-flooded heat pipe, that plexiglas cover could be damaged. Hence, not all input heat flux data are available for all the filling ratios. A very important point that needs to be considered in the operation of silicon heat pipes is unstable operation, i.e. fluctuations in temperature readings over relatively long periods of time, occurred often at filling ratios away from the optimum range and higher input heat loads. An example of unsteady operation is shown in Figure 2.22 for the filling ratio of 41.6 and input heat flux of 3.0 W/cm^2 (a higher degree of unsteady behavior was observed in other filling ratios). Inspecting the heat pipe carefully during unsteady operation, the reason might be attributed to the structure of the heat pipe. The outer grooves are located around 2 mm off the long edges and the end points of the grooves have about 3 mm distance from the short edges of the smaller o-ring. Since this space is covered with the plexiglas frame, there exists a very thin gap between

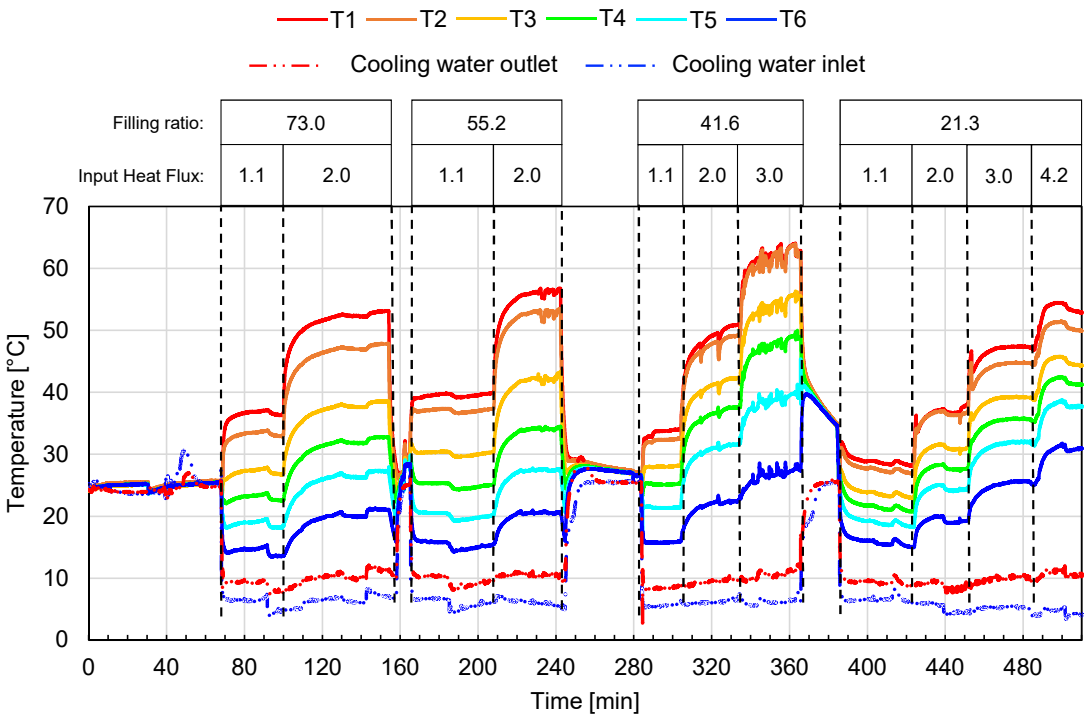

Figure 2.22: Transient temperature variation of heat pipe S-200 charged with DI water

the silicon piece and the plexiglas frame, which acts as a capillary structure. This gap causes the flow of working fluid from the condenser section to the evaporator. If the heat pipe has an excessive amount of working fluid, some may accumulate beyond the grooves end, or result in the bursting of the working fluid. Since the amount of transferred working fluid through this gap is not constant over time, and the bursting depends on this amount, such processes happen randomly and does not let the heat pipe reach a steady operation (temperature variation).

2.5 Experimental Failures

Due to the trial-and-error nature of experimental studies, some challenges faced while carrying out the experiments on each set of heat pipes, are described in this section.

2.5.1 Heat Pipe Charging

As the first proposed charging method for the first generation prototype aluminum heat pipes, micro syringe pumps, capillary tubes, and relevant valves are utilized. The filling procedure starts with vacuuming the heat pipe, follows by connecting it to a micro syringe pump filled with the working fluid for charging. The advantage of such method is the accuracy in the measurement of charged amount of the working fluid ($\pm 1\,\mu$L) by the user interface of a software. However, since the valves and fittings are not gas tight and the heat pipe is under vacuum prior to charging, this method let the ambient air penetrate the heat pipe. Figure 2.23–(a) shows the connections on the heat pipe with this charging method.

2.5.2 Water Incompatibility with Aluminum

As mentioned in section 2.1, the compatibility of the working fluid with the bulk material of a heat pipe is a must for its proper operation. Due to the superior properties of water, first generation prototype aluminum heat pipes were first charged with water. However, due to its wetting characteristics, the water couldn't wet the aluminum, especially the grooves surfaces. Figure 2.23–(b) shows a charged amount of water which is stuck to the plexiglas cover and the aluminum surface, while it couldn't enter the grooves. This resulted in changing the working fluid to IPA. Although its latent heat of vaporization is about one fourth of that of water, the payback of using IPA is its compatibility with aluminum which leads to proper operation of the heat pipes.

2.5.3 Damage on the Plexiglas due to Overheating

While performing the experiments on second generation aluminum heat pipes or silicon heat pipes, input heat loads could exceed $4 - 5\,\mathrm{W/cm^2}$. At some filling ratios away from the optimum ones, the temperature of the plexiglas cover or the plexiglas frame in the evaporator section exceed $60\,^{\circ}$C. Such high temperatures

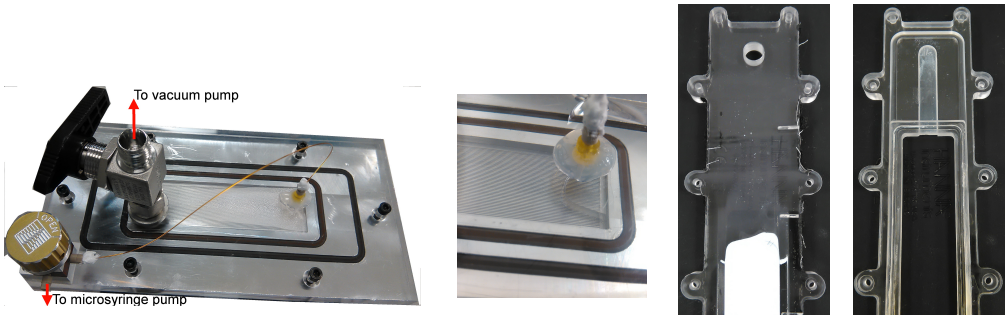

(a) (b) (c) (d)

Figure 2.23: Examples of failures during the experiments: **(a)** the first charging method, **(b)** incompatibility of water with aluminum surface, **(c)** and **(d)** burnt plexiglas cover pieces (Note: the scale of the photographs are not identical.)

along with the low chemical resistance of plexiglas against IPA[1], led the plexiglas pieces to be burnt or cracked. This happened to the plexiglas cover in second generation aluminum heat pipes assembly, shown in Figure 2.23–(c), and plexiglas frame in silicon heat pipes assembly, shown in Figure 2.23–(d). In one case, small detached pieces of plexiglas attached to the grooves on silicon and rendered it unusable.

[1]According to ePlastics®, continuous exposure of plexiglas to IPA at 50 °C is "not recommended. Immediate damage may occur such as severe crazing, cracking, or permeation losses." [60]

Chapter 3

Results and Discussion

Experiments were performed on the first generation prototype aluminum heat pipes, second generation aluminum heat pipes, and silicon heat pipes to investigate their thermal performance under different operating conditions. During the experiments, temperature variation on the bottom of the metal base, ambient, plexiglas top cover, and cooling water (for second generation aluminum heat pipes and silicon heat pipes) are recorded. In addition, a computational model is developed to quantify the heat input during the experiments on first generation aluminum heat pipes. Moreover, phase change heat transfer is simulated for one of the second generation aluminum heat pipes to predict its temperature variation. The experimental and computational results are given here.

3.1 Definition of the Filling Ratio

The fill charge, known as the amount of working fluid charged in a heat pipe, significantly affects its performance [26,61]. Although this value is mostly referred to as filling ratio, its definition may vary from one study to another. As an instance, filling ratio was defined as the ratio of the liquid volume to the internal volume of the flat plate heat pipe in [21]. In this case, filling ratio of unity

corresponds to a fully-flooded heat pipe and zero filling ratio demonstrates an empty one. In another study, it was defined as the total volume of liquid working fluid minus the dead volume inside the heat pipe over the volume of the grooves [15]. With such definition, an empty heat pipe has a filling ratio of zero. In present work, filling ratio is defined as the ratio of total volume of the liquid working fluid inside the heat pipe (V_{fluid}) over total colume of the grooves (V_{groove}). Therefore, filling ratio of zero corresponds to an empty heat pipe and filling ratio of a fully-filled heat pipe differs from a heat pipe to another, still has a value higher than unity.

3.2 Thermal Performance Indicators

Thermal resistance of different sections and effective thermal conductivity are of common parameters in the literature to characterize the heat removal performance of heat pipes. However, due to the geometry and operating conditions of the heat pipes in this work, the 1-D heat transfer criteria to apply such parameters are not met. In other words, there are 2-D and 3-D effects in the heat transfer from the heat source to the heat sink. Hence, the following parameters are defined and used as performance indicators of the heat pipes in this thesis:

3.2.1 Temperature Difference and Peak Temperature

The use of phase change heat transfer allows the heat pipes to operate with lower temperatures in the system, as well as lower temperature difference between the evaporator and condenser sections. In the current study, this difference is chosen to be one of the indicators of the phase change heat transfer performance of the heat pipes. Moreover, this definition is extended to include the peak temperature encountered as a second indicator of heat pipe thermal performance. Practically, electronic component cooling requirements dictate the system to operate below temperatures that would result in component failure, which is another manifestation of the above defined thermal performance indicators. With these definitions,

a better performing heat pipe is a device which transfers the same amount of heat with a lower temperature difference between the hot and cold junctions or with a smaller peak temperature in the system. Since this performance is a function of design as well as operating parameters, for a specified design, the thermal performance of a flat grooved heat pipe is a function of the filling ratio. In the present work, the filling ratio which results in the best thermal performance is defined to be the "optimum". The results show that the operation of a heat pipe with very high or very low filling ratios, away from the optimum, may be dominated by conduction alone with little heat transferred through phase change. In such a case, the device is operating at best marginally, at worst not at all as a heat pipe. Unless observed visually, or a wide scan of filling ratios is covered experimentally, the *modus operandi* of the device cannot be argued to be heat pipe.

3.2.2 Heat Pipe Effectiveness

A third indicator is introduced in the assessment of the thermal performance of a heat pipe. The effectiveness of a heat pipe, ε_{hp}, is defined as,

$$\varepsilon_{hp} = \frac{\Delta T_{dry}}{\Delta T_{operating}} \tag{3.1}$$

where, ΔT_{dry} and $\Delta T_{operating}$ are the temperature differences between the heat source and sink regions for the dry and operating conditions, respectively. The temperature difference between the heat source and the sink is at a maximum during dry operation (where the heat transfer is dominantly through conduction in the metal base), and reaches a minimum at the optimum operating point (where the input heat is being transferred mostly by the phase change of the working fluid). The effectiveness will be unity for dry operation—heat transfer through heat conduction in the metal alone—and will exceed unity with the start of phase change heat transfer. The effectiveness can be related to the "effective thermal conductivity" concept used in the literature. The reason for this new indicator of heat pipe performance is explained in the following sections, as results will show this parameter to be a function of not only the filling ratio but power input as well.

3.3 First Generation Prototype Aluminum Heat Pipes

Due to the dependency of the COP of the thermoelectric heating and cooling units to their operating conditions, the heat input and output to and from the heat pipes are not measured directly; therefore, these values are obtained with a simple 3-D computational model for two extreme values of filling ratio, fully-filled and dry. Since in these cases the heat transfer is through conduction in the metal base and working fluid, the values of their thermal conductivity are of great influence on the performance of the heat pipes. Thermal conductivity of IPA is set to $0.14\,\mathrm{W/m \cdot K}$. For that of aluminum, since the exact type of aluminum alloy is not known, a set of experiments with the heating and cooling methods used for the second generation aluminum heat pipes were performed on heat pipe G1-200 to find the temperature variation along the metal base. Knowing the heat input to the system, a computational model was used to match the experimental temperature readings with the model. Accordingly, thermal conductivity of aluminum found to be $140\,\mathrm{W/m \cdot K}$ and this value used as an input to the computational model on the heat pipes of first generation.

3.3.1 Simulation Results

The comparison of the experimental data and the simulation results can be seen in Figure 3.1. According to the results of the simulations, the input heat flux for the experiments is estimated to be in the range of $1.40 - 1.80\,\mathrm{W/cm^2}$. Although the same constant electrical power is supplied to the thermoelectric units, this variation in heat flux is attributed to the dependence of COP value on operating conditions.

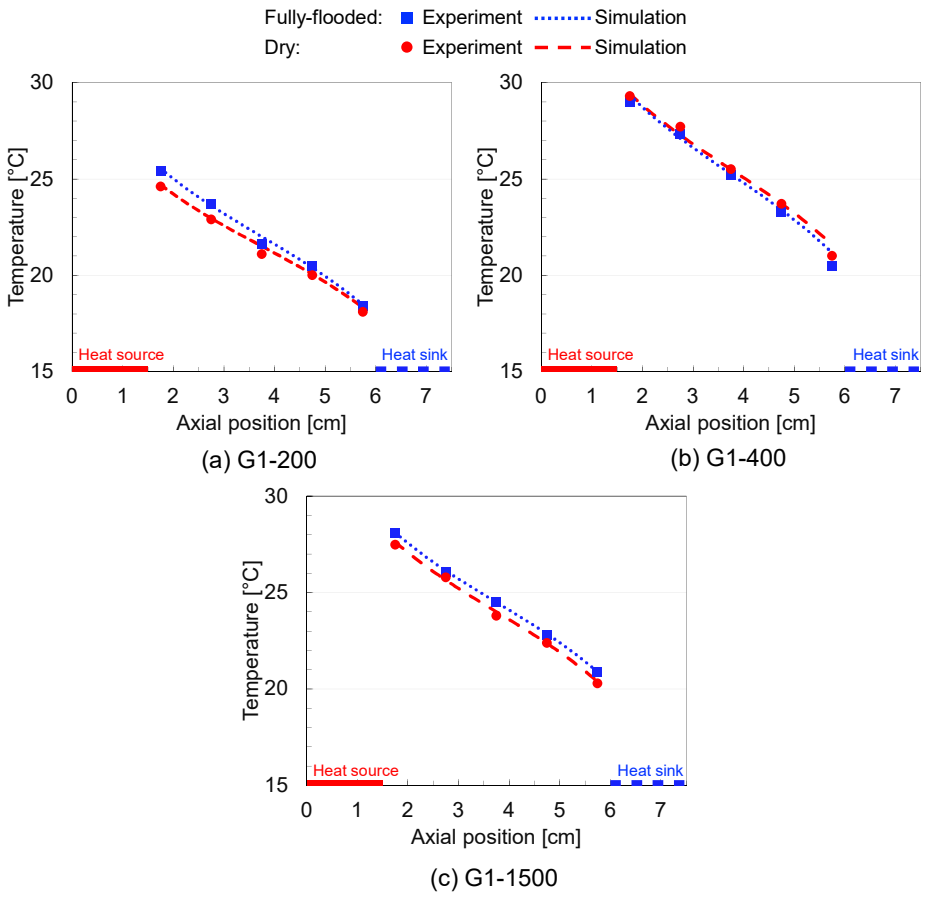

Figure 3.1: Simulated and measured temperatures of first generation prototype aluminum heat pipes

3.3.2 Experimental Results

3.3.2.1 Temperature Variation along the Heat Pipes

For each heat pipe, five different IPA amounts are used from fully-flooded to dry. Figure 3.2 shows the temperature differences between temperatures measured at locations described in Figure 2.1 (T_1 through T_5) and the plexiglas temperature (T_6) which is kept approximately equal to the ambient temperature. This is done because during the experiments both the ambient temperature, which is not controlled, and hence the plexiglas temperature varied. This referencing eliminates an erroneous interpretation of the temperature curves for different IPA extents.

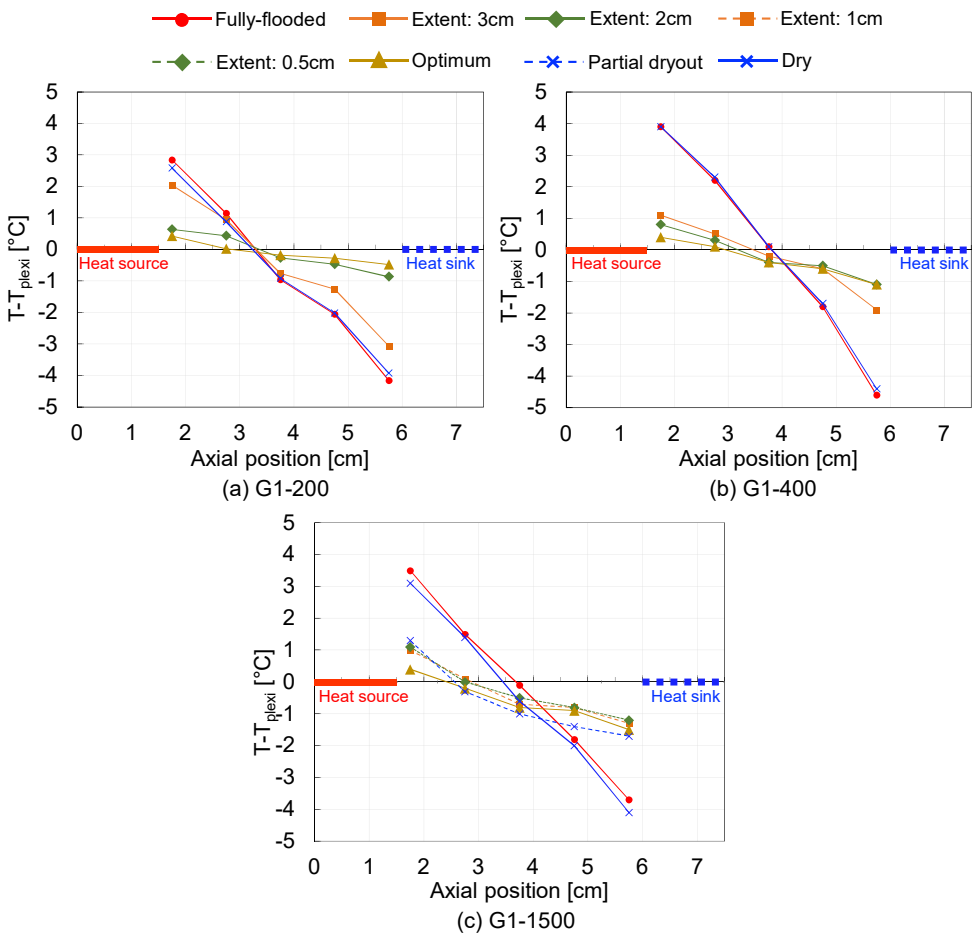

Figure 3.2: Temperature differences between thermocouples on the bottom of the metal base (T_1 through T_5) and the one on plexiglas (T_6) for first generation prototype aluminum heat pipes

It should be noted that because of the heavy weight of the experimental components, it was not possible to put the heat pipes in a vertical orientation during the IPA extent measurements (section 2.2.4). Hence, the average length of IPA extent is reported and the values of filling ratio are estimated. Estimated range of filling ratios corresponding to different cases are tabulated in Table 3.1. Due to inaccuracies in the measure of the liquid extent, the estimated range of optimum operating points is large, especially for higher groove densities. The temperature variations along the heat pipes are similar for the fully-flooded and dry cases, and displays a linear behavior. This is expected since in the absence of phase change, the heat transfer is due to conduction only. In the fully-flooded case,

Table 3.1: Estimated range of filling ratio for different liquid extents of IPA in first generation prototype aluminum heat pipes

G1-200		G1-400		G1-1500	
Case	**Filling ratio**	**Case**	**Filling ratio**	**Case**	**Filling ratio**
Fully-flooded	25.0	Fully-flooded	12.5	Fully-flooded	4.0
Extent: 3 cm	9.0 – 11.0	Extent: 3 cm	4.5 – 5.5	Extent: 1 cm	0.50 – 0.60
Extent: 2 cm	5.5 – 7.5	Extent: 2 cm	3.0 – 4.0	Extent: 0.5 cm	0.25 – 0.40
Optimum	0.8 – 2.5	Optimum	0.5 – 1.5	Optimum	0.15 – 0.20
Partial dryout	—	Partial dryout	—	Partial dryout	0.07 – 0.12
Dry	0.0	Dry	0.0	Dry	0.0

there is a possibility of heat transfer due to conduction and convection in the liquid. Both of these, however, are found to be very small; conduction due to the extremely small thermal conductivity of IPA compared to that of aluminum, and convection due to very small velocities in the liquid. Since the heat transfer in the fully-flooded case is through conduction in both the metal base and liquid, the temperature differences measured in the close proximity of the heater and the cooler are expected to be slightly lower compared to the dry case, where the heat transfer is through the metal base only. In Figures 3.2-(a) and (c), however, the temperature difference on the heater side of the dry case is lower than the fully-flooded case. The same trend is also seen in Figure 3.2-(a) in the proximity of the cooler side. This unexpected behavior can be attributed to the accuracy of the calculated temperature reading difference, which is estimated to be ($\pm 0.2\,^{\circ}$C). With the removal of IPA, the phase change complements conduction, the temperature curves flatten, and all temperatures approach the ambient temperature. This is characteristic of heat pipes, where the temperature difference between the high temperature and low temperature reservoirs are small, and these temperatures remain close to ambient for low heat flux values. At the optimum operating point, phase change is dominant, and the slope of the temperature curve is at its minimum, showing that heat conduction in the metal base is at a minimum. Once the temperature difference between the heater and cooler reaches a minimum at the optimum operating point, any additional removal of IPA forces the system to partial dryout and an increase in the temperature differences. The optimum

point is achieved with a small quantity of the working fluid, and therefore is very close to the dry operating condition. Although the estimates of filling ratios cover a wide range, it can be concluded that the filling ratio at the optimum point decreases with lower groove density.

3.3.2.2 Temperature Difference along the Heat Pipes

The temperature difference between the heater and cooler sections ($T_1 - T_5$) is given in Figure 3.3 for different operating conditions. For G1-200, the temperature difference between the heater and cooler is 6.9 °C (±0.2 °C) for the fully-flooded case, dropping gradually to 0.9 °C (±0.2 °C) for the optimum, and increasing to 6.5 °C (±0.2 °C) for the dry case. This shows that with the removal of IPA the system operates like a heat pipe, eventually reverting back to conduction only for the dry case. A similar performance is observed for G1-400 and G1-1500 where the temperature differences between the heating and cooling units are 8.5 °C (±0.2 °C) and 7.2 °C (±0.2 °C) for the fully-flooded, reaching a minimum of 1.5 °C (±0.2 °C) and 1.9 °C (±0.2 °C) at the optimum, and eventually reaching 8.3 °C (±0.2 °C) and 7.2 °C (±0.2 °C) for the dry operation, respectively. The operating characteristics of different groove densities are also apparent in the results. The majority of evaporation occurs near contact line within each groove; therefore increasing the number of grooves (i.e. groove density) enhances phase change heat transfer to the fluid [62]. A major fraction of the heat input is transferred through phase change rather than conduction through the heat pipe bulk material, resulting in a considerable reduction in the temperature difference between the heat source and sink. A difference in groove width and the corresponding fin width also changes the conduction in the fin cross-section; this effect, however, is believed to be minor compared to the effect of the increase in length of the contact line. The temperature difference between the heater and cooler sides can be considered as a measure of the effectiveness of a heat pipe. G1-200 with the highest groove density (i.e. the smallest groove size) has the best performance with a minimum temperature difference of 0.9 °C (±0.2 °C).

Another observation is the existence of a partial dryout in heat pipe G1-1500,

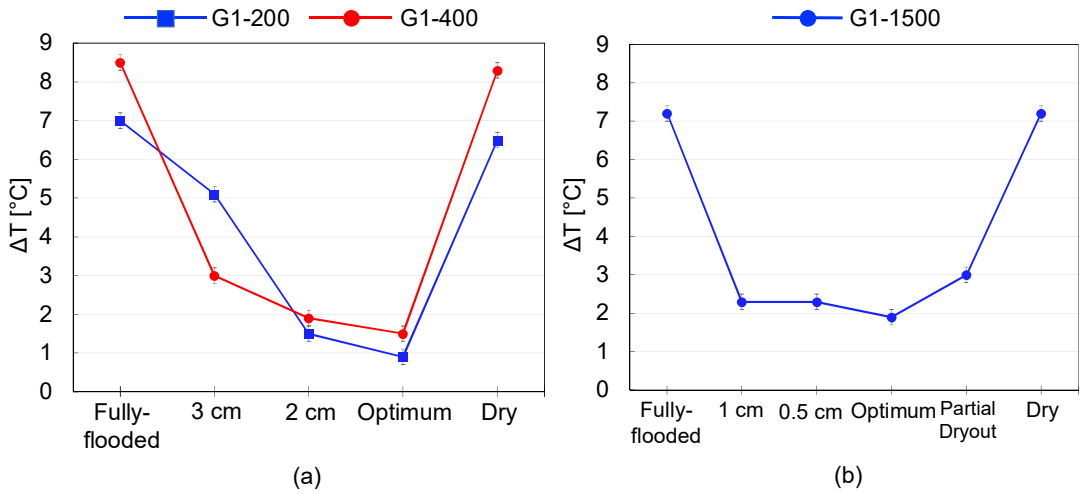

Figure 3.3: ΔT for different operating conditions for first generation heat pipes: **(a)** G1-200 and G1-400, **(b)** G1-1500

which is not seen in the other two samples. In G1-200 and G1-400, the amount of IPA left in the grooves in optimum operating condition is excessively small and an attempt to remove additional IPA resulted in a total removal of all remaining IPA, bringing the system to dry operating condition. In case of G1-1500, however, there is substantially more IPA left inside the grooves compared to G1-200 and G1-400 at the optimum operating point; therefore it is possible to remove more IPA from the system without rendering the grooves entirely dry. This enables the operation of the system with partial dryout conditions, where some of the grooves are void of liquid IPA in the vicinity of the heater unit.

3.4 Second Generation Aluminum Heat Pipes

The effect of groove density, filling ratio, and input heat flux is extensively studied on thermal performance of the second generation heat pipes. In this regard, heat pipes operated in a wide range of filling ratios under four different input heat flux values.

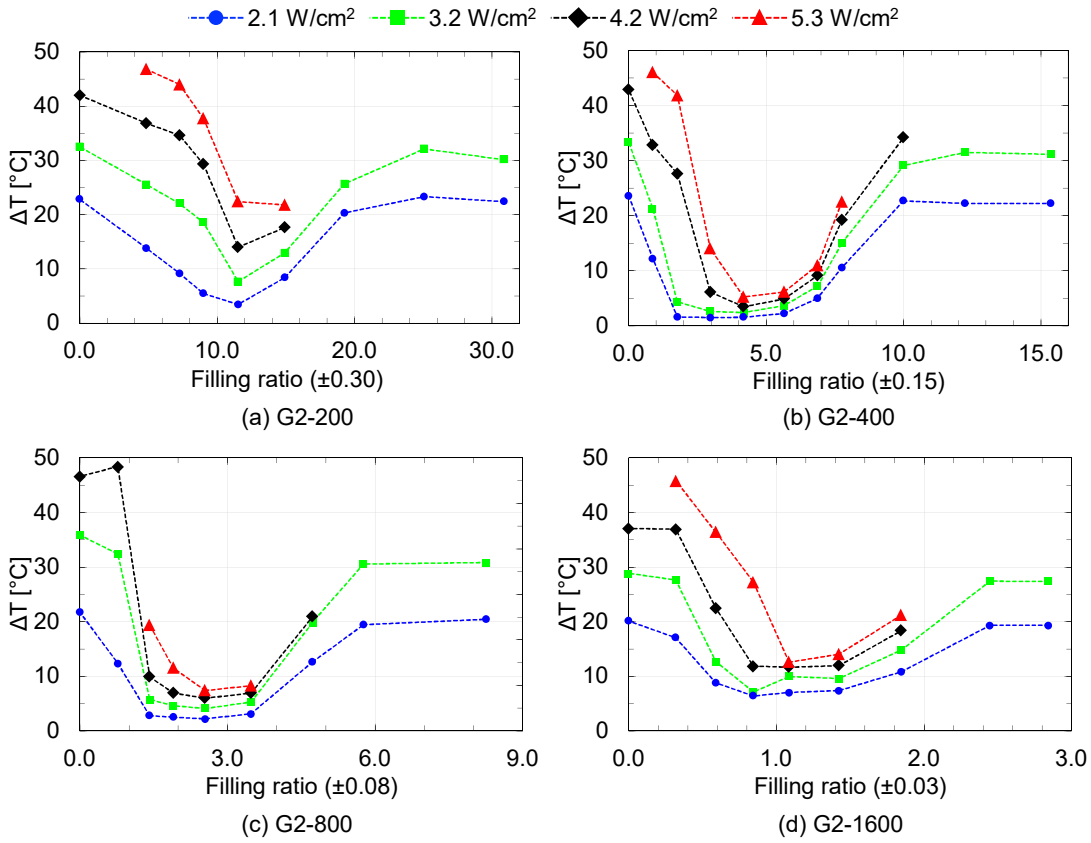

Figure 3.4: Variation of ΔT with filling ratio under different input heat fluxes for second generation aluminum heat pipes

3.4.1 Temperature Difference and Peak Temperature

The two most distant thermocouples, TC_1 and TC_5, are closest to the heater and cooler sections of the heat pipes (Figure 2.8). The temperature difference between the two, $\Delta T \equiv T_1 - T_5$, is plotted in Figure 3.4 for four heat pipes at different filling ratios under four input heat flux values. The highest value of the filling ratio in each graph corresponds to a fully-flooded heat pipe, while a filling ratio of zero corresponds to a dry (i.e. empty) heat pipe. All heat pipes show a similar variation of temperature difference as a function of filling ratio. When fully-flooded, the entire heat load is transferred through the aluminum base, IPA and the plexiglas top cover with thermal conduction. The bulk of the heat is transferred in the aluminum, due to negligible thermal conductivities of IPA and plexiglas ($0.14\,\mathrm{W/m \cdot K}$ and $0.18\,\mathrm{W/m \cdot K}$, respectively) compared to that of

Table 3.2: Variation of temperature difference and peak temperature with filling ratio and input heat flux for second generation aluminum heat pipes

			Temperature difference ΔT [°C] / Peak Temperature ($T_1 - T_{water}$) [°C]			
		Filling ratio	**2.1 W/cm²**	**3.2 W/cm²**	**4.2 W/cm²**	**5.3 W/cm²**
G-200	Fully-flooded	30.9	22.4/39.3	30.1/52.7	–	–
	Optimum	11.5	3.5/18.9	7.6/28.3	14.0/40.6	(21.8/53.1)[1]
	Dry	0.0	22.8/34.6	32.5/48.8	42.0/63.0	–
G-400	Full-flooded	15.4	22.2/36.3	31.1/50.9	–	–
	Optimum	4.2	1.6/(9.2)[2]	2.4/(15.0)[2]	3.5/(21.2)[3]	5.2/29.8
	Dry	0.0	23.5/36.1	33.3/50.6	42.9/65.4	–
G-800	Full-flooded	8.3	24.5/37.3	30.8/46.8	–	–
	Optimum	2.5	2.6/(9.8)[4]	4.1/(13.7)[4]	6.0/(19.1)[4]	7.4/(26.2)[4]
	Dry	0.0	25.3/37.7	35.6/53.0	46.0/69.2	–
G-1600	Full-flooded	2.8	19.3/35.2	27.4/49.8	–	–
	Optimum	0.8	6.4/15.5	7.1/20.6	(11.6)[5]/29.1	(12.6/35.4)[5]
	Dry	0.0	20.1/33.9	28.8/48.6	37.0/62.6	–

[1] Corresponds to filling ratio of 14.9.
[2] Corresponds to filling ratio of 1.8.
[3] Corresponds to filling ratio of 3.0.
[4] Corresponds to filling ratio of 1.9.
[5] Corresponds to filling ratio of 1.1.

aluminum ($140\,\mathrm{W/m \cdot K}$). As IPA is removed from the heat pipe and the filling ratio reduced, phase change heat transfer begins and the temperature difference along the heat pipe drops. This effect intensifies with successive removals of IPA reaching a minimum value of temperature difference. At this point the heat transfer *via* phase change is at a maximum and conduction at a minimum. Any further removal of IPA results in an increase in temperature differences, effectively a reduction in heat transferred through phase change and an increase in thermal conduction through the solid. This trend continues until the heat pipe cavity is totally void of any fluid—i.e. it is entirely dry—and the heat transfer is due to heat conduction in the metal base alone. Figure 3.5 shows the maximum temperatures in the system. Comparing Figure 3.4 to Figure 3.5, it can be seen that the minimum value of temperature differences and peak temperatures occur at approximately the same filling ratios for all cases studied. Based on the above definitions, the optimum operating points are the same for both factors of thermal performance. Importantly, the filling ratios at which the heat pipes operated at minimum value of temperature difference along them are noted in Table 3.2.

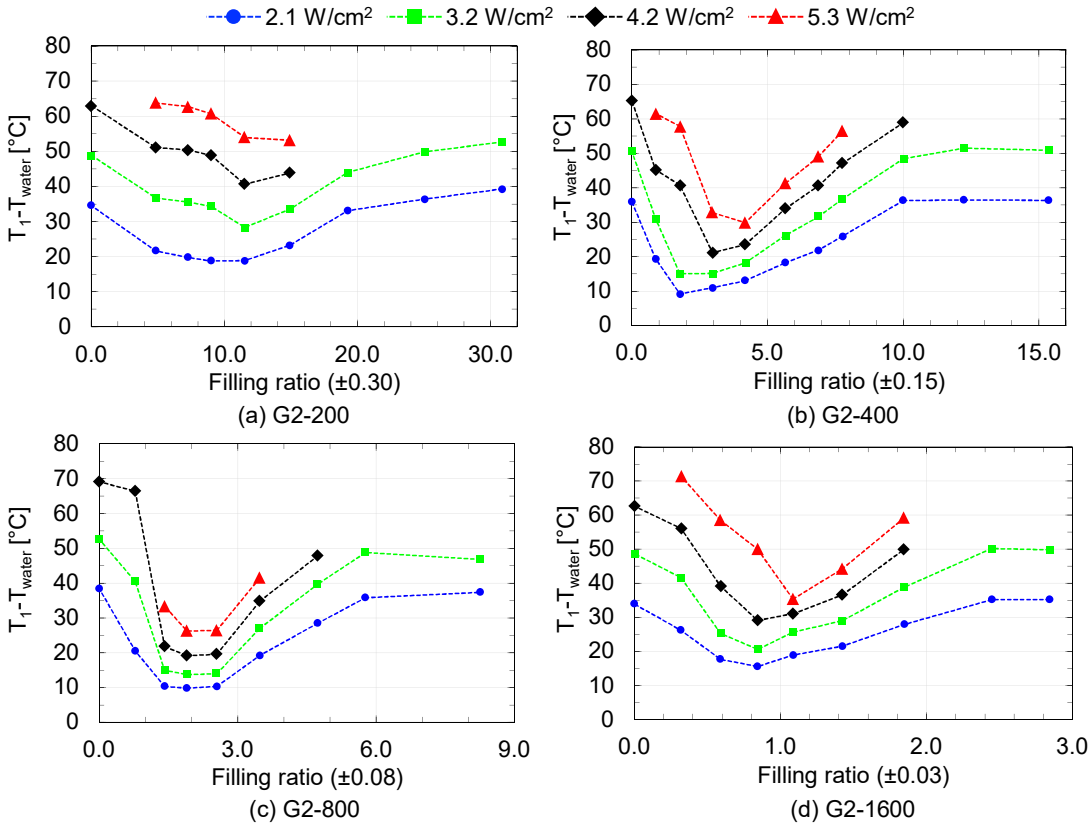

Figure 3.5: Variation of $T_1 - T_{water}$ with filling ratio for second generation aluminum heat pipes for different input heat flux values

Figure 3.5 shows the temperatures measured by the first thermocouple TC_1 of the heat pipes under different heat inputs. This thermocouple being the closest to the heater records the highest temperature readings, which is an indication of the highest temperature in the system. According to the aforementioned explanations, when the share of phase change in total heat transfer is high, the heat pipe operating temperature falls dramatically. As an instance, for heat pipe G2-400, T_1 at fully-flooded case is $46.3°C$ while at filling ratio of 1.8 it is $20.9°C$. In short, at optimum filling ratio, the heat pipes dissipate the same amount of heat as fully-flooded and dry cases while they operate in a much lower temperature range.

Table 3.3: Highest effectiveness values of second generation aluminum heat pipes under different input heat fluxes

Heat input $[W/cm^2]$	**2.1**	**3.2**	**4.2**	**5.3**
G2-200	6.5	4.1	3.0	–
G2-400	14.6	13.4	12.4	–
G2-800	6.5	6.6	–	–
G2-1600	3.1	4.0	3.1	–

3.4.2 Heat Pipe Effectiveness

The effectiveness of the heat pipes is a function of the filling ratio and the heat input, for a given design. The filling ratio is especially important, and an effectiveness value close to unity indicates that the heat pipe is actually not operating as it is supposed to, i.e. through phase change. The operating point where the effectiveness is at a maximum is desired, since this will result in the best possible use of a given design. The effectiveness is also expected to be a function of other design parameters, the distance between the heat source and sink being an important one, and also the effect of multi-dimensional heat conduction in the metal base. Figure 3.6 shows the variation of effectiveness with filling ratio under different input heat fluxes for the heat pipes. The highest values of ε_{hp} of the heat pipes are listed in Table 3.3 under different input heat fluxes. According to this table, G-400 is the most promising heat pipe in heat dissipation by phase change, while G-1600 is the least successful one. This can be attributed to the available surface for vaporization, since the majority of evaporation originates from a small area near the grooves wall tip, named micro region [62].

3.4.3 Temperature Variation with Axial Position

Figure 3.7 shows the temperature readings of thermocouples TC_1 to TC_5 for the optimum operating condition and under different input heat fluxes. It should be

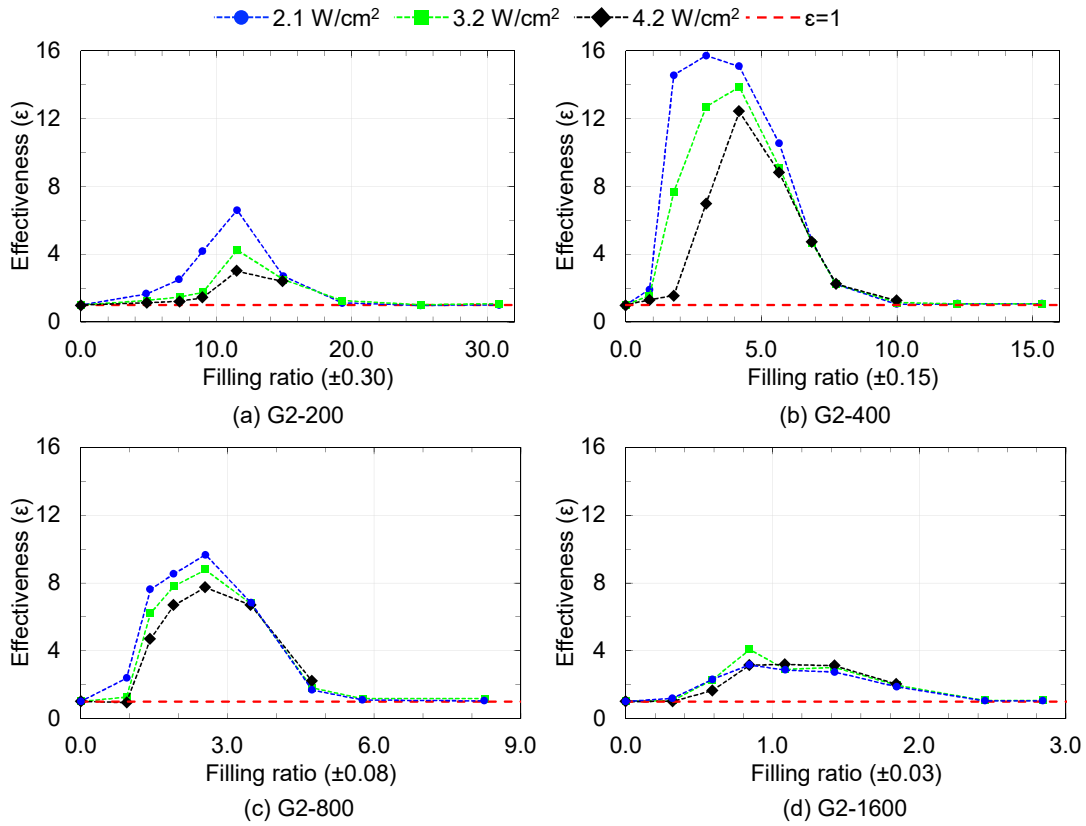

Figure 3.6: Variation of effectiveness with filling ration for second generation aluminum heat pipes under different input heat flux values

noted heat pipes G2-400 and G2-800 didn't undergo dryout at optimum filling ratio values of 4.2 and 2.5, respectively. Hence, their temperature distribution shows a linear behavior. However, heat pipe G2-200 operates under dryout even at its optimum filling ratio which is 11.5. Unlike the case of 2.1 W/cm^2, for input heat fluxes of 3.2, 4.2, and 5.3 W/cm^2 the dryout extent passes the first thermocouple. Therefore, a sudden temperature drop moving from TC_1 to TC_2. It should be noted that such temperature jump in the vicinity of the heat source is usually an indication of dryout when visualizing inside a heat pipe is not possible, as in cylindrical or flat heat pipes.

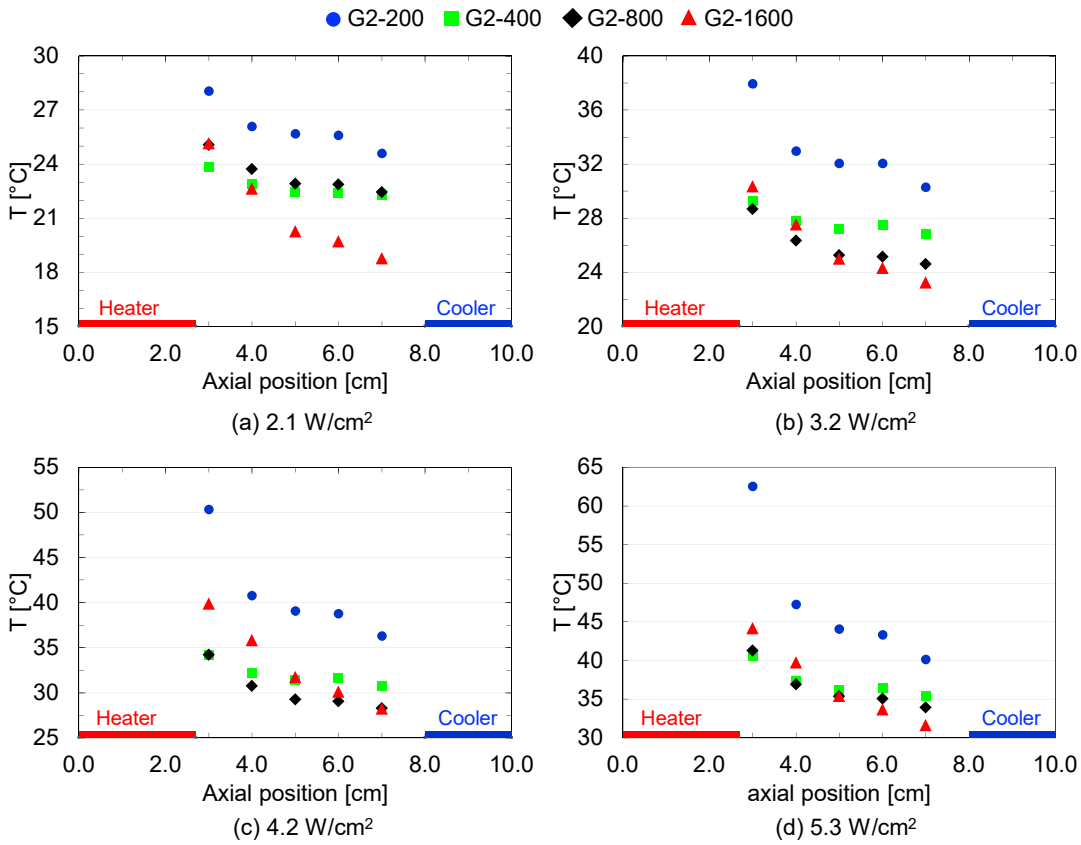

Figure 3.7: Variation of temperature with axial position under different input heat fluxes for second generation aluminum heat pipes working at their optimum filling ratios

3.4.4 Operation with Partial Dryout

When a heat pipe operates at the optimum filling ratio, removal of additional IPA results in a partial dryout, a condition in which a reduction in the amount of vaporization occurs, causing an increase in temperatures and a reduction in the amount of liquid flowing to the evaporator. As a consequence, some or all of the grooves become partially dry. This condition may result in a temperature jump at and in the near vicinity of the evaporator section. Moreover, once dryout initiates, increasing the heat input may lead it to extend further in the groove. Figure 3.8 shows the extent of dryout in four heat pipes. According to this figure, after onset, dryout extent increases with increasing the heat input and decreasing filling ratio.

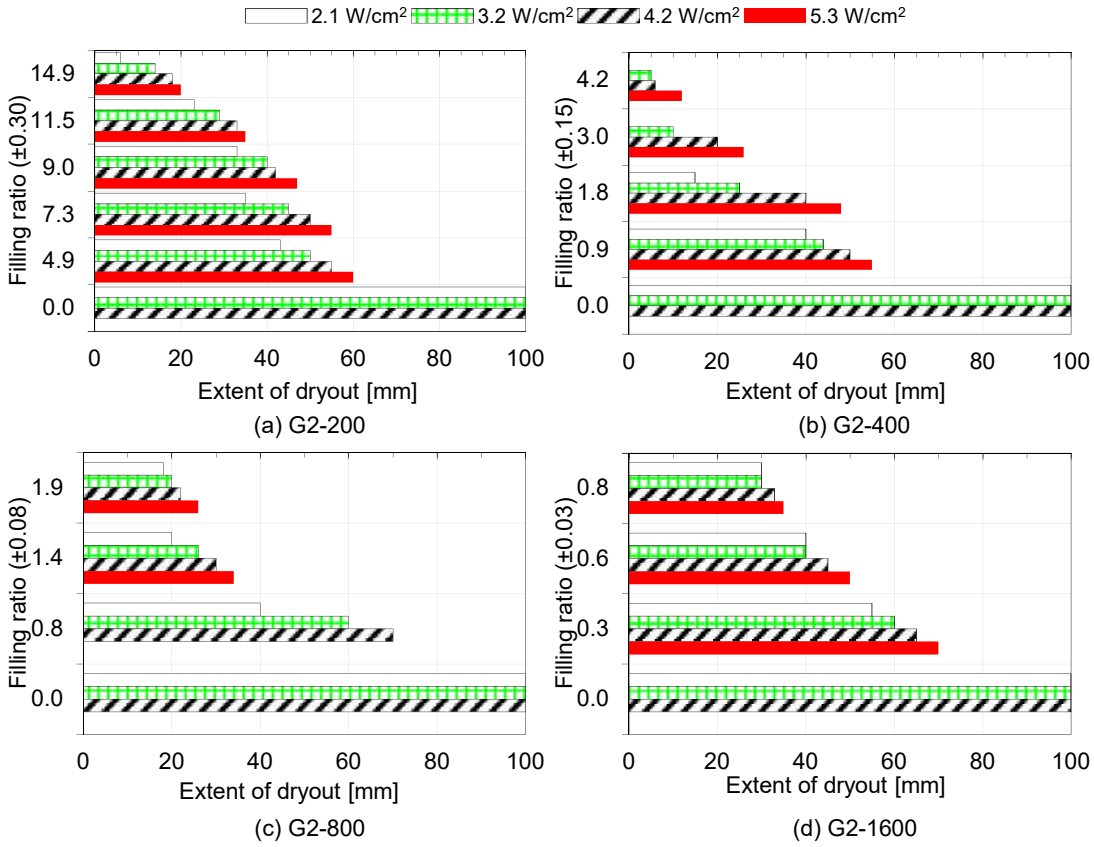

Figure 3.8: Variation of dryout extent with filling ratio for second generation aluminum heat pipes under different input heat fluxes

3.4.5 Verification of the Computational Model

After running a mesh independency analysis, the simulations are run using about 750 K quadratic elements which leads to about 1.130 M DOF. Figure 3.9-(a) shows the simulation results together with experimental temperature readings for heat pipe G2-800 operating at filling ratio of 2.5 under different input heat loads. The simulation results are tabulated in Table 3.4. The results reveal that about 90% of the heat input is transferred through the phase change of the working fluid through the evaporator. Moreover, relative error of each thermocouple compared to its corresponding location in the model is calculated and the average relative error of five thermocouples readings are reported in Table 3.4. Possible reason for the deviation of experimental results from the simulations is the fact that the filling ratio of the experiments is different than that of the simulations. However,

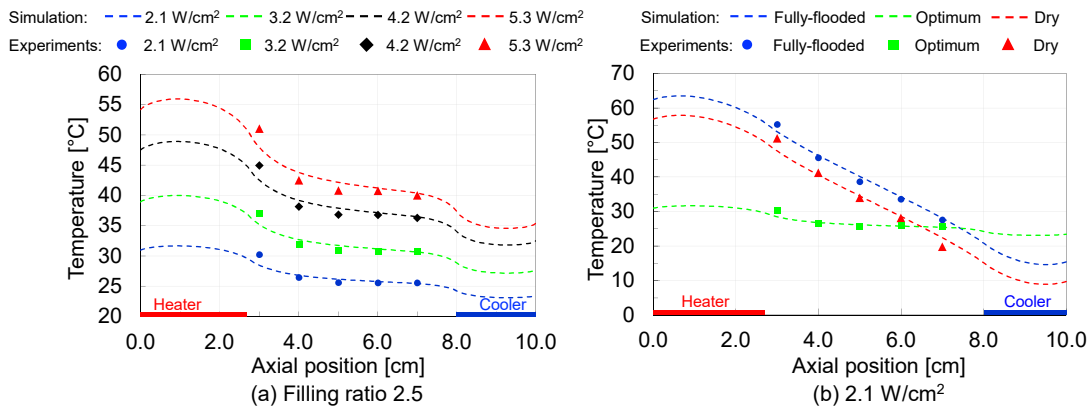

Figure 3.9: Experimental verification of computational model of heat pipe G2-800

the low values of average relative errors of the experimental results and the same trend of the thermocouples readings as to that of the simulations indicate that the model is able to predict the thermal performance of the heat pipe with a high accuracy. It should be noted that finding the optimum filling ratio by modeling requires a thorough numerical study, which is beyond the scope of this present preliminary work. As an instance, dependence of the maximum heat transport capacity to the filling ratio for a unit cell with varying groove width and depth and fin width are reported in [16]. Furthermore, the negligible difference between the values of $Q_{evaporator}$ and $Q_{condenser}$ in Table 3.4 corresponds to two factors of: (i) the convective heat transfer between the vapor of the working fluid and the bottom surface of the plexiglas cover, and (ii) the convective heat transfer between the vapor of the working fluid and the side walls of the recess on the metal base. Moreover, the difference between total heat input and $Q_{evaporator}$ is transferred probably through conduction in the metal base.

Figure 3.9-(b) shows the simulation and experimental results for three operating conditions fully-flooded, optimum, and dry under heat input of $2.1\,W/cm^2$. While fully-flooded, the whole heat input is transferred through conduction mostly in aluminum, resulting in a high temperature gradient in the heat pipe. For the optimum operating condition, the temperature gradient along the heat pipe reaches its minimum, showing that the most of the heat input is transferred through phase change. In dry case, the heat input is transferred through conduction in the metal base, which makes the heat pipe undergo a considerable

Table 3.4: Simulation results of heat pipe G2-800

Heat input $[W/cm^2]$	**2.1**	**3.2**	**4.2**	**5.3**
Q_{in} (Total heat input) $[W]$	8.0	12.0	16.0	20.0
T_{vapor} $[^\circ C]$	25.6	30.9	36.8	40.8
$Q_{evaporator}$ * $[W]$	7.1	10.7	14.2	17.8
$Q_{condenser}$ *$[W]$	-7.3	-11.0	-14.6	-18.3
$Q_{evaporator}/Q_{in}$ [%]	89	89	89	89
Average Rel. Error of Exp. Results [%]	2.3	2.4	2.7	3.1

* A positive value indicate the heat transfer from the groove walls to its surrounding, while a negative one shows the heat transfer from surrounding to the groove wall.

temperature gradient again. It is noteworthy that because of the limitations mentioned in section 2.5, the experimental and simulation results for heat inputs of 3.2, 4.2, and 5.3 W/cm^2 are missing.

Since the majority of the evaporation originates from the groove wall tip [62], named micro region, its temperature along the length of the grooves plays a key role in the performance of the heat pipe. Figure 3.10 shows the temperature distribution along the groove wall tip of 7 grooves of half width of the heat pipe (seventh groove being the one at the middle). Regarding the difference in the temperatures of the grooves, it should be noted that the 3-D effects mainly due to the conduction heat transfer through the metal base have an influence on the heat transfer mechanism. That difference is more noticeable on the parts of the grooves which are right above the heater and cooler because of 3-D geometry of the system and the high heat fluxes through the heater to the grooves and through the grooves to the cooler. Figure 3.11 depicts the temperature of the top surface of the plexiglas cover and bottom surface of the heat pipe under four different heat input values. The temperature distribution of the bottom side the aluminum base, i.e. the isothermal patterns, is a good indication of the conduction through it.

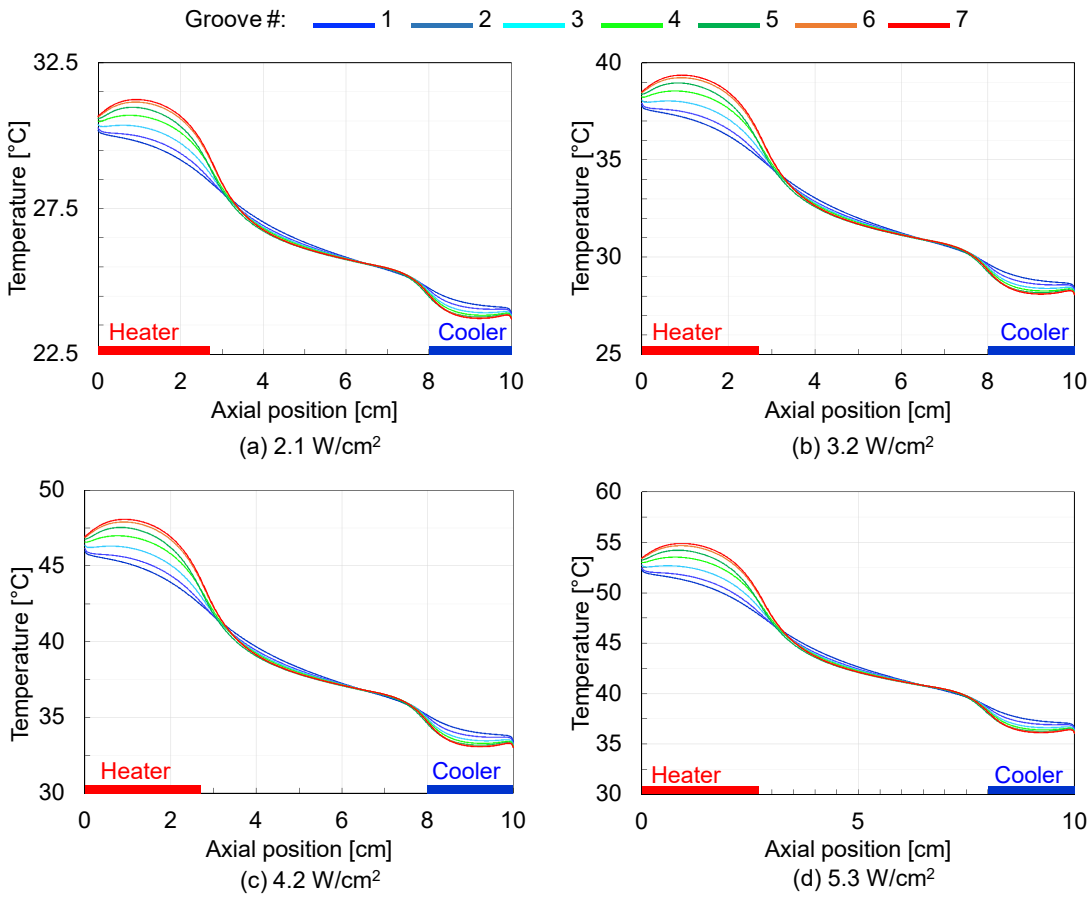

Figure 3.10: Simulated temperature distribution along the grooves of heat pipe G2-800 for different input heat flux values

3.5 Silicon Heat Pipes

The effect of working fluid, filling ratio, and input heat flux is extensively studied on thermal performance of heat pipe S-200. In this regard, it was charged with a wide range of filling ratios of DI water and IPA, and operated under different input heat fluxes.

3.5.1 Temperature Difference and Peak Temperature

For silicon heat pipes, thermocouples TC_1 and TC_2 are located on the heater electrode and TC_6 is the closest one to the heat sink (cooling water channels),

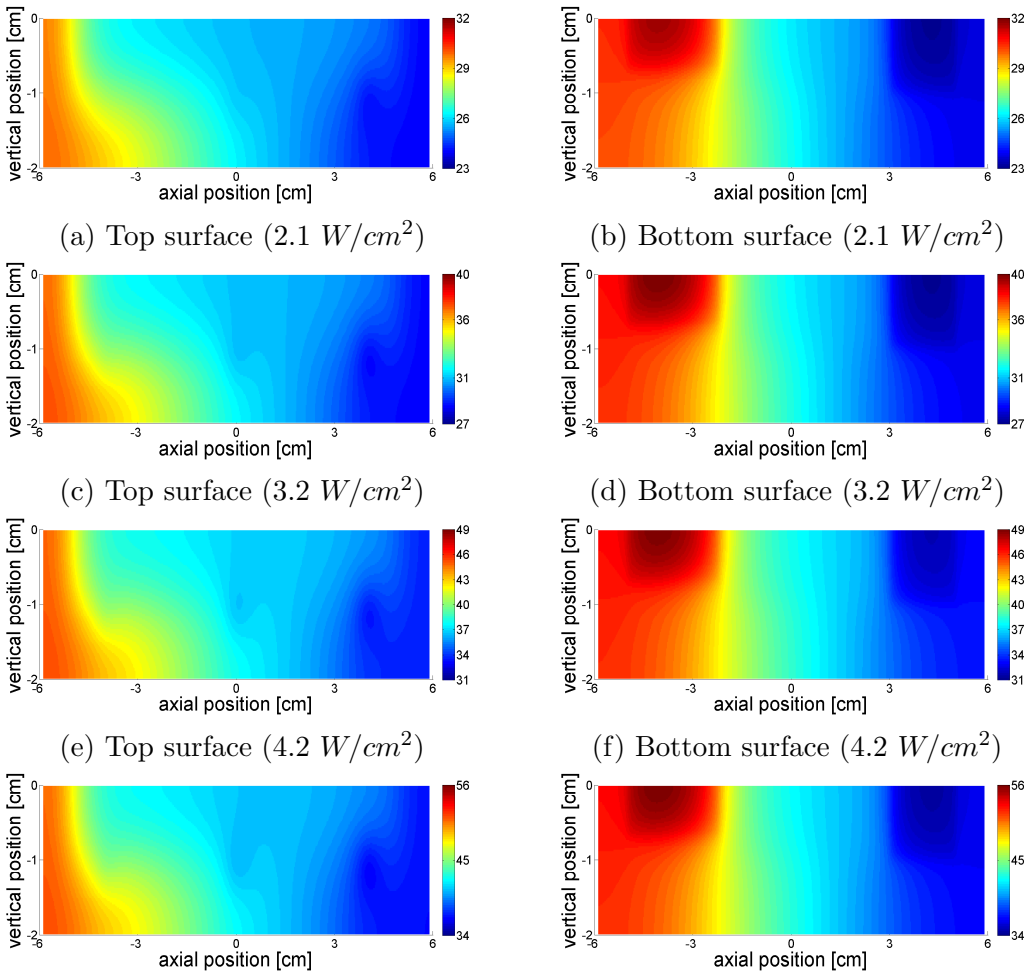

(a) Top surface (2.1 W/cm^2)

(b) Bottom surface (2.1 W/cm^2)

(c) Top surface (3.2 W/cm^2)

(d) Bottom surface (3.2 W/cm^2)

(e) Top surface (4.2 W/cm^2)

(f) Bottom surface (4.2 W/cm^2)

(g) Top surface 5.3 W/cm^2)

(h) Bottom surface (5.3 W/cm^2)

Figure 3.11: Temperature distribution of top and bottom surfaces of G2-800 heat pipe by the computational model under different input heat flux values

as depicted in Figure 2.18. Hence, the temperature difference between the two far-most thermocouples, i.e. $\Delta T \equiv T_1 - T_6$, indicates the performance of the heat pipes. Figure 3.12 shows the variation of ΔT along heat pipe S-200 with filling ratio, charged with water or IPA, under different input heat loads. Both working fluids exhibit a similar trend in ΔT as the filling ratio decreases from a fully-flooded heat pipe to a dry one. When fully-flooded, the input heat is transferred through conduction mostly in silicon. As some of the working fluid is extracted from the heat pipe, phase change heat transfer starts to occur. At optimum filling ratios, its share in the total heat transfer is at its maximum, while that of conduction is at its minimum. This is indicated by significantly lower values of

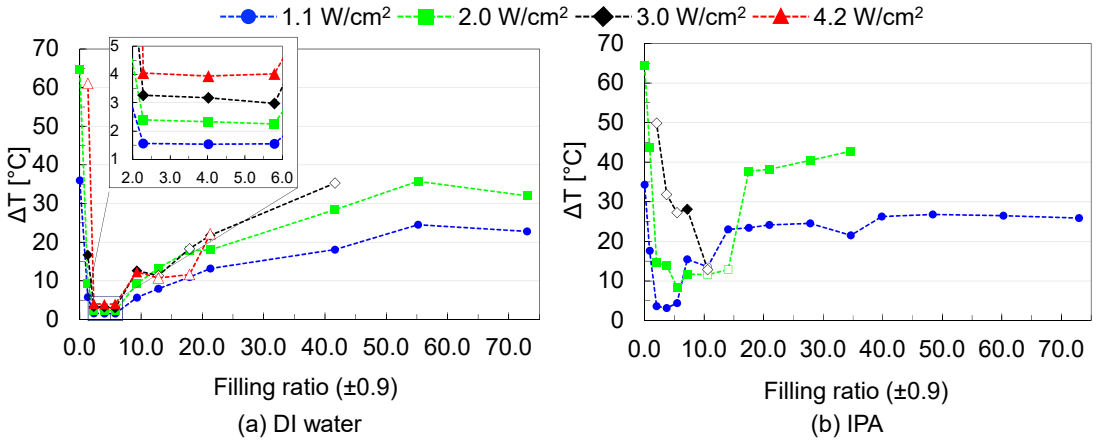

Figure 3.12: Variation of ΔT with filling ratio for heat pipe S-200 under different input heat fluxes (Note: the hollow data points correspond to unsteady operation of the heat pipe.)

ΔT compared to fully-flooded case. Further removal of the working fluid results in an increase in ΔT and, consequently, a decrease in share of phase change heat transfer until there remains no working fluid inside the heat pipe. In this condition, ΔT has a relatively large value corresponding to heat transfer through silicon. More importantly, because of the compatibility of DI water with silicon, operation of the heat pipe charged with water can be compared to that of charged with IPA. Since water has superior thermal and physical properties corresponding to its significant Merit number, its better performance is indicated by lower values of ΔT compared to those of IPA at a similar range of filling ratio. In other words, compared to IPA, water is capable of transferring the same amount of heat input with lower temperature difference along the heat pipe. Furthermore, the heat pipe charged with water was able to transfer higher input heat loads of 3.0 and 4.2 W/cm^2 steadily at filling ratios near the optimum range, while the one charged with IPA experienced unsteady operation under input heat loads of 2.0 and 3.0 W/cm^2.

According to the results of the experiments, temperature variation along the heat pipe is strongly dependent on the cooling water inlet temperature, T_{water} (corresponding to thermocouple TC_{10} in Figure 2.18). Any sudden or gradual change led the thermocouples TC_1 to TC_6 to change accordingly. This can be easily noticed from Figure 2.22 which depicts the temperature readings of the

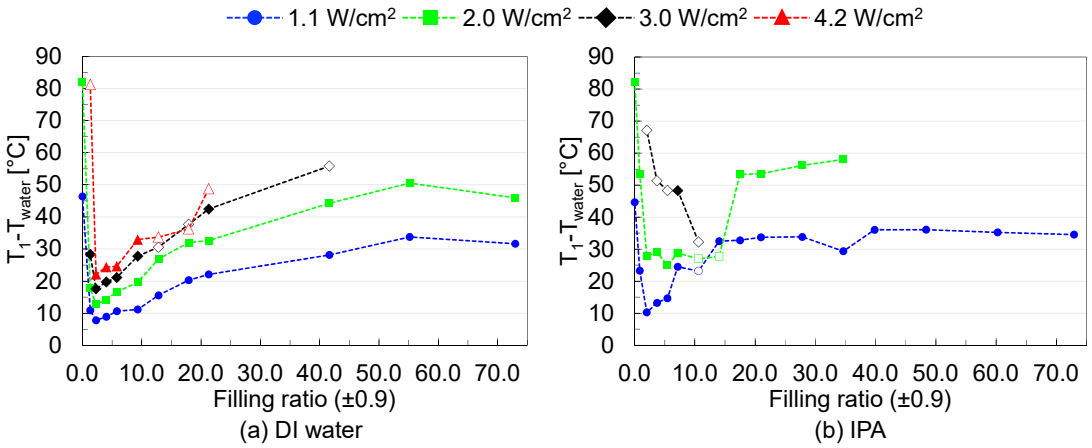

Figure 3.13: Variation of $T_1 - T_{water}$ with filling ratio for heat pipe S-200 under different input heat fluxes (Note: the hollow data points correspond to unsteady operation of the heat pipe.)

thermocouples over time. Therefore, water inlet temperature is considered as a reference to compare the peak temperature of the heat pipe. Furthermore, the difference between the peak temperature of the system, i.e. TC_1, and water inlet temperature found to be a strong function of filling ratio. The values of $T_1 - T_{water}$ are plotted in Figure 3.13 for heat pipe S-200 charged with water or IPA. Phase change enables a heat pipe to operate with a low temperature gradient and low peak temperatures as well. This is one of the reasons that they are devices of interest in applications where the localized hot spots must be avoided. According to Figure 3.13, near the range of optimum filling ratios, the heat pipe significantly lower the peak temperature in the heat pipe system compared to very high or very low filling ratios. As an instance, the values of $T_1 - T_{water}$ for the heat pipe charged with water are $31.7°C$ and $46.4°C$ under input heat load of $1.1 W/cm^2$ for fully-flooded and dry cases, respectively. This value was $7.8°C$ for the optimum filling ratio of 2.3. Moreover, the peak temperatures of the heat pipe charged with water were lower than those of the heat pipe charged with IPA, which can be considered as another indication for its better performance.

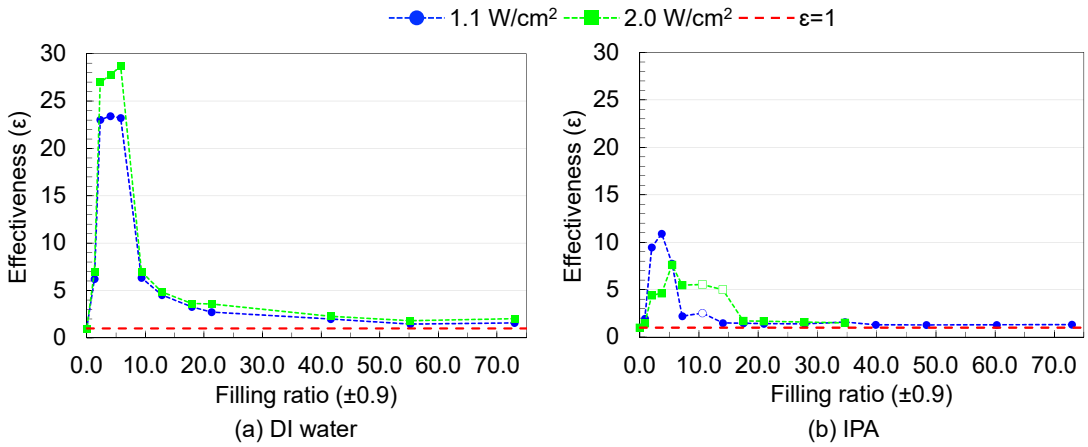

Figure 3.14: Variation of heat pipe effectiveness with filling ratio for heat pipe S-200 under different input heat fluxes (Note: the hollow data points correspond to unsteady operation of the heat pipe.)

3.5.2 Heat Pipe Effectiveness

Figure 3.14 shows the variation of effectiveness with filling ratio for heat pipe S-200 charged with different filling ratios of water or IPA under input heat loads of 1.1 and $2.0 W/cm^2$. Since the heat pipe charged with water exhibits lower values of ΔT during its operation at optimum filling ratios, the values of its effectiveness is higher compared to those of IPA. Along with more desirable thermophysical properties of water, the heat pipe charged with water does not operate with dryout at its optimum range of filling ratio. This enables the heat pipe to successfully transfer the input heat load through phase change at its maximum share. Hence, in both of the input heat loads of 1.1 and $2.0 W/cm^2$the effectiveness of the heat pipe charged with water is significantly higher than that of charged with IPA

3.5.3 Operation with Partial Dryout

The transparent top cover enables the visualization of the possible dryout during the operation of the heat pipe. Figure 3.15 show the variation of the extent of dryout with filling ratio for heat pipe S-200 under different input heat loads prior to dry operating condition. Expectantly, the extent of dryout increases by the

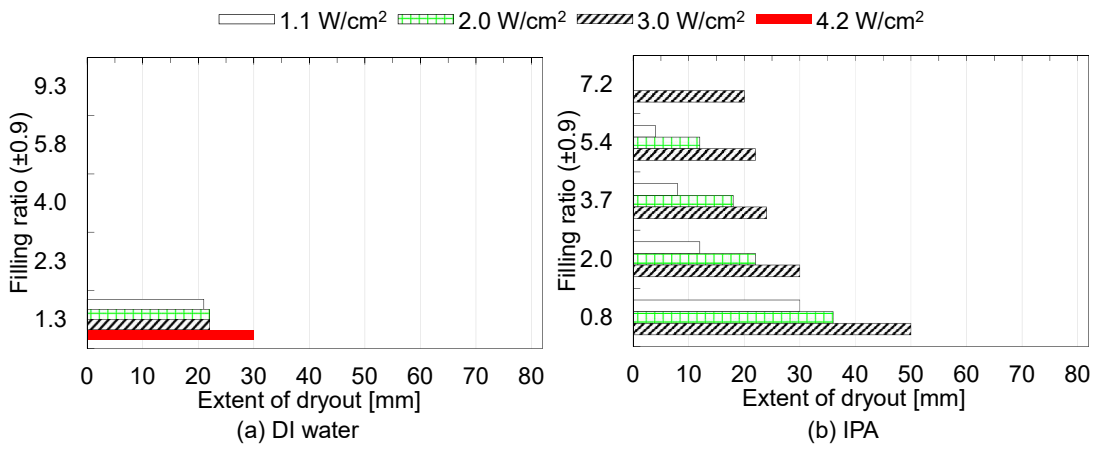

Figure 3.15: Variation of dryout extent with filling ratio for heat pipe S-200 under different input heat fluxes

heat load due to the higher rate of evaporation. For the heat pipe charged with IPA, the extent of dryout increases by decreasing the filling ratio, while for the case of water-charged heat pipe, dryout occurred at only one filling ratio prior to dry operating condition. With the help of its higher surface tension, water can provide more capillary pump in the same heat pipe. Consequently, the heat pipe charged with IPA experienced dryout in a wider range of filling ratio.

3.5.4 Heat Output Calculations

Knowing the inlet and outlet temperatures of the cooling water, the heat output of the heat pipe is calculated with the equation

$$Q_{out} = \dot{m} \cdot C_p \cdot \Delta T \tag{3.2}$$

where Q_{out} is the heat output from the heat pipe, $\dot{m}$ is the mass flow rate of cooling water, C_p is the specific heat of water ($4.2\,\mathrm{kJ/kg \cdot K}$), and ΔT is $T_{11} - T_{10}$ corresponding to rise in the cooling water temperature. Figure 3.16 shows the plot of calculated heat output against filling ratio for heat pipe S-200 charged with water and IPA. Input heat loads of 1.1, 2.0, 3.0, and 4.2 W/cm^2 correspond to 3.6, 6.6, 10.3, and 14.4 W, respectively. According to the input heat loads, the average relative error of heat output calculations are listed in Table 3.5. Based on

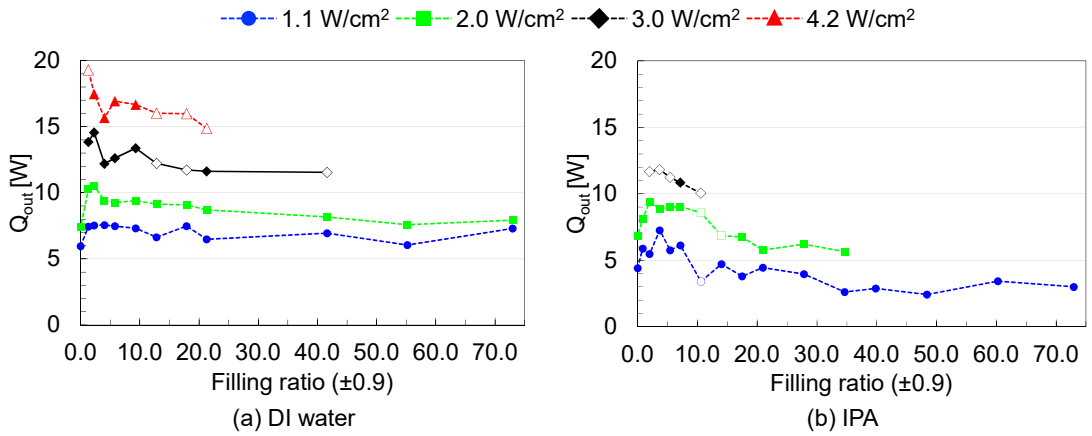

Figure 3.16: Variation of heat output with filling ratio under different input heat loads for heat pipe S-200 (Note: the hollow data points correspond to unsteady operation of the heat pipe.)

Table 3.5: Average relative error in heat output calculations for heat pipe S-200

Heat input [W/cm²]	**1.1**	**2.0**	**3.0**	**4.2**
Heat pipe charged with DI water	95.1%	35.0%	22.7%	15.4%
Heat pipe charged with IPA	34.1%	20.4%	8.9%	–

this table, the average relative error decreases with increasing the input heat load to the heat pipe. Although the relatively large values of the average relative error in heat output calculations make them not reliable enough to be interpreted, one possible source of error may be attributed to the change of the height of water inside the ice water reservoir during the experiments and subsequent water flow rate. For future experiments especially for heat pipe S-400, extra care is required to ensure the energy balance of the heat pipe. In this regard, switching inlet and outlet of the cooling water and inserting thermocouples directly to the PDMS piece are of possible solutions.

Chapter 4

Concluding Remarks

In the first phase of this research, three first generation prototype aluminum heat pipes with different groove densities are fabricated. Thermoelectric modules are used as the heat source and heat sink in the experiments. Moreover, a computational model is developed to quantify the input heat load. With the experience of prototypes, four aluminum heat pipes of second generation with different groove densities are fabricated and their thermal performance characterized. In their setup, a resistance heater and a copper block cooled by water flow are utilized as the heat source and sink. In addition, to simulate phase change heat transfer, a 3-D computation model is proposed for one of the heat pipes and verified by experimental results. At last, two silicon heat pipes with different groove densities are fabricated and experiments carried out on one of them. Two chromium sputtered electrodes are used as the heat source and cooling water flow in channels in a PDMS piece is the heat removal method. The thermal performance of each heat pipe is experimentally investigated under a wide range of filling ratios from fully-flooded to dry under different input heat loads, the optimum filling ratio is found by proposed thermal performance indicators, and extent of dryout is reported for different filling ratios and input heat fluxes.

The key findings of this thesis are as follows:

- Thermal performance of a flat grooved heat pipe is a strong function of filling ratio, groove density, and input heat flux.

- All heat pipes could properly transfer the heat input through phase change of the working fluid. However, the share of phase change depends on the filling ratio. For each heat pipe, the optimum filling ratio is selected by a minimum temperature difference along the heat pipe and reported.

- Among prototype heat pipes, the one with 0.2 mm grooves width showed the best performance. For second generation aluminum heat pipes, the one with 0.4 mm grooves width demonstrated minimum values of temperature difference and peak temperature.

- The computational model could simulate phase change heat transfer and is capable of predicting the temperature distribution along the heat pipe of interest, showing a strong agreement with the experimental results.

- As one of the performance limitations, the onset of dryout and its extent in different filling ratios are reported for all heat pipes. Beyond optimum filling ratios, further removal of the working fluid or increasing the input heat flux results in an increase in the extent of dryout.

- Compared to IPA, water could significantly boost the thermal performance of the silicon heat pipe by decreasing its minimum temperature difference, decreasing the peak temperature, and increasing its effectiveness by a factor of more than 2. Moreover, water could postpone the onset of dryout compared to IPA, which can be attributed to its higher Merit number than that of IPA.

There are some points that need to be considered for further studies, particularly for silicon heat pipes. The top cover used for the heat pipes in this study is decided to be plexiglas because of its transparency. Due to its low chemical resistance against some working fluids, using a pyrex cover would extend the maximum operational temperature range of the experiments, as well as the input heat flux. Moreover, for silicon heat pipes, improving the geometry of the frame

by decreasing the dead volume around the are of the grooves array would decrease the liquid flow in the gap between the frame and silicon piece. In addition, higher groove densities can be fabricated on silicon, e.g. grooves of 0.8 mm width. Hence, the optimum groove width can be selected having a more thorough understanding of dependency of thermal performance of silicon heat pipes on groove density. Furthermore, the vapor space can be fabricated in the top cover to decrease the number of the required materials, as well as the total thickness of the assembly.

Bibliography

[1] A. Faghri, "Review and advances in heat pipe science and technology," *Journal of Heat Transfer*, vol. 134, no. 12, p. 123001, 2012.

[2] A. Faghri, "Heat pipes: review, opportunities and challenges," *Frontiers in Heat Pipes (FHP)*, vol. 5, no. 1, 2014.

[3] S. Taze, "Modeling and fabrication of silicon micro-grooved heat pipes," Master's thesis, Bilkent University, Ankara, Turkey, 2015.

[4] ThermoLab Co. Ltd., 2009, `http://www.thermolab.co.kr/3443`, last visited on June 2017.

[5] C. Chan, E. Siqueiros, J. Ling-Chin, M. Royapoor, and A. Roskilly, "Heat utilisation technologies: A critical review of heat pipes," *Renewable and Sustainable Energy Reviews*, vol. 50, pp. 615–627, 2015.

[6] Y. Wang and G. Peterson, "Investigation of a novel flat heat pipe," *Transactions of the ASME-C-Journal of Heat Transfer*, vol. 127, no. 2, pp. 165–170, 2005.

[7] F. Lefèvre, J.-B. Conrardy, M. Raynaud, and J. Bonjour, "Experimental investigations of flat plate heat pipes with screen meshes or grooves covered with screen meshes as capillary structure," *Applied Thermal Engineering*, vol. 37, pp. 95–102, 2012.

[8] X. Li, M. Li, M. Li, R. Wu, Y. Wan, and T. Cheng, "Forming method of micro heat pipe with compound structure of sintered wick on grooved substrate," *Heat and Mass Transfer*, vol. 52, no. 3, pp. 581–593, 2016.

[9] T. Cotter, "Principles and prospects of micro heat pipes," in *Proceedings of the 5th International Heat Pipe Conference, Tsukuba, Japan*, vol. 1, pp. 328–335, 1984.

[10] Y. Cao and A. Faghri, "Micro/miniature heat pipes and operating limitations," *Journal of Enhanced Heat Transfer*, vol. 1, no. 3, 1994.

[11] Y. F. Maydanik, "Loop heat pipes," *Applied Thermal Engineering*, vol. 25, no. 5, pp. 635–657, 2005.

[12] M. Zaghdoudi, S. Maalej, J. Mansouri, and M. Sassi, "Flat miniature heat pipes for electronics cooling: State of the art, experimental and theoretical analysis," *World Academy of Science, Engineering and Technology, International Journal of Mechanical, Aerospace, Industrial, Mechatronic and Manufacturing Engineering*, vol. 5, no. 3, pp. 714–737, 2011.

[13] T. Kaya and J. Goldak, "Numerical analysis of heat and mass transfer in the capillary structure of a loop heat pipe," *International Journal of Heat and Mass Transfer*, vol. 49, no. 17, pp. 3211–3220, 2006.

[14] K. H. Do and S. P. Jang, "Effect of nanofluids on the thermal performance of a flat micro heat pipe with a rectangular grooved wick," *International Journal of Heat and Mass Transfer*, vol. 53, no. 9, pp. 2183–2192, 2010.

[15] S. Lips, F. Lefèvre, and J. Bonjour, "Nucleate boiling in a flat grooved heat pipe," *International Journal of Thermal Sciences*, vol. 48, no. 7, pp. 1273–1278, 2009.

[16] G. Odabaşi, *Modeling of multidimensional heat transfer in a rectangular grooved heat pipe*. PhD thesis, Middle East Technical University (METU), 2014.

[17] R. Hopkins, A. Faghri, and D. Khrustalev, "Flat miniature heat pipes with micro capillary grooves," *Journal of Heat Transfer*, vol. 121, no. 1, pp. 102–109, 1999.

[18] H. Lim, S. Kim, H. Im, K. H. Oh, and S. Jeong, "Fabrication and evaluation of a copper flat micro heat pipe working under adverse-gravity orientation,"

Journal of Micromechanics and Microengineering, vol. 18, no. 10, p. 105013, 2008.

[19] J.-S. Chen and J.-H. Chou, "Cooling performance of flat plate heat pipes with different liquid filling ratios," *International Journal of Heat and Mass Transfer*, vol. 77, pp. 874–882, 2014.

[20] X. Hao, B. Peng, Y. Chen, and G. Xie, "Experimental investigation on heat transfer performance of a flat plate heat pipe with MWCNTS-acetone nanofluid," *Journal of Heat Transfer*, vol. 139, pp. 1294–1304, 2017.

[21] S. Lips, F. Lefèvre, and J. Bonjour, "Combined effects of the filling ratio and the vapour space thickness on the performance of a flat plate heat pipe," *International Journal of Heat and Mass Transfer*, vol. 53, no. 4, pp. 694–702, 2010.

[22] R. N. Dean, D. K. Harris, A. Y. Palkar, and G. D. Wonacott, "Liquid metal-filled micro heat pipes for thermal management of solid-state devices," *IEEE Transactions on Industrial Electronics*, vol. 59, no. 12, pp. 4888–4894, 2012.

[23] M. J. Stubblebine and I. Catton, "Passivation and performance of inorganic aqueous solutions in a grooved aluminum flat heat pipe," *Journal of Heat Transfer*, vol. 137, no. 5, p. 052901, 2015.

[24] J. Supowit, T. Heflinger, M. Stubblebine, and I. Catton, "Designer fluid performance and inclination angle effects in a flat grooved heat pipe," *Applied Thermal Engineering*, vol. 101, pp. 770–777, 2016.

[25] J.-S. Chen and J.-H. Chou, "The length and bending angle effects on the cooling performance of flat plate heat pipes," *International Journal of Heat and Mass Transfer*, vol. 90, pp. 848–856, 2015.

[26] A. Bejan and A. D. Kraus, *Heat transfer handbook*, vol. 1. John Wiley & Sons, 2003.

[27] B. Kim and G. Peterson, "Analysis of the critical weber number at the onset of liquid entrainment in capillary-driven heat pipes," *International Journal of Heat and Mass Transfer*, vol. 38, no. 8, pp. 1427–1442, 1995.

[28] P. Nemec, A. Čaja, and M. Malcho, "Mathematical model for heat transfer limitations of heat pipe," *Mathematical and Computer Modelling*, vol. 57, no. 1, pp. 126–136, 2013.

[29] D. Reay, R. McGlen, and P. Kew, *Heat Pipes. Theory, Design and Applications.* Butterworth-Heinemann, 6 ed., 2014.

[30] A. Faghri, *Heat pipe science and technology.* Global Digital Press, 1995.

[31] W. W. Wits, J. van Es, and G. J. te Riele, "Automated charging of embedded heat pipe systems," *Heat Pipe Science and Technology, An International Journal*, vol. 3, no. 2-4, 2012.

[32] M. T. Ababneh, S. Chauhan, F. M. Gerner, D. Hurd, P. de Bock, and T. Deng, "Charging station of a planar miniature heat pipe thermal ground plane," *Journal of Heat Transfer*, vol. 135, no. 2, p. 021401, 2013.

[33] C. Li, Y. Luo, C. Zhou, Q. Shan, and X. Wang, "Charging method of micro heat pipe for high-power light-emitting diode," *Micro & Nano Letters*, vol. 10, no. 10, pp. 518–522, 2015.

[34] X.-d. Wang, G. Liu, L.-l. Zou, and Y. Luo, "Vacuum fluid charging and packaging technique for micro heat pipes," in *Electronic Packaging Technology (ICEPT), 2013 14th International Conference on*, pp. 46–49, IEEE, 2013.

[35] S. J. Kim, J. K. Seo, and K. H. Do, "Analytical and experimental investigation on the operational characteristics and the thermal optimization of a miniature heat pipe with a grooved wick structure," *International Journal of Heat and Mass Transfer*, vol. 46, no. 11, pp. 2051–2063, 2003.

[36] F. Lefèvre, R. Rullière, G. Pandraud, and M. Lallemand, "Prediction of the temperature field in flat plate heat pipes with micro-grooves–experimental validation," *International Journal of Heat and Mass Transfer*, vol. 51, no. 15, pp. 4083–4094, 2008.

[37] X. F. Yang, Z.-H. Liu, and J. Zhao, "Heat transfer performance of a horizontal micro-grooved heat pipe using CuO nanofluid," *Journal of Micromechanics and Microengineering*, vol. 18, no. 3, p. 035038, 2008.

[38] R. Revellin, R. Rullière, F. Lefèvre, and J. Bonjour, "Experimental validation of an analytical model for predicting the thermal and hydrodynamic capabilities of flat micro heat pipes," *Applied Thermal Engineering*, vol. 29, no. 5, pp. 1114–1122, 2009.

[39] F. Lefèvre, R. Rullière, S. Lips, and J. Bonjour, "Confocal microscopy for capillary film measurements in a flat plate heat pipe," *Journal of Heat Transfer*, vol. 132, no. 3, p. 031502, 2010.

[40] S. Lips, F. Lefèvre, and J. Bonjour, "Physical mechanisms involved in grooved flat heat pipes: experimental and numerical analyses," *International Journal of Thermal Sciences*, vol. 50, no. 7, pp. 1243–1252, 2011.

[41] J. Qu, H. Wu, and P. Cheng, "Start-up, heat transfer and flow characteristics of silicon-based micro pulsating heat pipes," *International Journal of Heat and Mass Transfer*, vol. 55, no. 21, pp. 6109–6120, 2012.

[42] Y. J. Youn and S. J. Kim, "Fabrication and evaluation of a slicon-based micro pulsating heat spreader," *Sensors and Actuators A: Physical*, vol. 174, pp. 189–197, 2012.

[43] Y. Tang, Z. Hu, J. Qing, Z. Xie, T. Fu, and W. Chen, "Experimental investigation on isothermal performance of the micro-grooved heat pipe," *Experimental Thermal and Fluid Science*, vol. 47, pp. 143–149, 2013.

[44] X. Li, J. Wang, Q. Hu, L. Bao, and H. Zhang, "Experimental and theoretical research on capillary limit of micro heat pipe with compound structure of sintered wick on trapezium-grooved substrate," *Heat and Mass Transfer*, vol. 49, no. 3, pp. 381–389, 2013.

[45] A. B. Solomon, A. R. Kumar, K. Ramachandran, B. Pillai, C. S. Kumar, M. Sharifpur, and J. P. Meyer, "Characterisation of a grooved heat pipe with an anodised surface," *Heat and Mass Transfer*, vol. 53, pp. 753–763, 2017.

[46] W. I. Aly, M. A. Elbalshouny, H. A. El-Hameed, and M. Fatouh, "Thermal performance evaluation of a helically-micro-grooved heat pipe working with water and aqueous Al_2O_3 nanofluid at different inclination angle and filling ratio," *Applied Thermal Engineering*, vol. 110, pp. 1294–1304, 2017.

[47] Y. Cai, Z. Li, J. Zhai, Y. Tang, and B. Yu, "Experimental investigation on a novel multi-branch heat pipe for multi-heat source electronics," *International Journal of Heat and Mass Transfer*, vol. 104, pp. 467–477, 2017.

[48] L. M. Poplaski, S. P. Benn, and A. Faghri, "Thermal performance of heat pipes using nanofluids," *International Journal of Heat and Mass Transfer*, vol. 107, pp. 358–371, 2017.

[49] H. N. Chaudhry, B. R. Hughes, and S. A. Ghani, "A review of heat pipe systems for heat recovery and renewable energy applications," *Renewable and Sustainable Energy Reviews*, vol. 16, no. 4, pp. 2249–2259, 2012.

[50] W. G. Anderson, J. H. Rosenfeld, D. Angirasa, Y. Mi, M. S. El-Genk, and M. J. Bragg, "Evaluation of heat pipe working fluids in the temperature range 450 to 700 K," in *AIP Conference Proceedings*, vol. 699, pp. 20–27, AIP, 2004.

[51] L. Jiang, J. Ling, L. Jiang, Y. Tang, Y. Li, W. Zhou, and J. Gao, "Thermal performance of a novel porous crack composite wick heat pipe," *Energy Conversion and Management*, vol. 81, pp. 10–18, 2014.

[52] J. Cheng, G. Wang, Y. Zhang, P. Pi, and S. Xu, "Enhancement of capillary and thermal performance of grooved copper heat pipe by gradient wettability surface," *International Journal of Heat and Mass Transfer*, vol. 107, pp. 586–591, 2017.

[53] G. Peterson, A. Duncan, and M. Weichold, "Experimental investigation of micro heat pipes fabricated in silicon wafers," *Journal of Heat Transfer*, vol. 115, pp. 751–751, 1993.

[54] M. Mehrali, E. Sadeghinezhad, R. Azizian, A. R. Akhiani, S. T. Latibari, M. Mehrali, and H. S. C. Metselaar, "Effect of nitrogen-doped graphene nanofluid on the thermal performance of the grooved copper heat pipe," *Energy Conversion and Management*, vol. 118, pp. 459–473, 2016.

[55] C. Oshman, Q. Li, L.-A. Liew, R. Yang, Y. Lee, V. M. Bright, D. J. Sharar, N. R. Jankowski, and B. C. Morgan, "Thermal performance of a flat polymer

heat pipe heat spreader under high acceleration," *Journal of Micromechanics and Microengineering*, vol. 22, no. 4, p. 045018, 2012.

[56] K. Park and H. Ma, "Nanofluid effect on the heat transport capability in a well-balanced oscillating heat pipe," *Journal of Thermophysics and Heat Transfer*, vol. 21, no. 2, pp. 443–445, 2007.

[57] Y. Ji, H. Ma, F. Su, and G. Wang, "Particle size effect on heat transfer performance in an oscillating heat pipe," *Experimental Thermal and Fluid Science*, vol. 35, no. 4, pp. 724–727, 2011.

[58] X. Yang, Y. Yan, and D. Mullen, "Recent developments of lightweight, high performance heat pipes," *Applied Thermal Engineering*, vol. 33, pp. 1–14, 2012.

[59] W. M. Haynes, *CRC Handbook of Chemistry and Physics*. CRC Press, 2014.

[60] ePlastics®, "Chemical resistance of plexiglass acrylic." `http://www.eplastics.com/Plastic/plastics_library/Chemical-Resistance-of-Plexiglass-Acrylic`, last visited on June 2017.

[61] B. Suman, "Modeling, experiment, and fabrication of micro-grooved heat pipes: an update," *Applied Mechanics Reviews*, vol. 60, no. 3, pp. 107–119, 2007.

[62] Y. Akkuş and Z. Dursunkaya, "A new approach to thin film evaporation modeling," *International Journal of Heat and Mass Transfer*, vol. 101, pp. 742–748, 2016.